

**QUANTITATIVE METHODS FOR THE ANALYSIS OF
HYDROCARBON OXIDATION PRODUCTS: A SMOG CHAMBER
STUDY**

Zoya Dobrusin

A thesis submitted to
the Faculty of Graduate Studies
in partial fulfillment of the requirements
for the degree of

Master of Science

Graduate Program in Chemistry
York University
Toronto, Ontario

August 2012

Abstract

The oxidation products from the reaction of beta-pinene with the hydroxyl (HO) radical were studied using the York University smog chamber. The main focus of this study was to look into methods of quantifying products with the API-365 APCI-MS/MS instrument. Being able to obtain quantitative information with this instrument would allow us to determine product yields and gain a better understanding of the instrument's sensitivity towards different classes of compounds. Linear calibrations were achieved through the use of analyte signals relative to the protonating reagent(s) (protonated water and its clusters) in the chemical ionization process.

Individual compound calibrations using analyte introduction via syringe pump were performed for reaction relevant products: nopinone and pinic acid. Nopinone calibrations, which were representative of gas phase products, were successful. On the other hand, pinic acid calibrations, meant to be more indicative of low volatility products, could not be properly achieved. The second type of calibration approach targeted to evaluate general instrument sensitivity towards classes of functional groups and to also reduce the dependence on commercially available standard compounds. This was done by deriving a relationship between instrument sensitivity and gas phase basicity (GB). This relationship was tested first by developing calibration curves (sensitivity/GB calibrations) using a few simple ketones and alcohols. The ketone calibration curve, showing good linearity, was then used to estimate the sensitivity of a reaction relevant ketone (nopinone).

Both calibration approaches were tested for their accuracy by using their measured sensitivities to estimate the concentration of a known amount of nopinone injected into the chamber. They were also both used to calculate the yield of nopinone in the beta-pinene/HO chamber experiment. The syringe pump calibrations showed good accuracy and were used to calculate a yield of 24 ± 5 %; a value in general agreement with other literature reported data. However, the sensitivity/GB calibrations did not show

sufficiently accurate results. The sensitivity/GB calibrations were still fully evaluated and several problem areas were identified for future research.

Acknowledgments

Firstly I would like to thank my supervisor Prof. Donald R. Hastie for his advice, support and guidance throughout my time in the lab and during my thesis. I appreciate his fostering of skills and professional growth that I feel will be of use in many future ventures. I would also like mention the past and current members of the Hastie group (Mehrnaz, Amanda, Julie, Janeen, Dana and Kim) who were not only available for academic discussion but were always a pleasure to work with. This also includes all the past and current members of the Centre for Atmospheric Chemistry (CAC), a community I felt very grateful to be a part of and whom with many I feel I have built long lasting friendships. And in particular Carol Weldon who was always extremely helpful with administrative issues or just available for a friendly chat.

I greatly value the feedback that Prof. Mozurkewich and Prof. Harris, members of my research evaluation committee, provided on my work. And also that Prof. Mozurkewich and Prof. McDade were able to be part of my examination committee.

I appreciate that Prof. Rudolph's, Prof. Organ's and Prof. Mozurkewich's groups generously allowed me access to their equipment and chemicals that were needed in order to complete my experiments. As well as, Greg Koyanagi and Voislav Blagojevic of Prof. Bohme's group who were helpful with instrumental difficulties and always available to share their wealth of knowledge. I would like to thank NSERC, the Charles Hantho and the Harold Schiff foundations for their financial support in my studies, as well as, Nick Karellas of the Ministry of the Environment for instrumentation.

Most importantly I would like to thank my family; my amazing parents (Yuri and Elena) and brother (Boris). They are my rocks of unconditional support and love. I feel so incredibly lucky to have them by my side.

Table of Contents

Abstract	iv
Acknowledgments.....	vi
Table of Contents	vii
List of Tables	xi
List of Figures	xiii
List of Abbreviations	xvii
1. Introduction.....	1
1.1. Organic Particle Components and Secondary Organic Aerosols	2
1.2. SOA Components Measurement Techniques	4
1.2.1. Off-Line Measurement Techniques	4
1.2.1.1. Sample collection and Handling	4
1.2.1.2. Off-line Instrumentation	5
1.2.2. On-Line Measurement Techniques.....	6
1.3. Studies in the York University Smog Chamber.....	8
1.3.1. Previous and Ongoing Hastie Group Studies in the York University Smog Chamber.....	8
1.3.2. This Current Study.....	9
2. Experimental.....	11
2.1. Mass Spectrometry.....	11
2.1.1. APCI Source Ion Formation	11
2.1.2. Quadrupole Mass Analyzer.....	13
2.1.3. Triple Quadrupole Mass Spectrometer	16
2.2. Calibration Approaches	21
2.2.1. Syringe Pump Calibrations	21
2.2.2. Exponential Dilution Flask Calibrations.....	22
2.2.3. Beta-Pinene Permeation Tube Calibrations	24
2.3. Smog Chamber Experiments	26
2.3.1. The Smog Chamber	26
2.3.2. Reagent Information	27
2.3.2.1. Chamber Seeding	27
2.3.2.2. HO Radical Production and Concentration Estimation	28
3. Results and Discussion	31

3.1. Initial API 365 Experiments with the Smog Chamber	31
3.1.1. Sampling Problems	31
3.1.1.1. Unsealed Ion Source	32
3.1.1.2. Filter Adsorption During Gas Phase Sampling.....	36
3.1.2. Product Identification Comparison between the TAGA and API Instruments	38
3.2. Obtaining Calibration Curves at Our Concentration Range	40
3.2.1. Derivation of Relative Signal Calibrations for Dimer Species	44
3.3. Reaction Relevant, Single Compound calibrations using a Syringe Pump	44
3.3.1. Gas Phase Calibration Set-Up.....	45
3.3.1.1. Nopinone in Methanol Solution.....	45
3.3.1.2. Pure Nopinone Sampling with Syringe Pump	47
3.3.1.3. Chamber Sampling Set-Ups.....	48
3.3.2. Dealing with Low Vapour Pressure Samples with the Syringe Pump Calibrations	52
3.3.2.1. Exploring Causes of the Signal Instability of Pinonic Acid Sampling	56
3.3.3. Summary of Syringe Pump Calibrations	57
3.4. Evaluating the General Sensitivity of the APCI-MS/MS Instrument	58
3.4.1. Deriving a Relationship between Sensitivity and Gas Phase Basicity	59
3.4.2. Analytes Chosen for Calibrations and Obtained Sensitivities	61
3.4.2.1. Calibrations of Alcohols and Ketones using the EDF Method.....	62
3.4.3. Applying the $\ln(\text{Sensitivity})$ vs. Gas Phase Basicity (GB) Relationship	66
3.4.3.1. Plotting Alcohol and Ketone $\ln(\text{Sensitivity})$ vs. ΔGB Graphs Separately	69
3.4.3.1.1 Deviation of $\ln(\text{Sensitivity})$ vs. ΔGB Ketone and Alcohol Slopes from the Theoretical Slope	69
3.4.3.1.2 Differences Between the $\ln(\text{Sensitivity})$ vs. ΔGB Ketone and Alcohol Slopes.....	69
3.4.3.2. Accuracy of $\ln(\text{Sensitivity})$ Estimated from $\ln(\text{Sensitivity})$ vs. ΔGB Graphs Calibration Curve and Average Experimental $\ln(\text{Sensitivity})$	72
3.5. Testing the Validity of the Calibrations for Chamber Reaction Relevant Compounds	75
3.5.1. Syringe Pump Accuracy Results.....	75
3.5.1.1. Data Acquisition and Evaluation Procedure	75
3.5.1.2. The Poor Accuracy of the Nopinone Dimer SRM Pair	77
3.5.2. Exponential Dilution Flask (EDF) Results	78
3.5.2.1. Direct EDF Sampling of Nopinone Problems	78
3.5.2.2. Nopinone Sensitivity Estimation	79

3.5.2.3. Nopinone Sensitivity Accuracy Testing: Set-Up A Results	81
3.5.2.4. Nopinone Sensitivity Accuracy Testing: Set-Up B Results	83
3.5.2.5. Possible Problems Associated with Estimation of Sensitivities from the Ketone Calibration	86
3.5.2.5.1 Shortcomings of Camphor as a Surrogate for Nopinone GB	86
3.5.2.5.2 Problems in the ln(Sensitivity) vs. ΔGB Calibration.....	87
3.5.3. Nopinone Yield Measurements	88
3.5.3.1. Nopinone Yield Measurements Using the Syringe Pump Calibration Method	90
3.5.3.2. Nopinone Yield Measurements Using Sensitivities of ln(Sensitivity) vs. ΔGB Graph of Ketones	93
3.5.3.2.1 Estimation of Instrument Sensitivity and Yield Calculation from a One-Point Calibration	94
3.5.3.3. Comparison to Literature Reported Gas Phase Nopinone Yields.....	96
3.5.4. Applying Calibrations to Evaluate Concentration from Signal and Determining Yields.....	99
4. Conclusions.....	100
4.1. Qualitative Data Acquisition.....	100
4.2. Quantitative Data Acquisition.....	102
4.2.1. Compound Specific Calibrations	102
4.2.2. General Instrument Sensitivity Evaluation	104
4.2.3. Calibration Accuracy and Yield Testing	105
5. Future Work.....	107
5.1. Low Vapour Pressure Compound Calibrations	107
5.1.1. Diffusion Tube Sample Introduction	107
5.1.2. The Use of a Heated Nebulizer.....	109
5.2. More work on ln(Sensitivity) vs. ΔGas Phase Basicity (GB) Calibrations	112
Appendix A. Calibration Compounds Information.....	115
Appendix B. Calculation of Analyte Concentration at the APCI Ion Source.....	116
Appendix C. Other Instrument Data from beta-Pinene/HO Chamber Experiments.....	117
Appendix D. Sample Saturation Mixing Ratio Calculation for Pinic Acid.....	119
Appendix E. Sample water droplet formation and evaporation rate for syringe	120
Appendix F. Time Constants of EDF Calibrations.....	121
Appendix G. ln(sensitivity) vs. Gas Phase Basicity (GB) data used for plotting calibration curves	122
Appendix H .EDF set-up B calibration data summary	123
Appendix I. Diffusion Tube Calculations [Nelson, 1971].....	125

References.....126

List of Tables

Table 2.1 Proton affinities for various water cluster sizes $H^+(H_2O)_n$	12
Table 2.2 Summary of scans used with the API 365 in these experiments.....	18
Table 2.3 Fragmentation pattern examples	20
Table 2.4 SRM pairs followed for nopinone calibrations (CE 10)	20
Table 3.1 The unaccounted flow rate from the leak in the APCI ion source when different exhaust pump rates were applied	33
Table 3.2 Products observed in the TAGA 6000E and API 365.....	39
Table 3.3 Summary of results from the slopes obtained using a nopinone/methanol solution in the syringe pump calibrations	47
Table 3.4 Summary of results from the slopes obtained using syringe pump calibration set-up B (1 st and 2 nd calibration results with changes in chamber conditions (reagent injection) in between.....	52
Table 3.5 Examples of intermediate gas phase basicities (GB) (GBs between that of water (660 kJ mol ⁻¹) and ammonia (819 kJ mol ⁻¹)) [Hunter et al., 1998].....	59
Table 3.6 Summary of sensitivities obtained from EDF calibration of alcohols and ketones	65
Table 3.7 Summary of calibration results for ln(sensitivity) vs. GB using the sensitivity obtained from using calibrations made from the signal of the most abundant ion.....	66
Table 3.8 Summary of calibration results for ln(sensitivity) vs. GB using the sensitivity obtained from using calibrations made from the sum of the signals of the three most abundant ions	71
Table 3.9 Absolute differences ($\Delta \ln S$) between the ln(sensitivity) or lnS calculated from ketone lnS vs. ΔGB calibration and experimentally measured lnS	74
Table 3.10 Absolute differences ($\Delta \ln S$) between the ln(sensitivity) or lnS calculated from alcohol lnS vs. ΔGB calibration and experimentally measured lnS	74
Table 3.11 Nopinone concentrations obtained from calibrations (actual nopinone injection value = 0.2ppm). The sensitivities used to calculate the concentrations are in Table 3.12.	76
Table 3.12 Sensitivities obtained from standard addition calibrations	76
Table 3.13 Calculated sensitivities of nopinone and calculated errors on the sensitivity (set-up A). The upper and lower ranges (min and max of the sensitivity) are also listed.	81
Table 3.14 The signal obtained for the 0.2 ppm of injected nopinone and the concentration calculated based on the sensitivity obtained from the slope of the ketone	

ln(sensitivity) vs. GB plot (set-up A). The concentration calculated from the upper and lower ranges (max and min) of the sensitivity are also listed.....	83
Table 3.15 Calculated sensitivities of nopinone and calculated errors on the sensitivity (set-up B). The upper and lower ranges (max and min) of the sensitivity are also listed.	84
Table 3.16 The signals obtained from set-up A re-calculated with set-up B sensitivities	85
Table 3.17 The signal obtained for the 0.2 ppm of injected nopinone and the concentration calculated based on the sensitivity obtained from the slope of the ketone ln(sensitivity) vs. Δ GB plot (set-up B). The concentration calculated from the upper and lower ranges (max and min) of the sensitivity are also listed.....	86
Table 3.18 Calculation of sensitivity changes with changes of GB (using set-up A data as starting comparison sensitivity).....	87
Table 3.19 Slopes from standard addition syringe pump calibrations from chamber experiments	91
Table 3.20 Nopinone product yields (%) using syringe pump calibrations	93
Table 3.21 Nopinone product yields (%) obtained from the sensitivities of the ln(sensitivity) vs. Δ GB graph of ketones	94
Table 3.22 Nopinone product yields (%) obtained from the instrument response to a 0.2 ppm nopinone injection following a beta-pinene chamber experiment.....	96
Table 3.23 Literature reported gas phase nopinone yields.....	98
Table A.1 SRM pairs used to calibrate compounds	115
Table A.2 SRM pairs followed for pinonic and pinic acid calibrations (CE 10).....	115
Table F.1 Time constant (τ_{fit}) for alcohols based on relative signal	121
Table F.2 Time constant (τ_{fit}) for ketones based on relative signal	121
Table F.1 Summary of alcohol ln(sensitivity) values vs. Δ GB.....	122
Table G.2 Summary of ketone ln(sensitivity) values vs. Δ GB	122
Table H.1 Ketone Δ GB values and lnS values for individual days and lnS taken as an average for EDF (set-up B (Figure 3.28 in Section 3.5.2.4)).....	123

List of Figures

Figure 1.1 A schematic of secondary organic aerosol (SOA) formation (Figure adapted from: [Seinfeld et al., 2003]).....	3
Figure 2.1 APCI Ion source with corona region expanded.....	12
Figure 2.2 (a) Schematic of the quadrupole mass analyzer with oppositely charged (Φ) two pairs of rods (see Equation 2.1 and Equation 2.2) (b) The radius and configuration of the rods where $r=1.1148r_0$ and r_0 is the radius of an imaginary rod that defines the separation between the four quadrupole rods	14
Figure 2.3 (a) Mathieu diagrams for the movement for an ion of mass m_i in the x and y directions as function of a and q ($u = x$ or y) (b) Superimposed x and y Mathieu diagrams from (a) with 4 intersecting areas (A, B, C and D) (Adapted from De Hoffmann et al (2008))	15
Figure 2.4 Stability diagram of m_1 , m_2 , and m_3 at the given values of a_u and q_u (where $u = x$ or y) and the scan line. Only m_2 follows a stable trajectory to the detector	16
Figure 2.5 Schematic of the triple quadrupole instrument.....	17
Figure 2.6 (a) Q1-MS/full mass spectrum of pure nopinone (where M =compound of mass of 138 u) (b) Product ion scan of m/z 139 of nopinone (where $M =$ compound of mass of 138 u). 19	19
Figure 2.7 Schematic of syringe pump sample introduction	21
Figure 2.8 Exponential dilution flask set-up.....	23
Figure 2.9 Schematic of beta-pinene permeation source set-up for calibration by GC-FID	25
Figure 2.10 beta-Pinene GC-FID calibration.....	25
Figure 2.11 Schematic of smog chamber experimental set-up	27
Figure 2.12 Schematic of experimental procedure in the smog chamber	27
Figure 2.13 \ln [beta-pinene] vs. time plot and HO concentration estimation from the first 30 min of the reaction profile.....	29
Figure 3.1 Schematic of the APCI ion source and adjacent areas; with the originally unsealed region leading to the interface region	35

Figure 3.2 Front face view of curtain plate which leads into the de-clustering/curtain gas region which is followed by the interface region (this is also the attachment point of the source). (*) region where EPDM rubber cord was placed.....	35
Figure 3.3 SRM time profiles with and without a filter in the sampling line for (a) nopinone (m/z 139/121) and (b) hydroxy nopinone (m/z 155/109)	37
Figure 3.4 Filter and no filter sampling over the course of a beta-pinene/HO chamber experiment.....	37
Figure 3.5 Raw nopinone signal (m/z 139/121) vs. nopinone concentration [M] and the protonating reagent ion signal as represented by the water clusters $H^+(H_2O)_n$ ($n=2$ and 3) at ion pair masses m/z 55/37 and m/z 37/19.....	41
Figure 3.6 Nopinone signal relative to protonating reagent ion signal vs. nopinone concentration.....	43
Figure 3.7 (a) Nopinone relative signal (m/z 139/121) in methanol solution vs. nopinone concentration	
(b) Methanol relative signal (m/z 51/33) vs. methanol concentration	46
Figure 3.8 Nopinone relative signal (m/z 139/121) vs. nopinone concentration	48
Figure 3.9 Syringe pump calibration set-up A: calibration and chamber sampling is done separately	49
Figure 3.10 Nopinone relative signal (m/z 139/121) vs. nopinone concentration with chamber sampling done between calibrations (set-up A).....	49
Figure 3.11 Syringe pump calibration set-up B: Sampling from calibration set-up and chamber was done simultaneously. The calibration was a standard addition.....	50
Figure 3.12 Nopinone relative signal (m/z 139/121) vs. nopinone concentration. Calibration was done using the standard addition method (set-up B). Using the same set-up first a calibration was done, the chamber conditions were changed (reagent injection) and finally a second was calibration done.	51
Figure 3.13 The structures of (a) pinic acid (b) pinonic acid.....	53
Figure 3.14 Calibration set-up for pinic and pinonic acids.....	54
Figure 3.15 SRM trace of m/z 185/167 (pinonic acid) during concentration variation via syringe pump flow rate changes (0.02, 0.05 and 0.07 $\mu\text{L min}^{-1}$).....	55
Figure 3.16 Calibration plots for the relative pinonic acid signal (m/z 185/167) vs. pinonic acid concentration	55
Figure 3.17 (a) Exponential decay of the relative signal of methanol SRM pair 51/33 vs time	
(b) Exponential decay of the relative signal of cycloheptanone SRM pair 113/95 vs time	
.....	63

Figure 3.18 (a) Calibration curve from the relative signal of methanol SRM pair 51/33 vs time obtained by the EDF method	
(b) Calibration curve from the relative signal of cycloheptanone SRM pair 113/95 vs time obtained by the EDF method	64
Figure 3.19 Graph of ln(sensitivity) vs. Δ GB for alcohols and ketones	67
Figure 3.20 Graph of ln(sensitivity) vs. Δ GB for alcohols	68
Figure 3.21 Graph of ln(sensitivity) vs. Δ GB for ketones	68
Figure 3.22 Graph of ln(sensitivity) vs. Δ GB for alcohols using the sum of the signals of the three most abundant ions.....	70
Figure 3.23 Graph of ln(sensitivity) vs. Δ GB for ketones using the sum of the signals of the three most abundant ions.....	71
Figure 3.24 Schematic of preferred protonation (a) alcohols (b) ketones	72
Figure 3.25 The EDF exponential decays for (a) beta-pinene (b) its nopinone impurity over time	79
Figure 3.26 The structures of (a) camphor (b) nopinone	80
Figure 3.27 Schematic of chamber sampling set-up to test the EDF calibration results (set-up A)	82
Figure 3.28 Schematic of chamber sampling set-up to test the EDF calibration results (set-up B)	84
Figure 3.29 Reaction time profile of m/z 139/121 over the course of a smog chamber experiment.....	89
Figure 3.30 Plot of nopinone formed, corrected for the reaction with HO radical plotted against beta-pinene consumed	92
Figure 3.31 (a) Nopinone (m/z 139/121) relative signal over the course of a beta-pinene chamber experiment	
(b) Nopinone (m/z 139/121) relative signal after a 0.2ppm injection into the chamber (with the lights off)	
.....	95
Figure 3.32 Proposed nopinone formation mechanism [MCM].....	98
Figure 5.1 Schematic of a diffusion tube	108
Figure 5.2 (a) Heated nebulizer probe cross section	
(b) Close up schematic of tip of heated nebulizer	
(Figure from: PE Sciex API System Reference Manual)	
.....	111

Figure B.1 APCI source flow inputs and (*) as the area in the source at which concentration calculated for use in calibrations.....	116
Figure C.1 Typical temperature and relative humidity time profile during a beta-pinene/HO experiments	117
Figure C.2 Example of a beta-Pinene/HO experiment particle size distribution.....	117
Figure C.3 Example NO and NO _x time profile during a beta-pinene/HO chamber experiment.....	118
Figure H.1 lnS vs. ΔGB of Ketones using EDF Set-Up B (Figure 3.28)	124

List of Abbreviations

AMS	aerosol mass spectrometry	O₂	oxygen
APCI	atmospheric pressure chemical ionization	O₃	ozone
bP	beta-pinene	PA	proton affinity
CEM	channel electron multiplier	PM	particulate matter
CFMD	counter flow membrane denuder	ppb	parts per billion
CID	collision induced dissociation	ppm	parts per million
Conc.	concentration	ppt	parts per trillion
CPC	condensation particle counter	PTR	proton transfer reaction
DC	direct current	Q	flow through the flask
DMA	differential mobility analyzer	RF	radio frequency
EDF	exponential dilution flask	SOA	secondary organic aerosols
EI	electron impact	SRM	selected reaction monitoring
EPDM	ethylene propylene diene monomer	TOF	time of flight
ESI	electrospray ionization	V	flask volume
FID	flame ionization detector	VOC	volatile organic compounds
FT-IR	Fourier transform infrared spectroscopy		
GB	gas phase basicity		
GC	gas chromatography		
H₂O	water		
HO	hydroxyl radical		
IC	Ion Chromatography		
HPLC	high performance liquid chromatography		
IPN	isopropyl nitrite		
LC	liquid chromatography		
lnS	natural log of relative instrument sensitivity		
<i>m/z</i>	mass to charge ratio		
MCM	master chemical mechanism		
MFC	mass flow controller		
MFM	mass flow meter		
MS	mass spectrometry		
MS/MS	tandem mass spectrometry		
N₂	nitrogen		
NO	nitrogen oxide		
NO₃	nitrate radical		
NO_x	sum of nitric oxide and nitrogen dioxide		
NP	nopinone		
NMR	nuclear magnetic resonance		

1. Introduction

Understanding the production and composition of atmospheric particulate matter (PM) has been one of the key research objectives of atmospheric chemists in the last century. PM has been linked to several adverse effects. These include contribution to climate change by acting as cloud condensation nuclei (CCN) [Twomey et al., 1984] and by absorbing or scattering solar radiation [Bauer et al., 2012]. PM and its production processes can also lead to enhanced instances of haze or smog ([Finlayson-Pitts and Pitts, 2000], [Dickerson et al., 1997]) and tropospheric ozone (O₃) [Kansal, 2009]. And very notably PM and its formation processes have been connected to increased rates of morbidity and mortality due to respiratory and cardiovascular complications ([Mauderly et al., 2008], [Kelly, 2003], [Zemp et al., 1999], [Gauderman et al., 2002]).

PM consists of components such as siliceous crustal minerals, trace metals, inorganic salts, water and carbonaceous (organic) material [Seinfeld et al., 2003]. The sizes of PM particles can vary greatly from as little as 30 angstroms (Å) to several hundred micrometers (µm). Particles with an aerodynamic diameter that is less than 2.5 µm are referred to as “fine” or PM_{2.5}; and those that are greater than 2.5 µm in diameter are referred to as “coarse”. Particles of different sizes usually have different compositions, removal processes from the atmosphere, optical properties and interactions in the respiratory tract; with the smaller PM_{2.5} particles being responsible for more of the adverse effects of PM listed above ([Seinfeld and Pandis, 2006], [Gauderman et al., 2002]). The organic fraction of PM and the smaller sized PM_{2.5} particles are of particular interest to atmospheric chemists.

1.1. Organic Particle Components and Secondary Organic Aerosols

The organic particle component category can be further split into two groups: primary organic aerosols (POA) and secondary organic aerosols (SOA). POA particles, usually composed of black (or elemental) carbon, are directly emitted into the atmosphere and can be formed from things like: biomass burning, combustion of fossil fuels and biological materials [Hallquist et al., 2009]. SOA is formed when volatile organic compounds (VOC) are emitted from either biogenic (e.g. plants, soil microbes, oceans) or anthropogenic sources (e.g. vehicle exhaust, industrial solvent use, landfills).

VOC emission estimates tend to vary greatly ([Guenther et al., 2000], [Atkinson, 2000]) but in general biogenic sources contribute to at least two thirds of total emissions [Cao and Hewitt, 1999]. In the atmosphere VOC can undergo photolysis or oxidation by oxidants such as O_3 and hydroxyl (HO) and nitrate (NO_3) radicals [Kansal, 2009]. The products of these VOC oxidation reactions can vary in volatility; those that are volatile remain in the gas phase, non-volatile stay in the particle phase and semi-volatile partitioning between the two phases. The non-volatile and semi-volatile products contribute to the organic fraction of PM by either forming new particles through nucleation or by condensing onto existing particles [Seinfeld et al., 2003]. A schematic of the process of SOA formation can be found in **Figure 1.1**.

Gas-particle partitioning depends on a variety of factors including semi-volatile compound structure and particle affinity, as well as, atmospheric conditions (e.g. NO_x (nitrogen oxide species; usually NO or NO_2)) levels and relative humidity ([Mauderly et

al., 2008], [Hallquist et al., 2009]). SOA tends to form the smaller and more harmful PM_{2.5} particles [Seinfeld and Pandis, 2006].

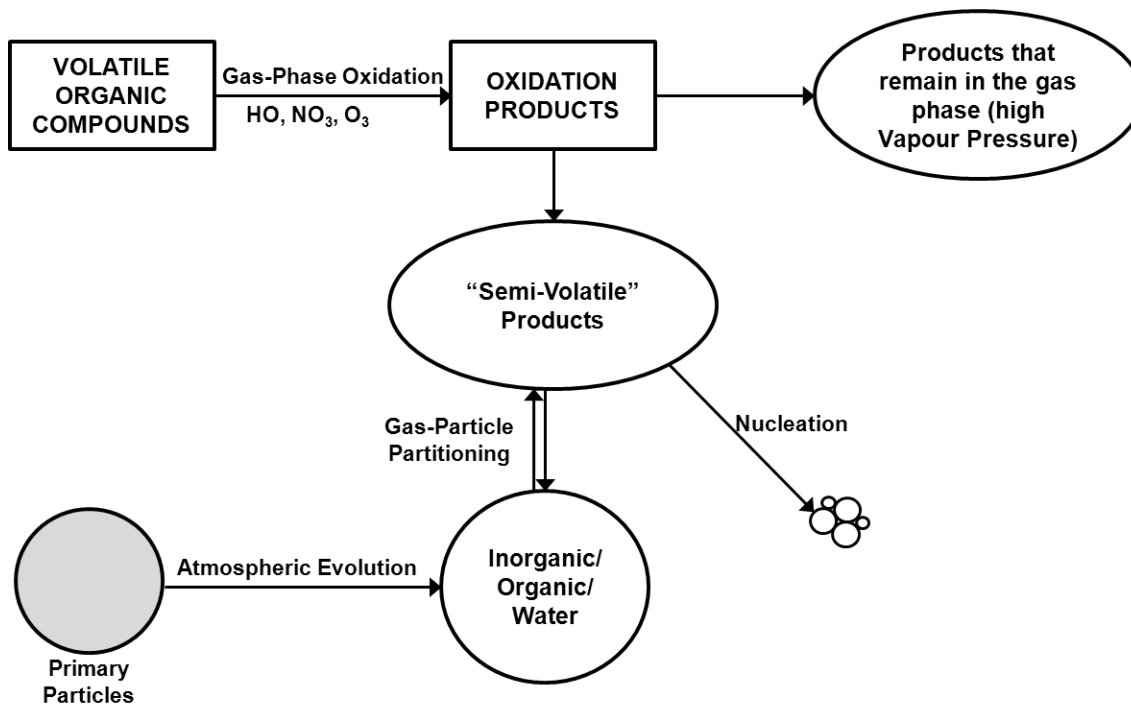


Figure 1.1 A schematic of secondary organic aerosol (SOA) formation (Figure adapted from: [Seinfeld et al., 2003])

There has been 10 000 to 100 000 of different VOC measured in the atmosphere [Hallquist et al., 2009]. Some of these VOC can undergo a number of transformation processes that lead to the production of SOA [Hallquist et al., 2009], thus it is important to gain knowledge into the formation mechanisms, as well as, composition and physical/chemical properties of SOA. This would help with the continuing task of compiling more detailed emission inventories of sources (VOC) and products (SOA) [Cao and Hewitt, 1999]; which would be valuable in tackling regulatory issues, as well as

modeling atmospheric transformations and fate of VOC and their products [Grosjean et al., 1993].

1.2. SOA Components Measurement Techniques

There are several types of instrumentation that can be used to measure SOA component and these can be broadly divided into offline techniques which require sample collection/preparation prior to analysis and online techniques which can acquire samples in-situ.

1.2.1. Off-Line Measurement Techniques

1.2.1.1. Sample collection and Handling

Off-line measurement techniques require the analyte sample to be collected in some kind of vessel or medium and go through processing (e.g. solvent extraction) and/or pre-concentration steps prior to being analyzed by a designated instrument. In one of the sample collection approaches, special filters (coated or uncoated) are fitted onto air samplers [McMurry, 2000]. Analytes to be analyzed from filters can be recovered through the use of solvent extraction or by thermal desorption. There are several issues associated with filter sampling; which include: volatilization of sampled semi-volatile compounds due to pressure drops in the sampler, adsorption of gases [Cadle et al., 1983], and evaporative losses during transport or storage [Wang et al., 1988].

Another technique is sampling VOC onto solid, adsorbent filled tubes (cartridges). They have the advantage of being compact and light, as well as, come in a variety of adsorbents (e.g. Tenax, silica gel and activated charcoal) depending on the

target compounds. However, this technique also has its disadvantages including: low capacity for polar VOC, chemical reactions (e.g. with O₃) and sample decomposition during sampling or thermal desorption [Cao and Hewitt, 1999].

The last sample collection technique discussed here is the use of a diffusion denuder [Possanzini et al., 1983]. These apparatuses have the ability to collect both gas and particle phase compounds separately. The separate collection is based on the different mobility of gases and particles in the gas phase. A laminar flow is drawn through a narrow assembly of tubes and the gases diffuse to coated walls; while particles pass through the tube onto a filter [Warneck and Williams, 2012] [Warneck and Williams, 2012]. This technique can have some issues with choosing the right coating and the avoidance of artifacts found due to sample-compound reactions with the coated denuder surfaces [McMurry, 2000].

1.2.1.2. Off-line Instrumentation

After the collection of material with one of the techniques described in **Section 1.2.1.1**, several instruments can be used for analysis. The most popular off-line analysis techniques are ones that are based on chromatographic separation principles. The first is the use of gas chromatography (GC) with a variety of detectors including: flame ionization detection (FID) and mass spectrometry (MS). GC separates analytes based on the principle of selective adsorption to material coated on the walls of a capillary column or its packing (the stationary phase) [Warneck and Williams, 2012] with analytes travelling through the column in a carrier gas flow (mobile phase). There are advantages to this method which include good sensitivity, low detection limit and a wide variety of

available column coatings which allow for the separation of a various number of compounds [Badjagbo et al., 2007].

The second technique is liquid chromatography, commonly: ion exchange (IC) or high-performance liquid chromatography (HPLC). IC usually uses a conductivity detector, while HPLC uses an optical detector. Similar to gas chromatography, these instruments separate compounds by temporary adsorption to a solid material (neutral for HPLC and charged in IC) on the column, but in this case material not adsorbed passes through the column in a liquid medium. HPLC is good for neutral, polar compounds and IC is useful for compounds that can be charged, such as organic acids and bases ([Warneck and Williams, 2012], [Hallquist et al., 2009]).

While both chromatographic instruments are still widely used, they mostly provide compound detection and quantification rather than molecular characterization. They also can only adequately detect select categories of compounds depending on the column or solvent used, missing valuable information that could be useful considering the wide variety of VOC. Their requirement for sample preparation prior to analysis also leaves room for contamination and sample loss, in addition to giving them very limited temporal and spatial resolution [Hallquist et al., 2009].

1.2.2. On-Line Measurement Techniques

On-line measurement techniques have the advantage of being able to do real-time, continuous monitoring of VOC and SOA; providing good temporal and spatial resolution. They also have reduced chance of sample contamination and loss, since sample

introduction is done with little or no preparations. The most widely used on-line measurement technique is mass spectrometry. Mass spectrometry is a technique that can offer high sensitivity, selectivity and speed [Gross, 2010]. It generally involves the ionization of analyte(s), separation of the analyte ions or their fragments by mass or mass-to-charge and finally detection. Separation is usually achieved by a suitable combination of electric and/or magnetic fields [Warneck and Williams, 2012].

An emerging mass spectrometry technique is aerosol mass spectrometry (AMS) which combines thermal desorption of aerosol components, followed by ionization using electron impact (EI) of the desorbed components and ion mass/charge separation usually done with a time of flight (TOF) mass analyzer [Jayne et al., 2000]. This technique does offer the advantage of sampling compounds in their aerosol form, as well as, superior resolution. However, the output information is mostly limited to the bulk composition of the aerosol with very little to no information on the individual organic species analyzed [Hallquist et al., 2009].

Two techniques that can be used to study VOC composition that do offer some individual compound characterization are: proton transfer reaction (PTR) and atmospheric pressure chemical ionization (APCI) mass spectrometry ([Lee et al., 2006], [McMurry, 2000]). They are both soft chemical ionization techniques, so commonly original molecular ion information can be retained. APCI is frequently used with quadrupole and ion trap mass analyzers ([Jost et al., 2003], [Warscheid et al., 2001]). While PTR-MS often uses quadrupole and TOF mass separation [Blake et al., 2009]. APCI forms ions through proton exchange reactions: proton transfer for positive ions and

proton abstraction for negative ions; with charge transfer to create molecular ions also a possibility. PTR as the name implies, creates ions through proton transfer with compounds that have a higher proton affinity (PA) than water [Hoffmann et al., 2002]. These techniques are also not without flaws, unless used in conjunction with a TOF mass analyzer that aids with elemental composition; they have difficulty distinguishing between isobaric/isomeric species. Furthermore, ion fragmentation, secondary ion-molecule reactions and clustering can occur in the respective ion sources and complicate analysis ([Ambrose et al., 2010], [de Gouw et al., 2003]).

1.3. Studies in the York University Smog Chamber

The York University smog chamber is a 8000L in volume structure that consists of a Teflon bag supported by two Teflon coated aluminum endplates. It is surrounded by a mylar covered frame that supports 24 UVA lights. The chamber's relatively large size decreases the chance of material loss to its walls. Chamber studies, in general are meant to provide a means to develop mechanistic understandings of individual chemical and physical processes that may occur in the atmosphere in a more simplified and controlled environment. Indoor smog chambers, although have the disadvantage of using artificial light, provide more reproducible control of photolytic conditions (light), temperature and relative humidity [Seinfeld et al., 2003].

1.3.1. Previous and Ongoing Hastie Group Studies in the York University Smog Chamber

The studies by the Hastie group in the smog chamber have been used to gain insight into SOA formation by examining the particle characteristics or reaction products

of singular or classes of VOC. Work by Andreea Barbu (2003) and Yael Bienenstock (2001) focused on particle yields and size distributions of aromatic VOC (toluene, meta-xylene and 1,3,5-trimethylbenzene). Janeen Auld's (2009) work dealt with on-line product analysis, time evolution profiles and mechanistic studies of gas phase photo-oxidation products of beta-pinene along with product identification of gas phase toluene products. Mehrnaz Sarrafzadeh (2012) is currently doing work on integrating a counter flow membrane denuder (CFMD) [Ruiz et al., 2006]; which uses the different diffusional properties of gases and particles to separate the two phase. Unlike the denuders mentioned in **Section 1.2.1.1** this one does not use any coatings and therefore does not need subsequent extraction, making it suitable to be incorporated into on-line analysis [Bennett et al., 2009]. Mehrnaz is using this feature of the CFMD to isolate particles formed from beta-pinene/HO reactions to see if these particles can undergo even further oxidation (or aging) with different oxidants (HO and O₃).

1.3.2. This Current Study

All oxidation product analysis from the smog chamber in our group is currently done by APCI-MS/MS (**Section 1.2.2**) ([Auld, 2009], [Sarrafzadeh, 2012]). So far this instrument, with smog chamber experiments, has only been used for qualitative information. The APCI-MS/MS is capable of obtaining quantitative data as shown in studies by Herrera (2008), Jost (2003) and Warscheid (2003). However, its sensitivity has been seen to vary daily or even over the course of an experiment due to the changes in the availability of chemical ionization reagents. It also can show deviations from linear concentration/signal relationships at higher concentrations [Sunner et al., 1988b].

The goal of this current study is to try and develop a method or methods that could be integrated and used in an experimental set-up that involves obtaining quantitative information from the smog chamber using APCI-MS/MS. Quantitative information would allow us to calculate product yields that pertain to our experimental conditions, potentially obtain product distributions in both the gas and particle phase and a better understanding of the instrument's sensitivity toward different classes of compounds.

2. Experimental

2.1. Mass Spectrometry

2.1.1. APCI Source Ion Formation

The air sample entering the APCI source can undergo direct ionization, at atmospheric pressure as long as it is in the gas phase. This source is capable of the production of both positive and negative ions. The ionization process starts off with the formation of a discharge current. The discharge current is a result of an electrical field formed when an electrical potential (~5kV) is applied between the corona discharge needle tip and the curtain plate (see **Figure 2.1**) [Kearle, 1977]. The corona created electrons collide with major components of air to form the ions: N_2^+ , O_2^+ , O_2^- , etc. via electron impact. In addition to the major components of air, water (H_2O) is also present at high amounts in the source. H_2O has a lower ionization potential than the primary ions so the primary ions can undergo charge transfer reactions to form H_2O^+ ions. Due to the high pressure conditions of the ion source the H_2O^+ ions can react with H_2O to form H_3O^+ and various other water clusters ($\text{H}^+(\text{H}_2\text{O})_n$ where $n=0,1,2,3,\dots$) through association reactions [Proctor et al., 1983]. Eventually an equilibrium cluster distribution is achieved of which the various species (different n values) depend on the source H_2O concentration and the preferred stabilities of some cluster species over others [Proctor et al., 1983].

In the ion source, both positive and negative analyte ions can be formed in various ways [Badjagbo et al., 2007]. However, in this study only positive ion formation with a particular reaction was of interest and is discussed here. In this reaction (**Reaction 2.1**) compounds (*CI*) that have a higher proton affinity (PA) than water (696 kJmol^{-1}) or its

water clusters (some listed in **Table 2.1** [Kawai et al., 2003]) can undergo proton transfer with either species to form $((CI+H)(H_2O)_m)^+$ ions. The hydrated molecular ions are usually reduced to the $(CI+H)^+$ ion or a low m value water cluster due to the ions passing through the curtain gas (N_2 (g)) region and the de-clustering potential (DP; DP=8 V in these experiments) applied between the orifice and the skimmer (**Figure 2.1**). CI compounds usually contain electronegative elements such as oxygen, nitrogen or sulphur.

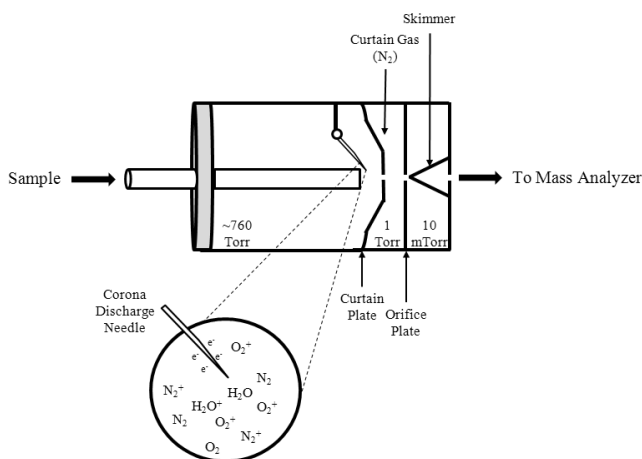
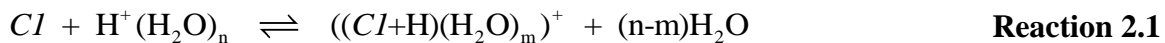
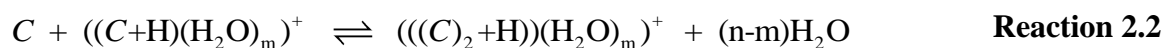


Figure 2.1 APCI Ion source with corona region expanded

Table 2.1 Proton affinities for various water cluster sizes $H^+(H_2O)_n$

Size (n)	Proton Affinity (kJ mol^{-1})
1	696
2	828
3	884
4	915

Clustering reactions are also common in our source conditions. These association reactions can occur due to the formed ions interacting with other species that are present in relatively high amounts in the source. Commonly observed clusters include protonated dimers of the same compound, $((C)_2+H)(H_2O)_m^+$ and are shown in the example in **Reaction 2.2**.



The formed ions then travel towards or away from the curtain plate (based on the chosen positive or negative polarity) under the influence of an electric field and pass through the curtain gas, orifice and skimmer; continuing onto the mass analyzer.

2.1.2. Quadrupole Mass Analyzer

Once the ions are produced in the ion source they need to be separated. In these experiments this separation, according to the ion's mass to charge ratio (m/z) was done using a quadrupole mass analyzer. A schematic of this analyzer is shown in **Figure 2.2a**. The ions leaving the ion source enter the quadrupole set-up in the z-direction. The quadrupole consists of four cylindrical shaped rods with a radius of $r=1.1148r_0$ where r_0 is the radius of the imaginary cylindrical rod that could be inserted in between the four rods (**Figure 2.2b**) [March et al., 1989]. Two pairs of diagonally separated rods are of the same electrical potential while the other two are of opposite potential. This potential consists of both a direct potential (DC) component ($U =$ magnitude DC voltage) and an radio frequency (RF) component ($V =$ amplitude of RF voltage) (described by **Equation 2.1** and **Equation 2.2**; where ω is the angular frequency in radians/sec or can also be

expressed as $2\pi f$ where f is the frequency of the RF amplifier of the mass analyzer (816 kHz in this case)).

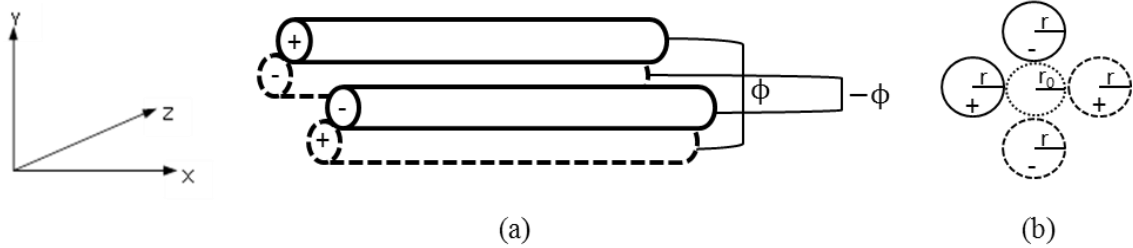


Figure 2.2

- (a) Schematic of the quadrupole mass analyzer with oppositely charged (ϕ) two pairs of rods (see **Equation 2.1** and **Equation 2.2**)
 (b) The radius and configuration of the rods where $r=1.1148r_0$ and r_0 is the radius of an imaginary rod that defines the separation between the four quadrupole rods

$$\phi = +(U - V \cos \omega t) \quad \text{Equation 2.1}$$

$$-\phi = -(U - V \cos \omega t) \quad \text{Equation 2.2}$$

The travelling ion will experience (depending on its charge) attraction or repulsion to the rods as the potential is switched periodically, this way it travels alternately in the xz and yz directions [De Hoffmann et al., 2008]. As long as its motion in these directions does not exceed a distance defined by $2r_0$ the ion will travel in a stable trajectory between the rods and reach the detector (the detector used in our instrument was a channel electron multiplier (CEM) (Photonis, Sturbridge, MA)). Otherwise the ion will either escape the mass analyzer or will be deactivated upon collision with the rods.

The motion of these ions is described by equations that were derived by E. Mathieu in 1866 [Gross, 2010]. The full derivation is not repeated here but the final

results are two functions (a_u and q_u); which define a stable trajectory for a given ion of mass m_i , at certain values of U and V (defined in **Equation 2.3** and **Equation 2.4**). And this is visually depicted by Mathieu diagrams for motion in the x and y directions (**Figure 2.3a**) for an ion of mass m_i . The superimposition of these two individual diagrams shows the stability diagram for this ion in the mass analyzer (**Figure 2.3b**). In this diagram, there are a_u and q_u values for which both x and y simultaneously are found to be stable but in practice only one region (A in **Figure 2.3b**) in which the U and V voltages are reasonably low is normally used [Downard, 2004].

$$a_u = a_x = -a_y = \frac{4eU}{m_i r_0^2 \omega^2} \quad \text{Equation 2.3}$$

$$q_u = q_x = -q_y = \frac{2eV}{m_i r_0^2 \omega^2} \quad \text{Equation 2.4}$$

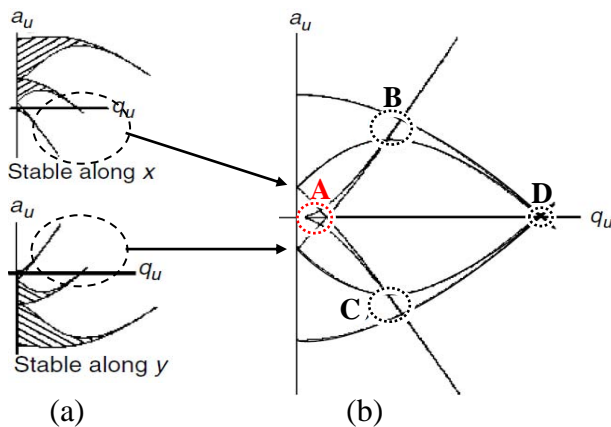


Figure 2.3

(a) Mathieu diagrams for the movement for an ion of mass m_i in the x and y directions as function of a and q ($u = x$ or y)

(b) Superimposed x and y Mathieu diagrams from (a) with 4 intersecting areas (A, B, C and D)

(Adapted from De Hoffmann et al (2008))

In order to obtain a mass spectrum, the mass analyzer scans through a series of a_u and q_u values (within the region A mentioned above) in order to transmit ions of different m/z . This scan is usually done at a constant $\frac{a_u}{q_u}$ (or $\frac{U}{V}$) ratio and can be visually seen in **Figure 2.4** as the “scan line”. Scanning means shifting the whole stability diagram along the scan line as each m/z value has its own unique diagram [Downard, 2004]. In the theoretical example of **Figure 2.4** the stability diagram of ion m_2 intersects with the scan line, which means that it will be transmitted while ions m_1 and m_3 will not be.

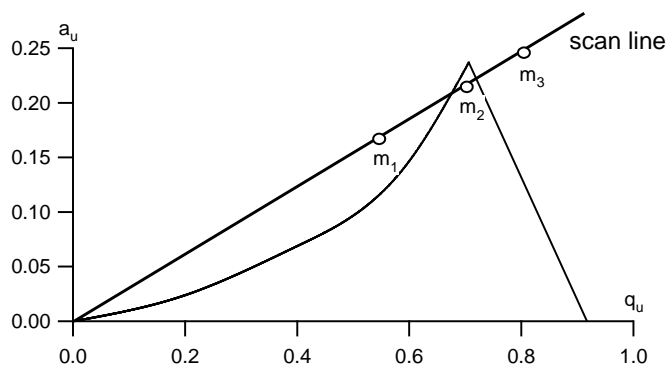


Figure 2.4 Stability diagram of m_1 , m_2 , and m_3 at the given values of a_u and q_u (where $u = x$ or y) and the scan line. Only m_2 follows a stable trajectory to the detector

2.1.3. Triple Quadrupole Mass Spectrometer

The instrument used in this analysis was the API 365 triple quadrupole mass spectrometer (MDS SCIEX, Concord, ON). A schematic of this type of instrument is shown in **Figure 2.5**. It has quadrupoles as described in **Section 2.1.2**; where Q1 and Q3 are usual mass scanning quadrupoles with both DC and RF components, while q_2 is a focusing quadrupole with only an RF component. RF only quadrupoles are used to transmit ions through the analyzer with minimum loss. As seen from **Figure 2.4**, if there

is no DC component, the slope of the scan line is equal to the q axis which means ions of all m/z can pass through [Gross, 2010]. This of course means that if required Q1 and Q3 could also and are used as RF only focusing quadrupoles. This set-up allows the instrument to further investigate ion properties by allowing not only to separate them, but to selectively separate and fragment them further using a process called collision induced dissociation (CID). In the CID used here a collision gas (nitrogen (N_2) (Linde, purity 99.999% +)) was added to the q_2 region. As ions move through this region they may collide with the collision gas molecules and upon this collision some of the ion's kinetic energy may be transferred into internal energy [Downard, 2004]. Usually upon multiple collisions enough energy can transfer to break bonds and fragment the ion into ion fragments that could be detected. In these experiments a collision energy of 10eV was sufficient to use where CID was required. A summary of the scans for the triple quadrupole that were used in these experiments is shown in **Table 2.2**. All masses that were attributed to compounds/ions or as input for scans were the nominal mass; which is based on the sum of the integer mass of the most abundant isotope of each element in the compound/ion and is measured in units of unified atomic mass (u).

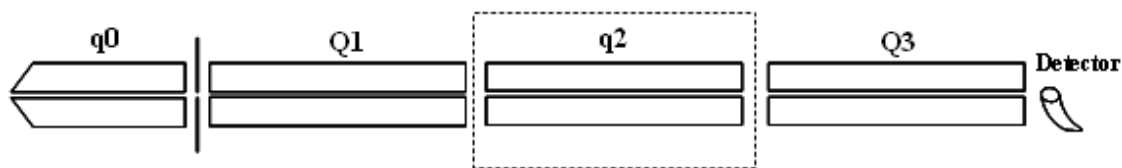


Figure 2.5 Schematic of the triple quadrupole instrument

Table 2.2 Summary of scans used with the API 365 in these experiments

Scan Mode	Operation of Q1	Operation of q2	Operation of Q3
Q1-MS/ Full Scan	Scan all m/z over entire desired mass range	-RF Only	RF Only
MS2/Product Ion Scan	Select one m/z (m_1) i.e. select “precursor”	-RF Only -CID (CE = 10eV)	Scan m/z of all resultant fragments up to the m/z value of m_1 i.e. scan “products”
Selected Reaction Monitoring (SRM)	Select one m/z (m_1) i.e. select one “precursor”	-RF Only -CID (CE = 10eV)	Select only one m/z for desired fragment (m_2) of m_1 i.e. select one “product”

The Q1-MS scan mode is typically used when first working with a particular analyte or set-up as it gives a general idea of the species present. **Figure 2.6a** shows a Q1-MS scan for a standard solution of nopinone (Sigma-Aldrich, purity 99.9% +) with the suspected, compound related peaks labelled.

A product ion scan can provide some insight into the structure or functionality of a specific ion as only the selected ion is fragmented. It can be used for chamber reaction product identification by comparing a product ion spectrum obtained during a chamber experiment and a product ion spectrum or a “fingerprint” obtained from analyzing a sample of a commercial available standard that is suspected to be the identity of the chamber reaction product. Often a commercial standard is not available, so then the m/z of the ion fragments in the product ion scan can help narrow down the functionality and structure of the suspected product. Some examples of common identifying fragments are

listed in **Table 2.3** and one example of an MS2 scan (for the m/z 139 ion) is shown in **Figure 2.6b**.

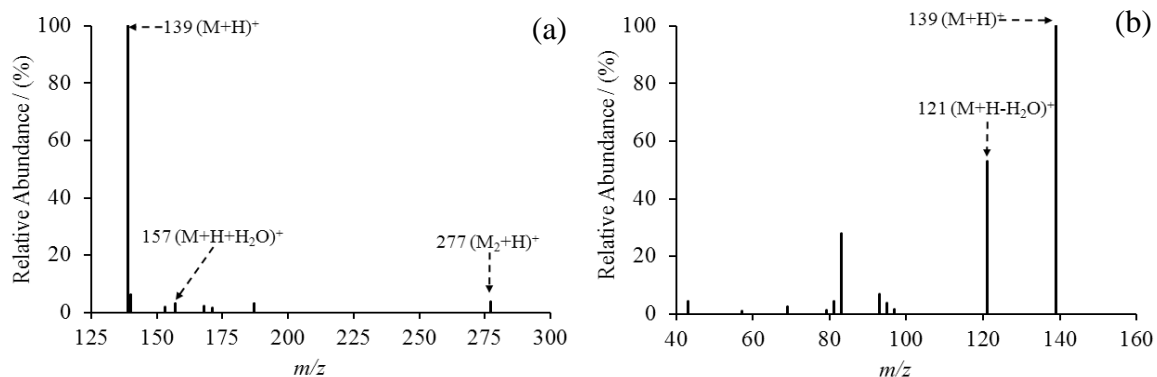


Figure 2.6

(a) Q1-MS/full mass spectrum of pure nopinone (where M=compound of mass of 138 u)
(b) Product ion scan of m/z 139 of nopinone (where M = compound of mass of 138 u)

The SRM scan only monitors a specific pre-cursor/product ion pair (SRM pair) and therefore if the pair is chosen correctly can offer the highest sensitivity toward a particular analyte. Using the help of knowledge gained from Q1-MS and product ion scans, SRM pairs were assigned to chamber reaction products. These SRM pairs were used to monitor products over the course of a chamber experiment; creating experimental time profiles. The SRM time profiles assist with product characterization through comparison of time profiles between products.

Due to the above mentioned high sensitivity, the SRM signal for analytes was used in generating calibration curves. The SRM pairs used for nopinone are shown in **Table 2.4** while pairs for other analytes are shown in **Appendix A (Table A.1)**. Often as seen for the nopinone SRM pairs, multiple pairs were followed for compounds in order to

be able to choose the best one in case a suspected interfering contaminant was present. The SRM signal reported in the calibration curves was an average of 1-10 min of stabilized SRM signal.

Table 2.3 Fragmentation pattern examples

Clues	Fragment m/z	Suspected Fragment Identity
oxygen presence	-18	H ₂ O
carbonyl group	-28	CO
nitrate group	-46	NO ₂
	-63	HNO ₂
odd number(s) of nitrogen(s) even m/z		
alkyl chain	-14	CH ₂

Table 2.4 SRM pairs followed for nopinone calibrations (CE 10)

Nopinone Pairs (M= nopinone with nominal mass of 138 u)		
m/z of precursor/product ion pairs	Mass loss (u) from precursor	Suspected identity of the observed precursor ion and its mass loss
139/121	-18	(M+H) ⁺ with (1 x H ₂ O) loss
157/139	-36	(M+H ₂ O+H) ⁺ with (1 x H ₂ O) loss
157/121	-18	(M+H ₂ O+H) ⁺ with (2 x H ₂ O) loss
277/139	-138	(M ₂ +H) ⁺ with (1 x M) loss

2.2. Calibration Approaches

2.2.1. Syringe Pump Calibrations

The set-up used for syringe pump calibrations and their results will be further discussed in **Section 3.3.1**. But in general the sample introduction was as shown in **Figure 2.7**. Where the analyte standard is in its pure form or dissolved in methanol or water (H₂O) was introduced in liquid form using a 1, 5 or 10µL syringe mounted on a syringe pump (Harvard Apparatus, Holliston, MA). The liquid syringe output entered an air stream of purified air from an Aadco clean air generator (Aadco Instruments Inc., Cleves, OH). Provided the compound/solution was of sufficiently high volatility at room temperature or if the set-up was heated to accommodate lower volatility compounds the output of the airflow contained the sample in its gas form. Changing the syringe pump flow rate or air flow varied the analyte concentration at the output. The sample was diluted downstream to further change the concentration. The gas phase analyte concentration (ppm) calculations are as outlined in **Appendix B**. The concentrations stated/calculated are estimated to have an error of 10-15% due to errors in factors such as the syringe volume, syringe pump rate, Aadco flow rate, operator error, etc.

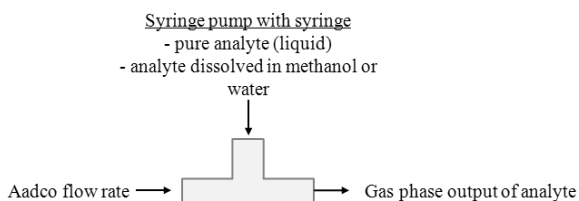


Figure 2.7 Schematic of syringe pump sample introduction

2.2.2. Exponential Dilution Flask Calibrations

The exponential dilution flask (EDF) calibration technique was first developed by Lovelock in 1961. It involves a known amount of analyte or mixture of analytes being introduced into a flask, allowed to mix or assumed to be mixed instantaneously and then through the introduction of a controlled flow of dilution gas into the flask, have the output concentration of the flask decline in an exponential manner [Greenhouse et al., 1990]. This is a widely used technique for medium/high volatility compounds that are sampled by a gas detector; which is thought to be appropriate for many of the analytes sampled in this study. It is convenient since it can generate a large number of concentration values with a single analyte(s) injection. This reduces the analysis time as well as decreases systematic error [Inman et al., 1982].

The set-up can take many forms but the one used in this study is shown in **Figure 2.8 a,b**. The sample was introduced into an Aadco air flushed, 5 Litre, 3-neck round-bottom flask, via an injection of 0.025-0.1 μ L of sample using a 0.5 μ L syringe (Hamilton Company, Reno, NV) through a septum. The sample was allowed to mix isolated from any diluent gas flow for at least 15 min (**Figure 2.8a**) and then the 4-way valve was switched (**Figure 2.8b**) to allow for the diluent gas to flow into the flask and provide an exponentially decaying analyte concentration at its output. A magnetic stirrer was used in order to encourage uniform mixing of the analyte in the flask using turbulent flow in addition to the normal gas phase diffusional mixing the sample undergoes [Ritter et al., 1976].

Knowing the initial concentration (C_0) in the flask (calculation is similar to the syringe pump concentration calculations in **Appendix B**) and obtaining a signal that is linearly proportional to sample concentration, then at any time (t) (where t is time after the diluent gas is introduced into the flask) the sample concentration (C) can be calculated using **Equation 2.5**. Low concentration values were required for the calibrations so the output of the flask was further diluted prior to entering the APCI source by a flow of humidified air through a water bubbler, as well as, another Aadco air stream. As with the syringe pump calibrations (**Section 2.2.1**) concentrations stated/calculated were estimated to have an error of 10-15%.

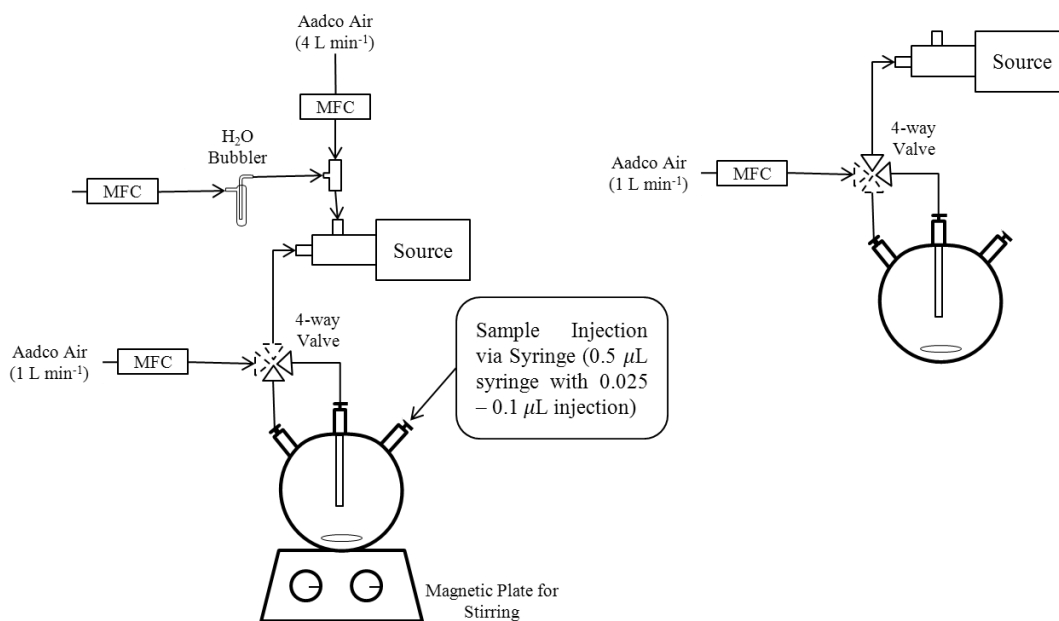


Figure 2.8 Exponential dilution flask set-up

- (a) sample introduction into the flask and a minimum 15 minutes of mixing time
- (b) the same set-up as in (a) with the 4-way valve switched in position to allow for flow of dilution gas into flask and output for source sampling

$$c = c_0 \exp^{-\frac{t}{\tau}}$$

Equation 2.5

where $\tau \equiv \frac{\text{volume of the flask (L)}}{\text{flow of the diluent gas through the flask (Lmin}^{-1})} = \frac{V}{Q}$

2.2.3. Beta-Pinene Permeation Tube Calibrations

The beta-pinene concentration was measured since it was necessary in order to be able to obtain product yield measurements. Unfortunately, this compound shows low sensitivity with the APCI-MS/MS so it was not optimal to measure it with that instrument. Instead the beta-pinene concentration was monitored by GC/FID using a Hewlett Packard 5890 Gas Chromatograph (GC), equipped with a non-polar Supelco SPB-1 capillary column (30m×0.53mm×0.5µm film) and a flame ionization detector (FID). This instrument was calibrated against a standard generated by diluting the emission from a beta-pinene (Aldrich, purity 99%) containing permeation tube (KINTEK, La Marque, TX) using a varying Aadco air flow. The 7.5cm long sealed Teflon permeation tube was stored in a temperature-controlled, insulated housing. The permeation tube emits beta-pinene at a constant rate if held at one temperature. The temperature used was (100 ± 0.1°C); monitored by a CN9000A temperature controller (OMEGA, Laval, QC). The permeation rate was determined by weighing the permeation tube every few months and determining its mass loss. The average permeation rate was found to be 75 ng min⁻¹. A low flow (15 ml min⁻¹) of N₂ (Linde, purity 99.999% +) was used to sweep the emitted beta-pinene from the tube toward the GC-FID, and through the Aadco dilution air flow. A schematic of this permeation tube calibration set-up is shown

in **Figure 2.9** and an example of a result from this type of calibration is shown in **Figure 2.10**.

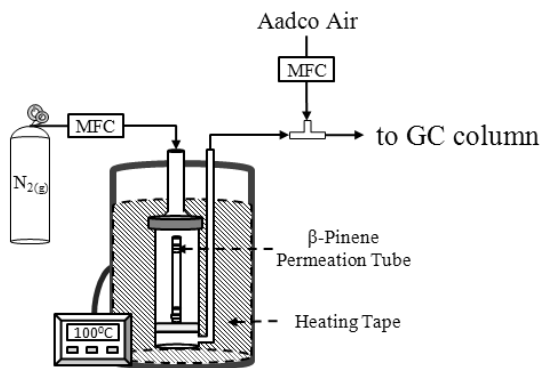


Figure 2.9 Schematic of beta-pinene permeation source set-up for calibration by GC-FID

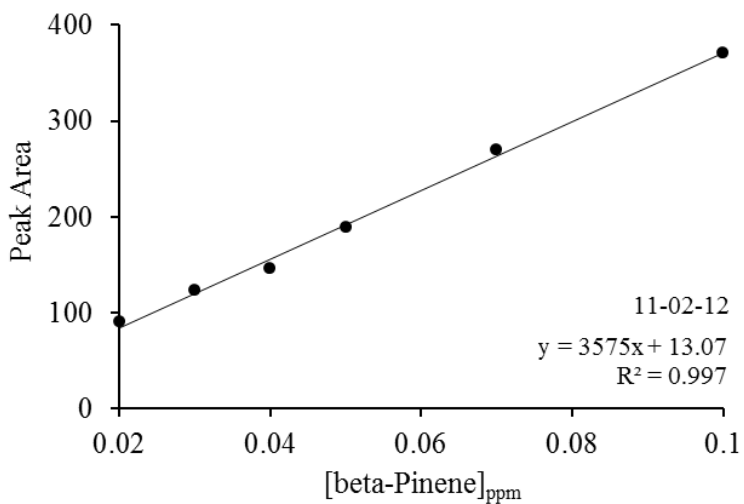


Figure 2.10 beta-Pinene GC-FID calibration

2.3. Smog Chamber Experiments

2.3.1. The Smog Chamber

Experiments for the photooxidation reaction by HO (hydroxyl radicals) of beta-pinene were done in the York University smog chamber. The cylindrical smog chamber is 8m³ in volume and has transparent Teflon walls and two Teflon coated aluminum endplates. The outside is a mobile frame covered with Mylar. To the inside of the frame, 24 ultraviolet lights with a radiation window of 350-400 nm (Philips F40BL, 40 Watt) are attached. Reagent injections were done in the endplate that is opposite to sampling with an internal fan to aid the mixing of the chamber contents. Reagents were allowed to mix at least 60 minutes prior to initiation of the reaction. Withdrawal of air for instrument sampling was balanced by a continuous supply of Aadco air. Between experiments, which were done at least 24 hours apart, the chamber was flushed with 30 L min⁻¹ of clean air. Since the desire was to keep conditions fairly consistent between experiments, the temperature and relative humidity of the chamber were monitored before and during experiments using an Omegaette HH311 humidity and temperature meter (OMEGA, Laval, QC). The temperature over the course of the experiment started at 24⁰C (lights off) and rose to as high as 30⁰C (lights on); the average relative humidity was 11% (profile in **Appendix C (Figure C.1)**). A schematic of this set-up is in **Figure 2.11** and the experimental procedure is summarized in a scheme in **Figure 2.12** as well as further discussed in **Section 2.3.2**.

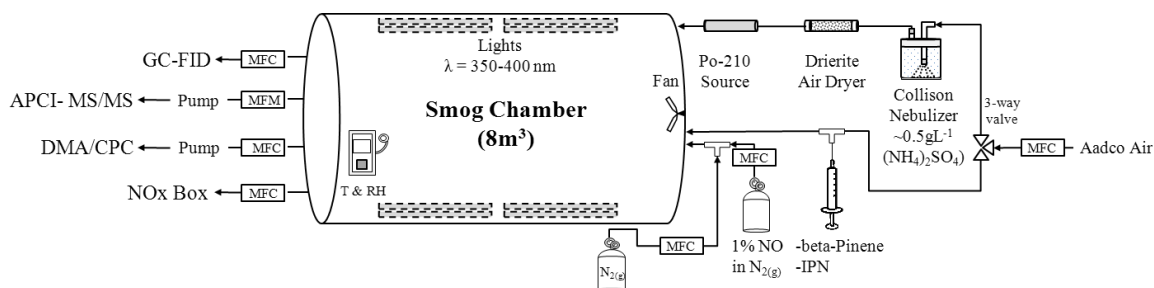


Figure 2.11 Schematic of smog chamber experimental set-up

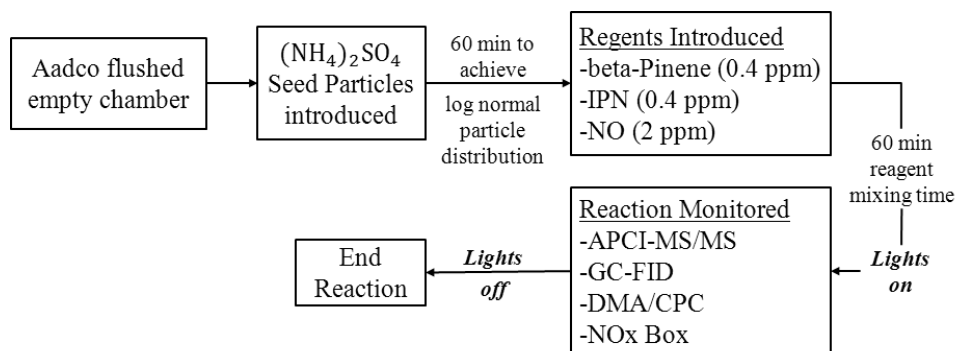


Figure 2.12 Schematic of experimental procedure in the smog chamber

2.3.2. Reagent Information

2.3.2.1. Chamber Seeding

The experiments here were done in the presence of inorganic seed particles. In these seeded experiments, particle growth was primarily through condensation; which was the growth mode that was found to give the most reproducible chamber data [Bienenstock, 2001]. The seed particles were generated by passing Aadco air through a Collision nebulizer (BGI, Waltham, MA) containing a 0.5 gL^{-1} solution of ammonium sulphate $(\text{NH}_4)_2\text{SO}_4$ in water. The formed particles were then passed through a calcium sulphate

drier to reduce their humidity. Before the particles entered the chamber they also passed through a Po-210 charge neutralizer to decrease losses that may have occurred due to highly charged particles interacting with transfer lines and chamber walls. The particle size distribution (**Appendix C (Figure C.2)**) was monitored by combining the mass discerning, differential mobility analyzer (DMA) (TSI, Shoreview, MN) and the particle counting ability of a condensation particle counter (CPC) (TSI, Shoreview, MN). Prior to the introduction of other reagents, the particles were allowed to stabilize in the chamber until a log normal particle size distribution was achieved (approximately 60 minutes).

2.3.2.2. HO Radical Production and Concentration Estimation

Isopropyl nitrite ((CH₃)₂CHONO) (IPN), that was synthesized in-house using a modified version of the method used by Noyes (1936), was used as the HO radical source. The HO radicals were generated upon photolysis of IPN that was initiated by the chamber lighting system as described in reactions **Reaction 2.3**, **Reaction 2.4**, and **Reaction 2.5** below:



The turning on of the chamber lights and therefore the start of HO production in the presence of beta-pinene initiated the reaction. The actual HO concentration obtained from these reactions was estimated using the rate of beta-pinene depletion. The depletion could be measured using the calibration data from the GC-FID as outlined in **Section**

2.2.3. It was observed that for at least the first 30 minutes of the reaction, a plot of \ln ([beta-pinene]) vs. time (**Figure 2.13**) is linear. In these 30 minutes the reaction is assumed to be pseudo first order due to an approximately constant HO radical concentration and therefore the slope of the plot of this data represents the pseudo first-order rate constant: $k_{HO}[HO]$. Knowing the rate constant (k_{HO}) for reaction of HO with beta-pinene ($7.43 \times 10^{-11} \text{ cm}^3 \text{ molecule}^{-1} \text{ s}^{-1}$) ([Atkinson, 1997]) it was then possible to estimate the HO concentration using **Equation 2.6**. Based on the experimental conditions here the HO concentration estimated from this method was found to be 0.1 ppt.

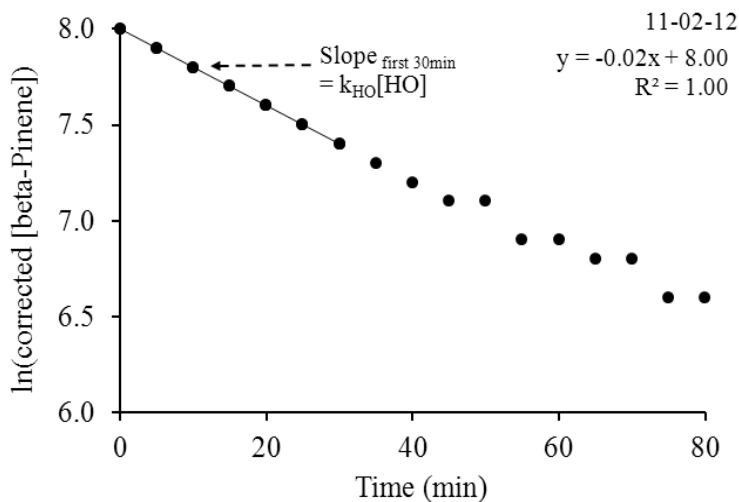


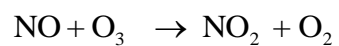
Figure 2.13 \ln [beta-pinene] vs. time plot and HO concentration estimation from the first 30 min of the reaction profile

$$\frac{d[\text{beta-pinene}]}{dt} = (\text{slope}_{1\text{st}30\text{ min}}) \times [\text{beta-pinene}] = k_{HO}[HO][\text{beta-pinene}] \quad \text{Equation 2.6}$$

Since the desire was to focus on the yield due to HO radical oxidation, 2 ppm

Nitric oxide (NO) (1%NO/N₂, Air Liquide) was injected in an effort to suppress ozone

(O₃) (**Reaction 2.6**) that may form from NO₂ photolysis as the experiment proceeds. The concentration of NO gas injected was monitored by a 42S Chemiluminescence NOx Analyzer (TE Inc., Franklin, MA) (example profile in **Appendix C (Figure C.3)**).



Reaction 2.6

3. Results and Discussion

3.1. Initial API 365 Experiments with the Smog Chamber

Any quantification attempt with the APCI-MS/MS for beta-pinene/HO would need to incorporate previous knowledge from qualitative analysis done by Auld (2009). This previous analysis dealt with both the gas phase sample introduction into the APCI-MS/MS as well as identifying suspected products of the beta-pinene/HO reaction done in the smog chamber with the same instrument. This previous work was done on a TAGA 6000E (MDS SCIEX, Concord, ON) while in this study the API 365 was used (**Section 2.1.3**). Both instruments are previously described, (**Section 2.1.3**) triple quadrupole instruments with an APCI ion source (**Section 2.1.1**). The switch was made to the API 365 since it is a more user friendly, modern, and compact instrument. From empirical evidence when comparing the two instruments, the API 365 also had a higher signal to noise ratio and therefore sensitivity. It also has the ability to scan at least 30 SRM pairs in one experimental time period versus only 8 in the TAGA 6000E, so more ion pairs can be followed on the same timescale and with less user intervention. To build on the previously gained knowledge from the TAGA 6000E, experiments had to be duplicated to see if any adjustments needed to be made in the newly employed API 365 instrument.

3.1.1. Sampling Problems

When comparing the API 365 and TAGA 6000E instruments, two sampling related problems were seen: the first was an unsealed ion source and the second was adsorption due to a Teflon filter that was used during gas phase chamber sampling.

3.1.1.1. Unsealed Ion Source

The major problem was that the APCI ion source for the API 365 was very poorly sealed and therefore not isolated from the room environment. The problem was discovered when it was found that the input and output flow rates at the ions source (**Figure 3.1**) were not balanced. This was especially evident when input into the source was dependent on the amount of air flow being pulled by a pump placed at the ion source exhaust. In these instances the amount of air pulled into the source was significantly lower than the pump flow rate; indicating a leak. This caused several problems. The first was contamination, as room air component peaks (e.g. from acetone) were seen in large amounts in the mass spectrometer; interfering with experiment relevant peaks. The second problem was that since the main goal of this study was to develop calibration methods it was important to have a proper idea of all the input and output flows at the source to have an accurate picture of the analyte concentration going into the mass spectrometer.

The source of the leak was investigated. It was tested by pulling air from the ion source exhaust using a pump at various flow rates that were controlled using a mass flow meter (MFM). The resultant input, which was from the smog chamber, into the source was tracked using a magnehelic pressure drop flow meter. It was very difficult to get any flow from the chamber at lower flow rates but sampling could be achieved at higher pump rates. However, as seen in **Table 3.1** the sampling that was obtained from the chamber was still smaller than the leaking air flow.

Table 3.1 The unaccounted flow rate from the leak in the APCI ion source when different exhaust pump rates were applied

Pump at Source Exhaust (L min⁻¹)	Flow Rate from Chamber (L min⁻¹)	Unaccounted for Flow (L min⁻¹)
18.3	5.8	12.5
14.9	5.2	9.7
10.6	4.6	6

The source of the leak was carefully explored. It was initially thought that the source of the leak must have originated at the ion source; in either its seal to rest of the instrument or at various input/output points. This was thought because this was the only piece that was removed with any regularity and whose seals would be subject to wear and tear. However, after extensive leak testing at the source it was found that it could not have been the cause of the leak.

The cause of the leak was found by greatly over-pressurising the source with input of air and physically feeling for escaping air. The problem was determined to be a completely un-sealed area that surrounds the curtain plate and proceeds on through to the interface region. In this region there are various points for air to exchange with the lab environment. This area is shown schematically in **Figure 3.1** and more visually in **Figure 3.2**. The cause of this defect was not initially apparent but further prodding into the origin of the instrument revealed that the area was intentionally left unsealed by the manufacturer. This was because the instrument was initially designed to be used with an electrospray ionization (ESI) ion source.

In electrospray ionization, a dilute solution is pumped through a small metal capillary at a very slow flow rate ($\mu\text{L min}^{-1}$), as liquid emerges from the capillary it experiences forces from an electric field due to voltage applied at the capillary tip and the orifice plate. The process of the liquid emerging from the capillary and transforming into a finer mist as ionization proceeds is assisted with a nebulizing gas (usually nitrogen) [Harris, 2006]. The interface region in the API 365 was intentionally left unsealed to allow exchange with lab air so that this nebulization gas can escape and prevent over pressurization of the source without the need of additional controls.

Sampling with the APCI source, specifically where analyte movement in the source is very dependent on airflows rather than an electric field as with ESI was not the original intention of the instrument. This is in contrast with the source in the TAGA 6000E instrument; which was designed for the purpose of trace gas analysis (TAGA = Trace Atmosphere Gas Analyser) [Perkin Elmer Sciex] and was more originally suited for this type of sampling. Modifications needed to be done to the API 365 source so that it could be used for the purpose of gas analyte sampling in the manner required for our experiments.

The modification and long term solution for this leak problem was the placement of an EPDM rubber sealing cord (Able O-Rings and Seals, North York, ON) tucked in tightly in the gap between the stainless steel housing and the adjacent Teflon component ((*) in **Figure 3.2**). This greatly reduced the leak to less than 0.8 L min^{-1} overall; which was found to be an acceptable range and reduced the contamination from the room air that was seen in the mass spectrum.

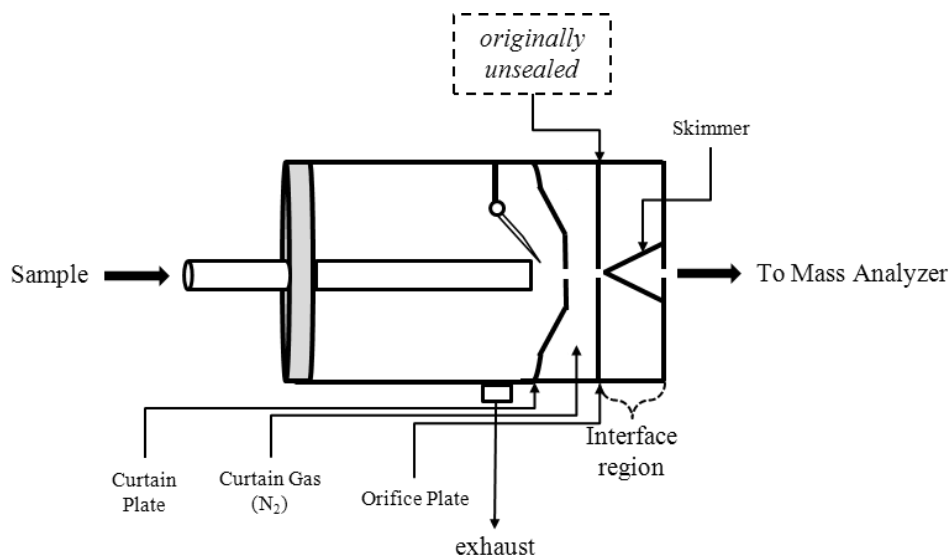


Figure 3.1 Schematic of the APCI ion source and adjacent areas; with the originally unsealed region leading to the interface region

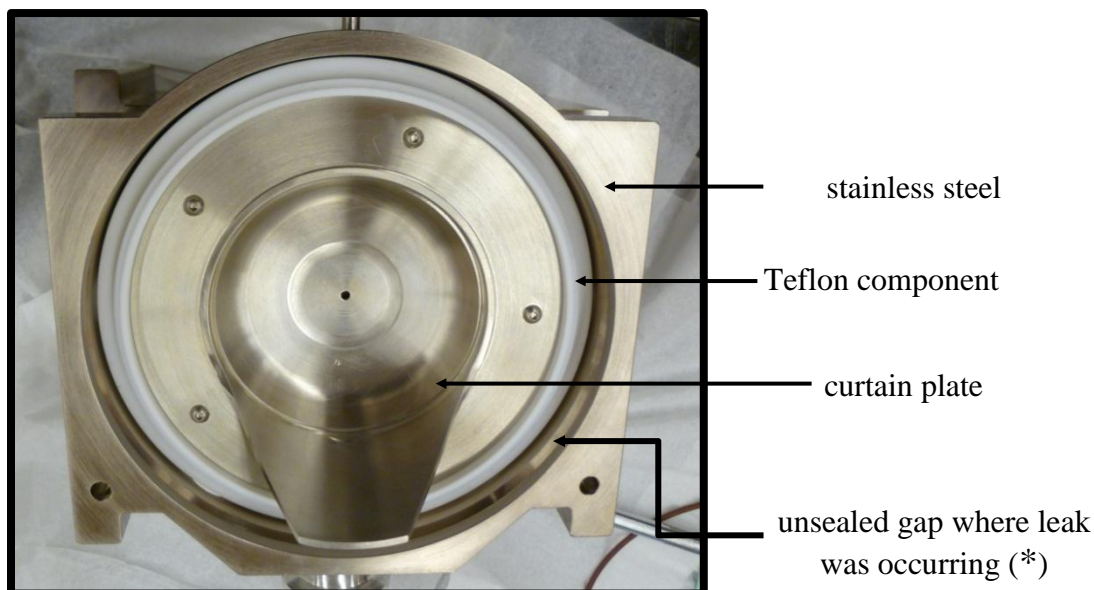


Figure 3.2 Front face view of curtain plate which leads into the de-clustering/curtain gas region which is followed by the interface region (this is also the attachment point of the source). (*) region where EPDM rubber cord was placed

3.1.1.2. Filter Adsorption During Gas Phase Sampling

During and after the testing for the API 365 leak problem, another sampling problem was discovered. This sampling problem had to do with the in-line 25mm diameter quartz fiber filter (PALL (Canada) Ltd, Toronto, ON). It was found that in previous (TAGA 6000E) APCI-MS/MS chamber experiments the filter was in place during gas phase sampling to ensure isolation of the gas from the particle phase. During the API 365 experiments the filter was removed when the source leak problem was a factor; this was done to reduce airflow resistance during sampling from the chamber. It was found that the SRM profiles with the filter consistently had time delays before a detectable signal change was seen over the course of a beta-pinene/HO chamber experiment. While with the no filter sampling, in most cases, the time delay was negligible. Examples of these two observations are shown in **Figure 3.3** for nopinone (**a**) and hydroxyl nopinone (**b**). For these examples, SRM profiles were obtained during a sample beta-pinene chamber experiment with air flow sampled by the APCI-MS/MS that either went through the filter or bypassed it. The selection of the mode of air flow was done by manually switching a 3 way valve every 2.5 minutes over the course of the experiment (set up in **Figure 3.4**).

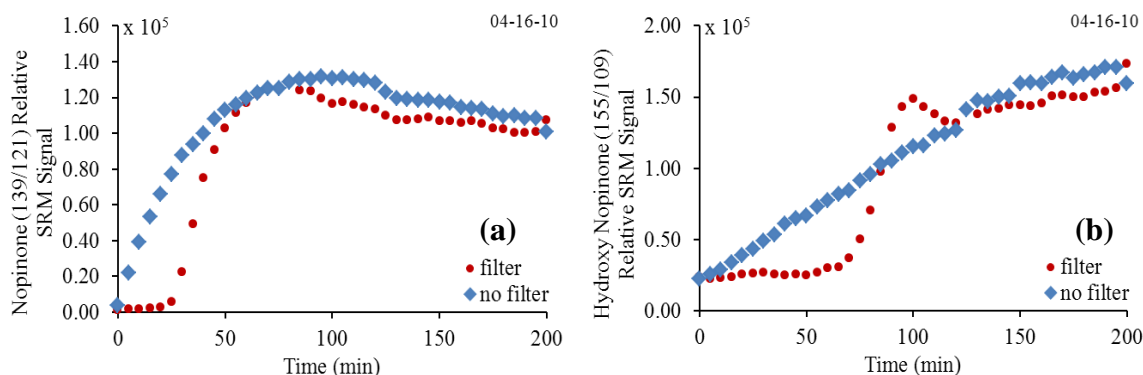


Figure 3.3 SRM time profiles with and without a filter in the sampling line for (a) nopinone (m/z 139/121) and (b) hydroxy nopinone (m/z 155/109)

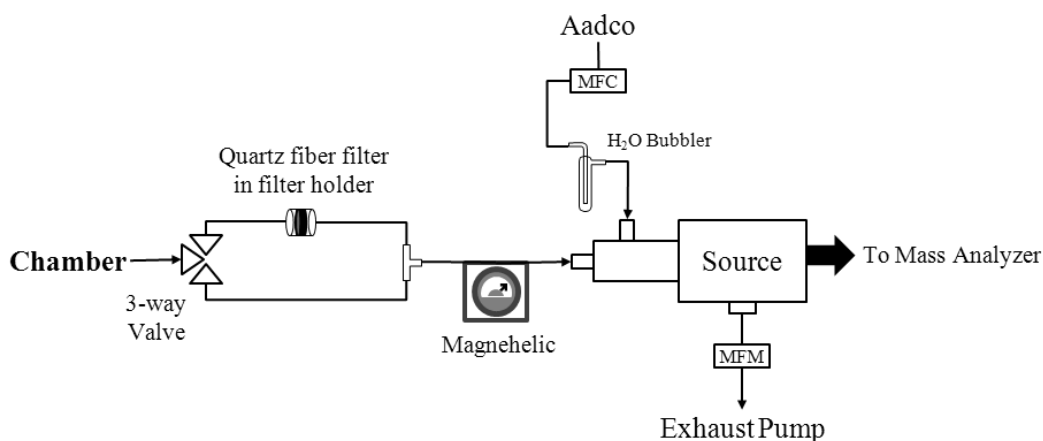


Figure 3.4 Filter and no filter sampling over the course of a beta-pinene/HO chamber experiment

Quartz fiber filters are often used in atmospheric sampling due to their high particle collection efficiency and low cost however there are two main artifacts that may occur when using quartz filters. The first is the adsorption of organic gases onto the filter and the second is evaporation of particulate matter during sampling [Kirchstetter et al., 2001]. The adsorption case may be used to explain the observed delay in SRM time profile on-sets. If adsorption is occurring then the gas products will adsorb until the

filter is saturated at which time the gases can pass through the filter and continue on to the ion source. The evaporation case is an unlikely reason since there are immediate onsets in the absence of the filter, indicating an initial presence of gas phase products.

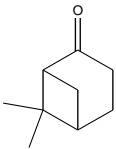
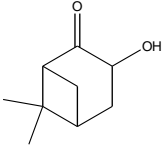
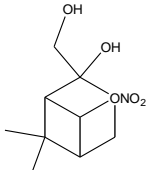
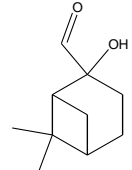
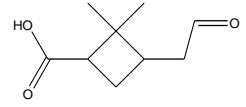
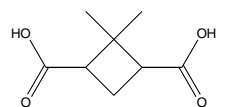
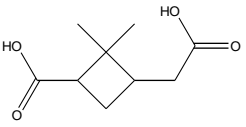
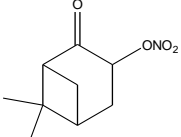
With the filter adoption interfering with getting an accurate picture of the SRM time profiles, all subsequent chamber experiments were done without the filter in place. It was decided that since the APCI source can only sample analytes in the gas phase; that the lower vapour pressures of particle phase products would be sufficient enough to separate the two phases as long as sampling was done at room temperature.

3.1.2. Product Identification Comparison between the TAGA and API Instruments

After the source was sufficiently sealed and mode of gas phase sampling from the chamber was finalized; the API 365 was tested for its ability to detect some products already identified by the TAGA 6000E. Q1-MS, product ion and SRM scans were used to identify products. A detailed description of these products is found in [Auld, 2009], but a select list of products is in **Table 3.2** below. All seven (not counting isomers) of the tested products were seen by both instruments and were confirmed either by fingerprint comparison, fragmentation pattern analysis or with help from their SRM time profile(s).

With the incorporation of the API 365 instrument with chamber sampling, as well as, the re-acquisition and comparison of key qualitative data from previous work done on the TAGA 6000E, further elements of the beta-pinene/HO chamber reaction could be explored. One such element is to gain quantitative information regarding these identified products and this attempt at quantification is investigated in the rest of this study.

Table 3.2 Products observed in the TAGA 6000E and API 365

Nominal Weight (<i>u</i>)	Suggested Identity	SRM Pairs (<i>m/z</i>)	Structure	TAGA	API
138	Nopinone	139/121 157/139 157/121		✓	✓
154	Hydroxy nopinone (multiple isomers)	155/109		✓	✓
231	Dihydroxy nitrate	232/151		✓	✓
168	C10 hydroxy aldehyde	169/151		✓	✓
170	Pinalic 3-acid	171/153 171/135		✓	✓
	Norpinic acid	173/127 173/109		✓	✓
186	Pinic acid	187/169 187/141		✓	✓
199	Nitrooxy nopinone (multiple isomers)	200/154		✓	✓

3.2. Obtaining Calibration Curves at Our Concentration Range

Once some of the chamber products could be qualitatively characterized and the API 365 APCI MS/MS instrument was modified in order to be functional for the purpose of our experiments; the quantification of chamber products using this instrument was attempted. It was seen in previous quantitative APCI-MS/MS studies in our group, as well as in studies by Sunner et al. (1988a,b) and Jost et al. (2003) that the signal of the protonated analyte ion $((M+H)(H_2O)_m)^+$ is linearly proportional to the sampled analyte (designated as M) concentration. However, if [M] gets too high, the protonating reagent ions (in this case $H^+(H_2O)_n$ ions) get depleted, causing the instrument signal to saturate and eventually fall off with increasing [M]. For cases with compounds of higher proton affinities (PA), where more extensive protonating reagent depletion occurs, this reversal in sensitivity takes place at lower concentrations [Sunner et al., 1988b]. The same observation was seen in this current study as it is demonstrated in **Figure 3.5**.

The signal of nopinone (SRM pair m/z 139/121) (from syringe pump calibrations) decreases when its concentration exceeds 0.1 pmm. This fall off in the nopinone signal is accompanied by a loss of the protonating reagent ion signal (SRM pairs m/z 55/37 and 39/17) as show in **Figure 3.5**. This calibration is obviously unusable since the linear range falls within a region outside the concentration range of nopinone required in this study, making the effective range of calibrations limited.

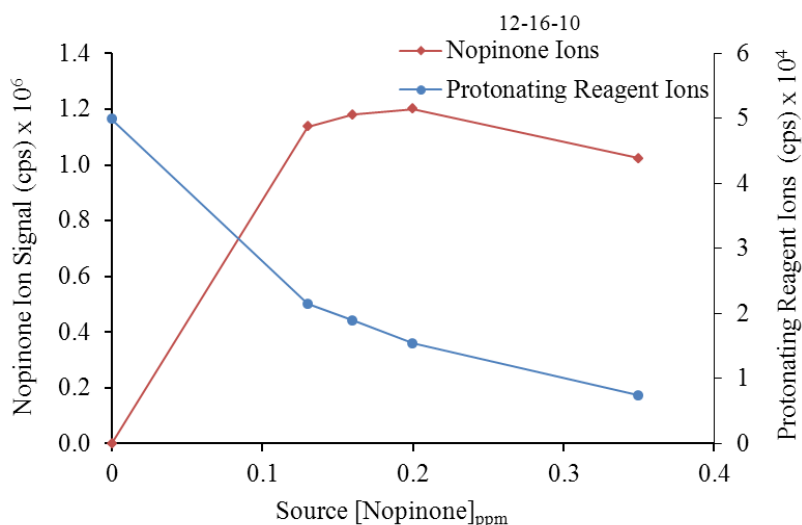
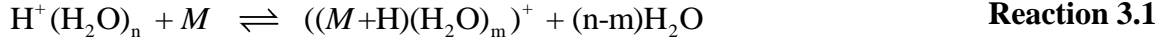


Figure 3.5 Raw nopinone signal (m/z 139/121) vs. nopinone concentration [M] and the protonating reagent ion signal as represented by the water clusters $H^+(H_2O)_n$ ($n=2$ and 3) at ion pair masses m/z 55/37 and m/z 37/19

In order to attempt to address the above issue a closer look was taken at the process of the proton transfer reaction to form $((M+H)(H_2O)_m)^+$ ions (**Reaction 3.1**) and how it is related to the sensitivity of the sampled analytes (M). It was found by Sunner et al. (1988b) that compounds of intermediate PA (mostly oxygen bases; ones of most interest in this study) have the formation of their $((M+H)(H_2O)_m)^+$ ions governed by equilibrium reactions in the ion source. This knowledge allows the species in **Reaction 3.1** to be expressed as part of equilibrium constant (K_{eq} in **Equation 3.1**). Water vapour was present in large excess in our ion source over the analyte and ion concentrations, leading to the assumption that its concentration in the source was approximately constant. This assumption and the rearrangement of the expression in **Equation 3.1**, allows for the concentration of the analyte [M] to be expressed in terms of the other reaction components (**Equation 3.2**).



$$K_{\text{eq}} = \frac{[(\text{M}+\text{H})(\text{H}_2\text{O})_m]^+ [\text{H}_2\text{O}]^{(n-m)}}{[\text{H}^+(\text{H}_2\text{O})_n] [\text{M}]} \quad \text{Equation 3.1}$$

$$[\text{M}] = \text{C} \times \frac{[(\text{M}+\text{H})(\text{H}_2\text{O})_m]^+}{[\text{H}^+(\text{H}_2\text{O})_n]} \quad \text{where } \text{C} = \frac{[\text{H}_2\text{O}]^{(n-m)}}{K_{\text{eq}}} \quad \text{Equation 3.2}$$

However, due to the extensive de-clustering that takes place in the curtain gas and orifice/skimmer region of the ion source (see **Section 2.1.1**) no info is provided in the observed spectra on the actual $\text{H}^+(\text{H}_2\text{O})_n$ and $(\text{M}+\text{H})(\text{H}_2\text{O})_m^+$ cluster distribution prevailing in the ion source [Sunner et al., 1988a,b]. Additionally ion transmission efficiencies are reduced due to the pumping capabilities of the instrument and quadrupole mass discrimination against higher mass ions [Sunner et al., 1988a]. To try and get around the information lost through these ion loss processes; it can be assumed that the sum of the ion intensities of all the hydrate clusters of a given species ($\sum I_{[(\text{M}+\text{H})(\text{H}_2\text{O})_m]^+}$) is directly proportional to the sum of the corresponding ion concentrations present in the ion source ($\sum [(\text{M} + \text{H})(\text{H}_2\text{O})_m]^+$). In this case **Equation 3.2** becomes **Equation 3.3**:

$$[\text{M}] = \text{C}' \times \frac{\sum I_{[(\text{M}+\text{H})(\text{H}_2\text{O})_m]^+}}{\sum I_{[\text{H}^+(\text{H}_2\text{O})_n]}} \quad \text{Equation 3.3}$$

Where I = ion intensity and $\text{C}' = \text{constant} \times \frac{[\text{H}_2\text{O}]^{(n-m)}}{K_{\text{eq}}}$

The expression in **Equation 3.3** requires the sum of all reagent ions but can be simplified in cases where [M] is changing but [H₂O] is constant [Sunner et al., 1988b]. In these cases (including the experiments done in this study) using the intensity of the most

abundant ion for M and one or two of the observed water cluster ions is sufficient. For M the maximum observed quasi-molecular signal was due to the $(M+H)^+$ or the $((M+H)(H_2O))^+$ ions. In all cases the only water clusters with significantly detectable signal were: a large peak due to $(H^+(H_2O)_3)$ ions and a smaller one due to $(H^+(H_2O)_2)$ ions at m/z 55 and 37 respectively. **Equation 3.4** is further modified to reflect this information where m/z 55 and m/z 37 are represented by their SRM pairs of m/z 55/37 and m/z 37/19.

$$[M] = C'' \times \frac{I_{[(M+H)(H_2O)_m]^+}}{\sum I_{[H^+(H_2O)_n]}} = C''' \times \frac{I_{[(M+H)(H_2O)_m]^+}}{I_{m/z\ 55/37} + m/z\ 37/19} \quad \text{Equation 3.4}$$

Where the m value (0, 1, 2, 3...) corresponds to that of the most abundant ion

It was observed that using the relationship shown in **Equation 3.4** which relates the analyte concentration to the relative signals of the analyte and water cluster ions, greatly improved the linearity and dynamic range of nopinone calibration curves (**Figure 3.6**). This form of calibration was used for all the calibrations discussed below in which they are referred to as the relative signal calibrations.

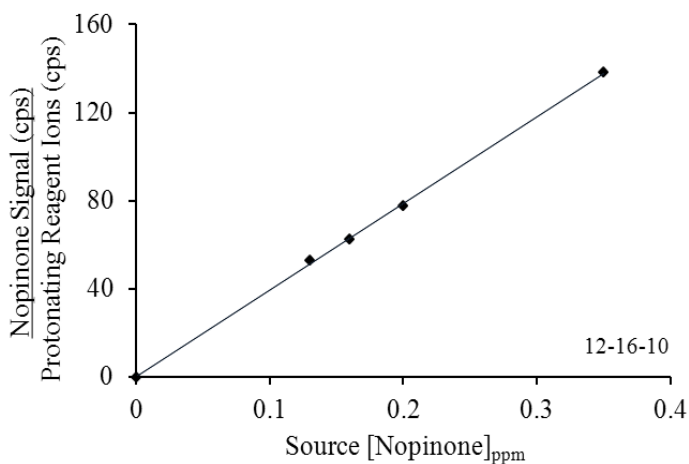
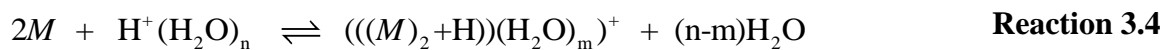
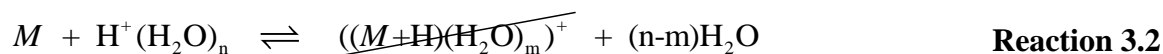


Figure 3.6 Nopinone signal relative to protonating reagent ion signal vs. nopinone concentration

3.2.1. Derivation of Relative Signal Calibrations for Dimer Species

In some cases where the M concentration was particularly high the formation of dimers (see **Section 2.1.1**) became significant. A way to improve the linearity of calibrations for these type of species was taken by formulating dimer ion formation, $((M)_2+H)(H_2O)_m^+$, using the net result (**Reaction 3.4**) of **Reaction 3.2** and **Reaction 3.3** and deriving an expression for the dimer relative signal (**Equation 3.5**) using the same manner as done for the monomer species in **Equation 3.1** through **Equation 3.4**.



$$[M] = C^{m''} \times \sqrt{\frac{I_{[(M)_2+H](H_2O)_m]^+}}{I_{m/z\ 55/37} + I_{m/z\ 37/19}}} \quad \text{Equation 3.5}$$

3.3. Reaction Relevant, Single Compound calibrations using a Syringe Pump

For these experiments the initial goal was to obtain calibration curves using sample input via syringe pump so that yield measurements could be obtained for beta-pinene photo-oxidation products. Set-up(s) were sought that allowed for the sampling of both gas and particle phase products so compounds were chosen to represent ones that could be found in those two phases. The product selected for gas phase quantification was nopinone. From a practical point of view it was a good product for initial tests since it was commercially available and had a good observed sensitivity with the APCI-MS/MS. But more importantly nopinone, along with formaldehyde, is considered to be a major

gas phase product of beta-pinene oxidation by HO radical ([Orlando et al., 2000]; [Larsen et al., 2001]). Its reported yields in the gas phase are high: generally ranging from 25 [Larsen et al., 2001] to 30% [Arey et al., 1990], and with one as high as 78% [Hatakeyama et al., 1991].

The other product that was attempted to be quantified was pinic acid. It was chosen in order to try and generate a calibration set-up that could be used with particle phase sampling. Pinic acid was the first candidate since it was detected by Larsen et al. (2001) to be the highest product in concentration in the aerosol phase with a yield of 0.2-0.3%.

3.3.1. Gas Phase Calibration Set-Up

3.3.1.1. Nopinone in Methanol Solution

Nopinone was used to try and develop a method for gas phase calibrations. Initially the calibration for nopinone was done using a methanol solution with syringe pump. This approach was done for a variety of reasons. Firstly it was done in order to be able to see if the use of a solution allows for the access of a wider range of concentrations than that solely accessible from syringe pump flow variation. Secondly to be able to use a solution that allows for low concentrations while still using higher syringe flow rates; which was found to give better signal stability. Two calibrations were done on the same day using an identical set-up but between the calibrations the syringe was re-filled with the solution.

The calibration turned out to be unusable since the sensitivity of the instrument, represented by the slope of the linear fit line, was not in agreement between the two

calibrations. A representative result from two such calibrations is shown in **Figure 3.7a**. In this particular example the sensitivity changed by approximately a factor of two between the two calibrations (200.3 and 90.1 respectively). This change (other examples in **Table 3.3**) made it impossible to tell which calibration was truly representative of the instrument's sensitivity at a given time.

In order to see if this problem was compound, set-up or instrument related, the signal of methanol was also followed. The results of the methanol calibrations are shown in **Figure 3.7b**. In the case of methanol, as seen in **Figure 3.7b** and **Table 3.3**, the sensitivity did not undergo a significant change (sensitivity of 0.039 (Run 1) decreased to 0.037 (Run 2)). This indicated that this reproducibility problem was not instrumental or set-up related but rather specific to nopinone. These experiments indicated that nopinone could not be reliably sampled in the form of a nopinone/methanol solution.

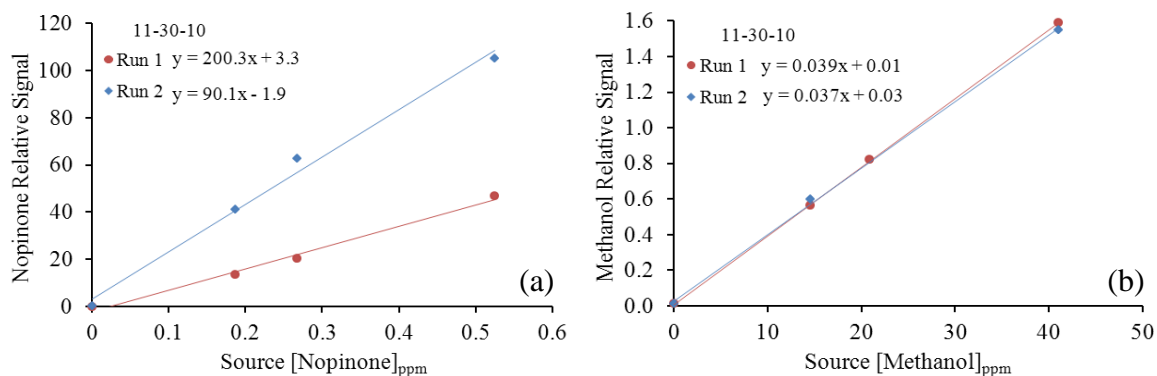


Figure 3.7

- (a) Nopinone relative signal (m/z 139/121) in methanol solution vs. nopinone concentration
 (b) Methanol relative signal (m/z 51/33) vs. methanol concentration

Table 3.3 Summary of results from the slopes obtained using a nopinone/methanol solution in the syringe pump calibrations

Date	Calibration	Nopinone (<i>m/z</i> 139/121) Slope	Methanol (<i>m/z</i> 51/33) Slope
11-30-10	1 st	80 ± 4	3 x 10 ⁻² ± 1 x 10 ⁻⁴
	2 nd	251 ± 11	3 x 10 ⁻² ± 3 x 10 ⁻⁵
12-01-10	1 st	289 ± 20	4 x 10 ⁻² ± 5 x 10 ⁻⁴
	2 nd	224 ± 16	4 x 10 ⁻² ± 2 x 10 ⁻³
12-02-10	1 st	90 ± 7	4 x 10 ⁻² ± 3 x 10 ⁻⁴
	2 nd	174 ± 7	4 x 10 ⁻² ± 1 x 10 ⁻³

* Errors based on errors on the slope from the regression fit

3.3.1.2. Pure Nopinone Sampling with Syringe Pump

Sampling pure nopinone with the syringe pump was attempted next. This form of sampling gave a great improvement over the reproducibility than was seen for the nopinone/methanol solution. A representative result for this set of experiments is shown in **Figure 3.8**. Once again the only thing that separated the two calibrations was a re-fill of the syringe. This time the slopes agree with each other (within error). The reason(s) for the irreproducibility of the results for the methanol-nopinone solutions were never ascertained so pure nopinone was then used for all future experiments.

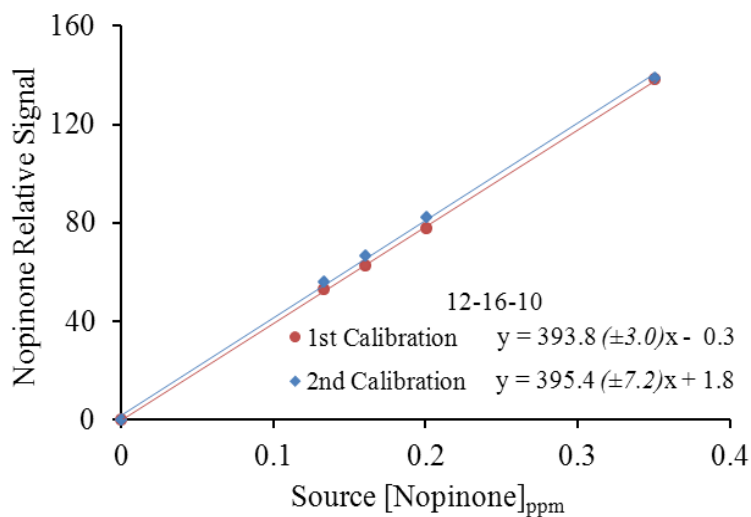


Figure 3.8 Nopinone relative signal (m/z 139/121) vs. nopinone concentration

3.3.1.3. Chamber Sampling Set-Ups

The goal of this study was to be able to generate product yields. For this purpose the generated calibrations needed to be applicable to data obtained from chamber sampling. Initially calibrations were attempted using set-up A (**Figure 3.9**). In this sampling procedure, a calibration was done, the calibration set-up was replaced by the chamber sampling line and finally the calibration set-up was reconnected and one more calibration was performed. **Figure 3.10** shows an example of a result from this type of experiment. As it is seen the calibrations done prior and post chamber sampling gave sensitivities (167.2 (prior) and 300.4 (post)) that were not in agreement, once again making these calibrations ineffectual. It was suspected that despite taking care in preserving similar conditions; the system was disrupted when switching between the calibration set-up and chamber sampling. For this reason even more precautions needed to be taken to minimize disturbance in the source conditions.

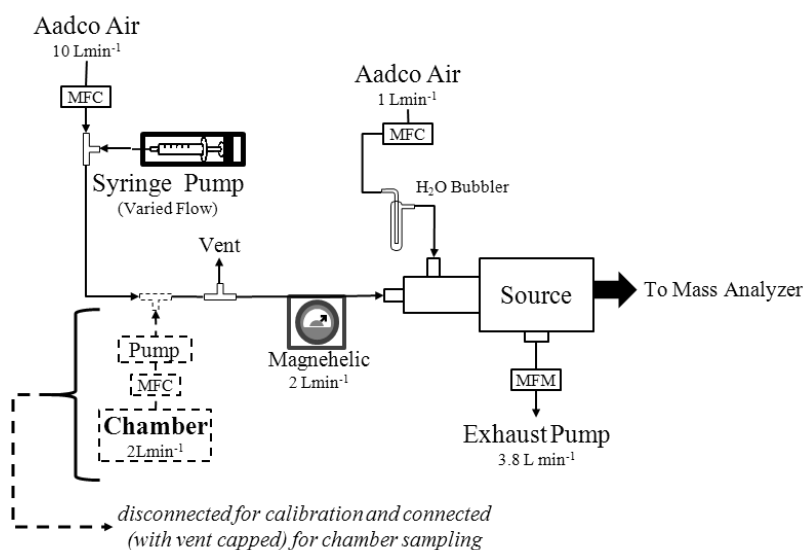


Figure 3.9 Syringe pump calibration set-up **A**: calibration and chamber sampling is done separately

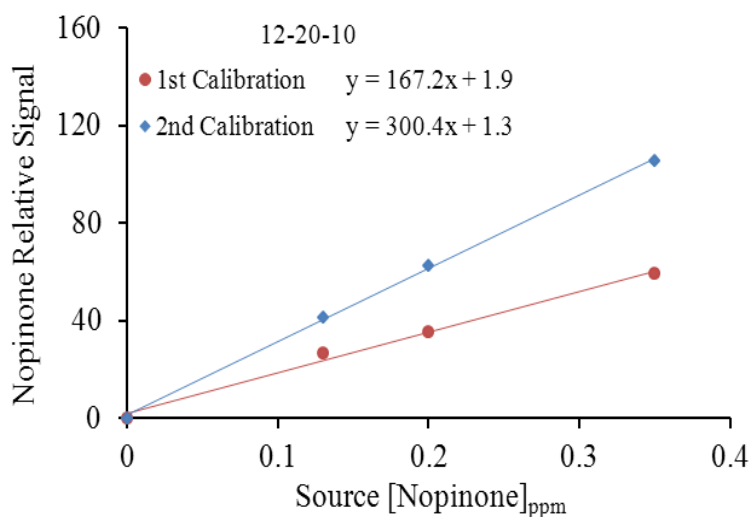


Figure 3.10 Nopinone relative signal (m/z 139/121) vs. nopinone concentration with chamber sampling done between calibrations (set-up **A**)

Measures to diminish changes in ion source conditions were taken in calibrations and sampling done via set-up B (**Figure 3.11**).

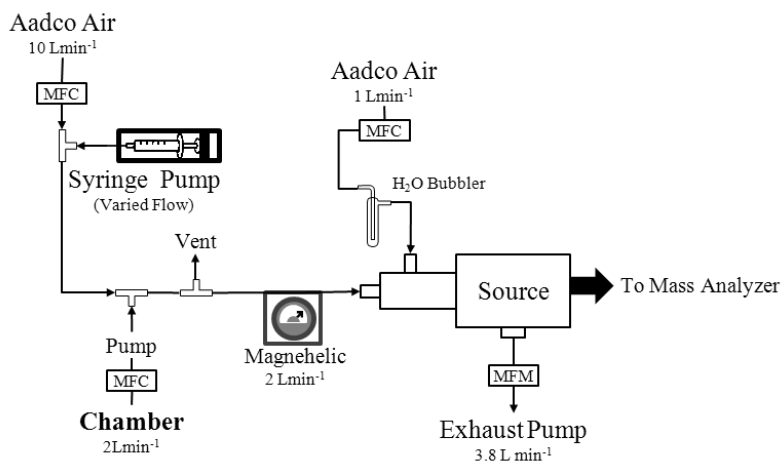


Figure 3.11 Syringe pump calibration set-up B: Sampling from calibration set-up and chamber was done simultaneously. The calibration was a standard addition.

Calibrations done using this set-up were carried out using the standard addition method. This meant that calibrations were done while simultaneously sampling the chamber and any signal due to the chamber contents was part of the background signal in the calibrations. Typically a syringe pump calibration was done while sampling an empty, flushed chamber, followed by changes in the chamber conditions (e.g. injection of nopinone into the chamber) and a second calibration was done in the same manner as the first but with a different background nopinone signal. Changes between the first and second calibrations were meant to simulate nopinone signal acquisition that would be done during a beta-pinene/HO experiment (for which the calibrations would be applied to). This set-up/method gave much better results in terms of the reproducibility of the

slopes/sensitivity. An example of this is shown visually in **Figure 3.12**. The differences between the two slopes (487.8 ± 9 (first) and 504.0 ± 10 (second)) in **Figure 3.12** exceeded their errors; however the differences were very minor and lead to small differences in calculated concentrations. For example, for a nopinone relative signal of 200, the concentration calculated using the slope of the first calibration (487.8) was 0.41ppm and with the second (504.0) 0.40ppm; results that were sufficiently similar for the purpose of these experiments. Reproducible sensitivities were also seen in other calibration done over the course over the same experimental day and on other days as seen in **Table 3.4**. The standard addition method (set-up B) was used for all subsequent syringe pump calibrations and quantitative chamber experiments.

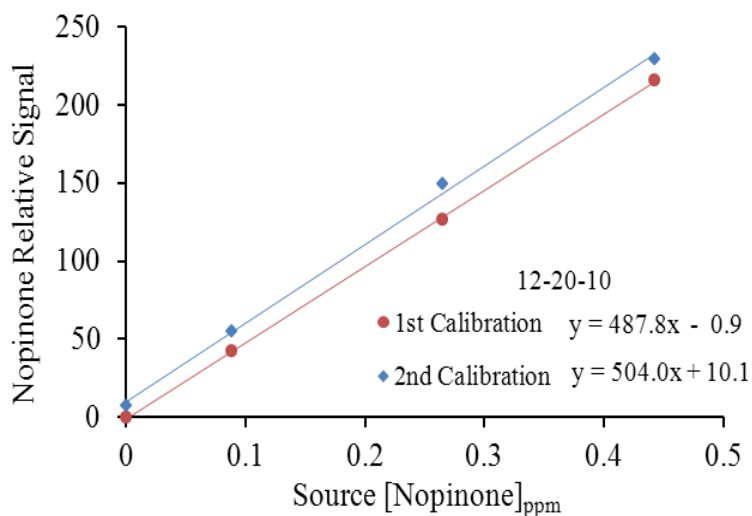


Figure 3.12 Nopinone relative signal (m/z 139/121) vs. nopinone concentration. Calibration was done using the standard addition method (set-up B). Using the same set-up first a calibration was done, the chamber conditions were changed (reagent injection) and finally a second was calibration done.

Table 3.4 Summary of results from the slopes obtained using syringe pump calibration set-up B (1st and 2nd calibration results with changes in chamber conditions (reagent injection) in between

Date	Calibration	Nopinone (<i>m/z</i> 139/121) Slope
12-20-10	1 st	488 ± 9
	2 nd	504 ± 10
01-13-11	1 st	212 ± 5
	2 nd	226 ± 11
01-24-11	1 st	274 ± 4
	2 nd	273 ± 11

* Errors based on errors on the slope from the regression fit

3.3.2. Dealing with Low Vapour Pressure Samples with the Syringe Pump Calibrations

Pinic acid was the product of beta-pinene oxidation by hydroxyl reaction that was used to represent other lower vapour pressure compounds and to try and develop a calibration set-up for these compounds to use with the syringe pump sample introduction. In order to use the commercially available pinic acid (Sigma-Aldrich, unknown purity) in calibrations, a solution had to be generated since it was in its solid form. Distilled water was found to be a solvent in which pinic acid readily dissolved in and was the preferred solvent of choice since water is already a part of the ionization process that takes place in the APCI source (**Section 2.1.1**). The calibration was first attempted using the same set-up as was used for the sampling of nopinone (see **Section 3.3.1.2**). However, no visible signal for the pinic acid could be obtained. After using its vapour pressure at room temperature (3.2×10^{-5} Pa) [ACD/Labs Software] to calculate its saturation mixing ratio and obtaining a very low value of 0.3 ppb (calculation in **Appendix D**) it was clear that

the solution needed to be heated prior to sampling by the APCI source. Unfortunately, pinic acid purchased from Sigma-Aldrich is only available in small amounts (5 mg) for this reason a surrogate compound of pinonic acid was used in its place to attempt to generate a calibration system since a large amount of solution was required to experiment with set-up adjustments. Like pinic acid, pinonic acid is also soluble in water and is structurally very similar (**Figure 3.13**). The SRM pairs used to follow the calibrations are outlined in **Appendix A (Table A.2)**.

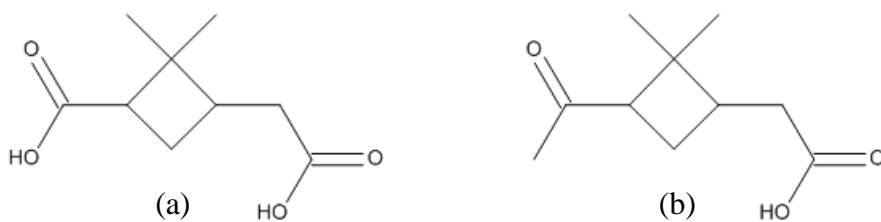


Figure 3.13 The structures of (a) pinic acid (b) pinonic acid

After attempting a few different set-ups, a system that could produce a signal for pinonic acid as well as be used to generate calibration curves was built and is shown in **Figure 3.14**. In this set-up, the acid is introduced once again via syringe pump and the sample travels along stainless steel tubing that is heated using a tape heater (OMEGA, Laval, QC) and then introduced inside the source using a heated inlet. Both the tape and the inlet heater were set to 200⁰C however due to the flow of Aadco air and the cooling associated with it, the temperature of the inside of the tubing and at the location at which the acid sample was introduced was measured to be only 100⁰C. Although it is desired to keep the temperature at the higher set value, calculations for the saturated mixing ratio

show that at 100⁰C the ratio is 3ppm (calculations in **Appendix D**); which is much higher than the concentrations sampled during the calibrations, making this temperature sufficient.

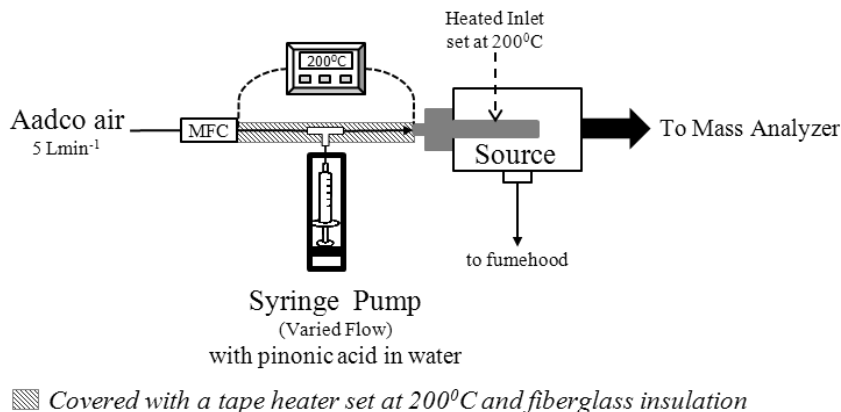


Figure 3.14 Calibration set-up for pinic and pinonic acids

Figure 3.15 shows the trace of the SRM signal as the syringe pump rate is varied to achieve different concentrations. It is seen that the points for these calibrations were difficult to obtain as the signal at each concentration point took a long time to stabilize and at higher concentrations/flow rates became very unsteady, severely limiting the range of the calibrations. If the analysis time was long enough then some calibration curves (**Figure 3.16**) could be achieved by selecting stable signal regions. These calibration curves showed good linearity (with $R^2 > 0.98$) and reproducible sensitivity in a given day (1st and 2nd calibrations **Figure 3.16**). However, the range of these calibrations was extremely limited and selection of stable regions subjective. Attempts at lower concentrations were limited by the pump flow rate/syringe size and any increase in Aadco air dilution contributed further to the undesirable cooling along the heated transfer

lines. Higher concentrations were limited since the instability seen in the signal (**Figure 3.15**) was only further enhanced and even visible pooling of solution in the lines occurred if the solution volume was excessive or dilution airflow too reduced.

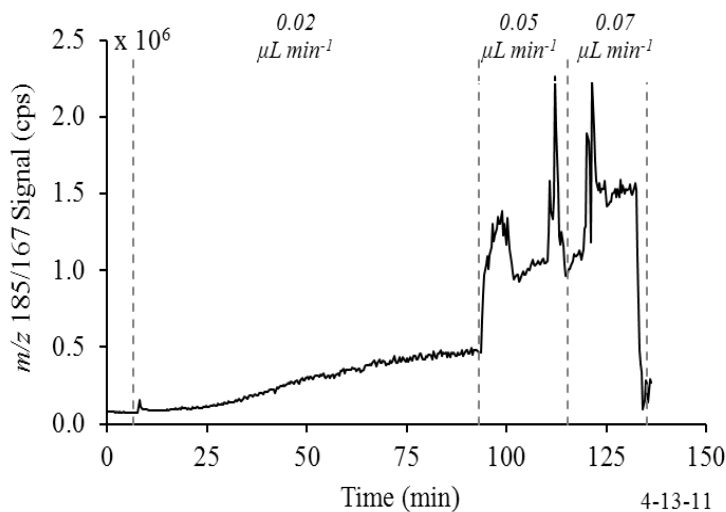


Figure 3.15 SRM trace of m/z 185/167 (pinonic acid) during concentration variation via syringe pump flow rate changes (0.02, 0.05 and 0.07 $\mu\text{L min}^{-1}$)

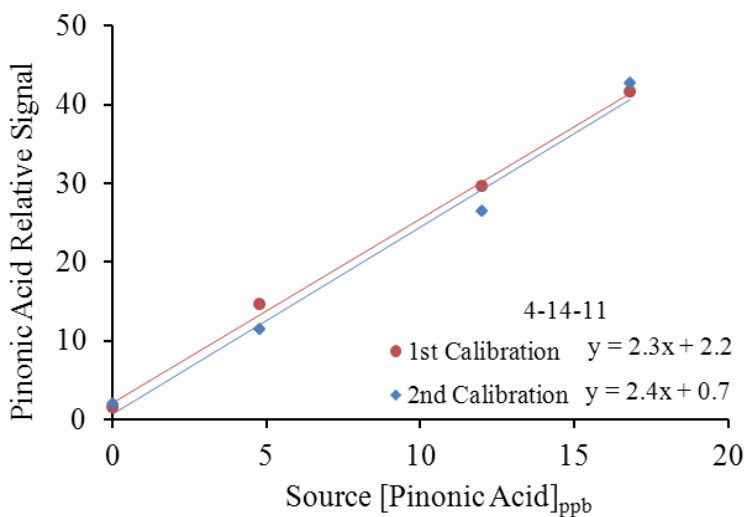


Figure 3.16 Calibration plots for the relative pinonic acid signal (m/z 185/167) vs. pinonic acid concentration

3.3.2.1. Exploring Causes of the Signal Instability of Pinonic Acid Sampling

It was attempted to further investigate the instability of the signal. At first it was thought that the diameter of the syringe could be an issue, but varying syringe sizes (10, 25 and 50 μL syringes, with successively larger diameters) produces comparable, unstable results. Secondly it was thought that the sample was not completely evaporating upon leaving the syringe tip. However, calculations (**Appendix E**) estimating the droplet radius at a given flow rate indicated that the evaporation of the droplet occurs on a fast enough time (1.2 seconds) that it should not factor into changes in the signal. Despite this material deposition on the syringe tip could occur and cause spikes in the signal. Thirdly since it was not possible to measure the temperature at all points of the set-up it was possible that there were areas of higher or lower temperatures; which could cause pooling of material and spikes/dips of the signal. Lastly since water is used as the solvent, there could be issues of incomplete dispersion of the sample into the gas phase due to the high surface tension of the water. In the manual for the API 365 instrument (MDS SCIEX) there are guidelines which outline liquid chromatography sampling by the instrument. In the outline it indicates that 425°C is minimum temperature that should be present in order to achieve complete nebulization of a sample that is dissolved in water. Limited by the equipment and safety of the set-up used, any values even close to this high temperature range could not be achieved. Solutions for the signal instability and overall sampling of these lower vapour pressure compounds could not be found at this time.

3.3.3. Summary of Syringe Pump Calibrations

A reliable set-up for sampling nopinone using syringe pump sample introduction was developed and used to obtain reproducible calibrations and successful integration with chamber sampling. With results also positive for another high vapour pressure analyte (methanol) this set-up is likely applicable to sampling other gas phase products. Preliminary results were also obtained for a syringe pump set-up that could be used to calibrate for lower vapour pressure, particle phase products. However, along with the complication that these lower vapour pressure compounds are in solid form and require to be dissolved prior to sampling, the calibration results showed large instability in the obtained signal and a very limited calibration range. Attempts to look at possible remedies to these problems were unsuccessful and at this time a set-up for sampling lower vapour pressure compounds was not achieved.

3.4. Evaluating the General Sensitivity of the APCI-MS/MS Instrument

Compound specific, syringe pump calibrations were found to be successful in sampling a reaction relevant gas phase analyte (nopinone); however these calibrations were reliant on the condition that a standard or a close surrogate is available to be used to generate calibration curves. The fact remained that the majority of the products formed in the beta-Pinene/HO chamber reactions did not have commercially available standards. Additionally the identities of some products are not yet fully defined; other than their key functional group(s). So it was desirable to try and develop a calibration method in which the general sensitivity of the instrument towards specific groups of compounds could be better evaluated. And that this sensitivity is preferably related to a quantity that would either be available in literature or could be calculated. One such quantity is gas phase basicity (GB) whose relationship to sensitivity is derived below. The analytes of interest in these experiments were ones of intermediate GBs (defined by Kabarle (1977) as compounds with GBs between that of water and ammonia) with examples of these GBs listed in **Table 3.5**. For these compounds ion formation in the ion source is governed by an equilibrium (**Section 3.1**) in which the forward reaction, which leads to proton transfer to the analyte from protonated water clusters $H^+(H_2O)_n$ and formation of protonated analyte ions $((M+H)(H_2O)_m)^+$, is favoured for compounds with higher GBs. In other words compounds with higher GBs have higher sensitivities.

Table 3.5 Examples of intermediate gas phase basicities (GB) (GBs between that of water (660 kJ mol⁻¹) and ammonia (819 kJ mol⁻¹)) [Hunter et al., 1998]

Compound	Gas Phase Basicity (kJ mol ⁻¹)	Compound	Gas Phase Basicity (kJ mol ⁻¹)
Methanol	724.5	Acetone	782.1
Ethanol	746	Cyclopentanone	794
n-Propanol	756.1	2-Pentanone	800.9
n-Butanol	758.9	3-Pentanone	807
i-Butanol	762.2	Cyclohexanone	811.2
2-Propanol	762.6	Cycloheptanone	815.9
t-Butanol	772.2		

3.4.1. Deriving a Relationship between Sensitivity and Gas Phase Basicity

In the hypothetical gas phase reaction of basic compound A (**Reaction 3.5**) the tendency of A to accept a proton is quantitatively described by its GB_A and proton affinity (PA_A). Where GB_A is equal to the negative of the free energy of **Reaction 3.5** (-ΔG_{Reaction 3.5}⁰) and PA_A is equal to the negative enthalpy change for **Reaction 3.5** (-ΔH_{Reaction 3.5}⁰) ([Hunter et al., 1998], [Gross, 2010]).



The expression for free energy in **Equation 3.6** can then be written in terms of GB and PA in **Equation 3.7** with the entropy (TΔS⁰) term approximately the same (30 kJ mol⁻¹) for the compounds investigated here.

$$\Delta G_{\text{Equation 3.6}}^0 = \Delta H_{\text{Equation 3.6}}^0 - T\Delta S_{\text{Equation 3.6}}^0 \quad \text{Equation 3.6}$$

$$PA_A = GB_A - T\Delta S_{\text{Equation 3.6}}^0 \quad \text{Equation 3.7}$$

And in the case of equilibrium:



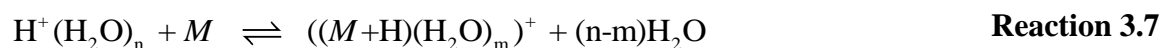
Then the equilibrium constant (K_{eq}) can be described as:

$$K_{eq} = \frac{[(A+H)^+][B]}{[(B+H)^+][A]} \quad \text{Equation 3.8}$$

And combining the information in **Equation 3.6**, **Equation 3.7** and **Equation 3.8**, the GB_A can be related to the K_{eq} by **Equation 3.9** [Gross, 2010].

$$GB_A = -\Delta G^0 = RT \ln K_{eq} \quad \text{Equation 3.9}$$

This equilibrium is also seen in the reaction that occurs in the APCI ion source and is written out once again in **Reaction 3.7** where the proton transfer occurs between the introduced analyte (M) and protonated water clusters ($H^+(H_2O)_n$).



In **Section 3.1** an expression was derived from K_{eq} to relate the analyte concentration [M] to ion intensity (I) measured by our mass spectrometer (**Equation 3.10**).

$$[M] = C''' \times \frac{I_{[(M+H)(H_2O)_m]^+}}{I_{m/z \ 55/37 + m/z \ 37/19}} \quad \text{where I = ion intensity} \quad \text{Equation 3.10}$$

$$\text{Where } C''' = C'' \frac{[H_2O]^{(n-m)}}{K_{eq}}$$

Which can be rearranged back into the equilibrium constant (K_{eq}):

$$K_{eq} = \frac{[H_2O]^{(n-m)}}{C''} \times \frac{I_{[(M+H)(H_2O)_m]^+}}{[M] (I_{m/z \ 55/37 + m/z \ 37/19})} \quad \text{Equation 3.11}$$

κ

S

$$K_{\text{eq}} = \kappa \times \text{Sensitivity}(S) \quad \text{Equation 3.12}$$

Where $\kappa = \frac{[\text{H}_2\text{O}]^{(n-m)}}{C}$ = constant and S = slope of relative signal vs. concentration calibration curve

This expression for K_{eq} (**Equation 3.12**) can then be substituted into **Equation 3.9** to relate the slope of the relative signal calibration curves or sensitivity (S) to the GB (**Equation 3.13** and **Equation 3.14**).

$$\text{GB} = \text{RTln}K_{\text{eq}} = \text{RTln}(\kappa \times S) = \text{RTln}(\kappa) + \text{RTln}(S) \quad \text{Equation 3.13}$$

$$\ln(\text{Sensitivity}) = \ln(S) = \left(\frac{1}{\text{RT}}\right) \text{GB} - \ln(\kappa) \quad \text{Equation 3.14}$$

This shows that the $\ln(\text{Sensitivity})$ is directly proportional to GB which potentially allows a quantity that is measurable by our instrument through calibration curves (sensitivity) and a value that can be found in literature or calculated (GB) to be related.

3.4.2. Analytes Chosen for Calibrations and Obtained Sensitivities

It would be desirable to explore the sensitivity of the groups of compounds that are seen as oxidation products of beta-Pinene. However, the lack of standards and literature GB values, as well as, the fact that most of the products are complex and multifunctional in nature made attempting to use them in this initial sensitivity/GB relationship investigation not practical. Instead a selection of two groups of single functionality compounds (alcohols and ketones) that had a good representation of standards and literature GB values available were chosen. By choosing compounds in these categories

of varying size and shape, a homologous sensitivity series could be established. Once again Q1-MS and product ion scans were done so that SRM pairs could be established to monitor analytes using the mass spectrometer. The analytes used and their respective SRM pairs followed are listed in **Appendix A (Table A.1)**.

3.4.2.1. Calibrations of Alcohols and Ketones using the EDF Method

EDF was introduced in **Section 2.2.2** as one of the calibration techniques used in this study. It was chosen for the alcohols and ketones due to its mentioned ability to generate calibration curves quickly. As with the syringe pump calibration curves the relative $\left(\frac{I_{[(M+H)(H_2O)_m]^+}}{I_{m/z\ 55/37 + m/z\ 37/19}}\right)$ rather than raw signal had to be used in order to try and achieve a linear signal and concentration relationship. The relative signal that was followed was from the SRM ion pair responsible for the most abundant ion (**Table A.1**).

It was also found that using the time constant ($\tau_{\text{predicted}}$) based on the flow through the flask (Q) and flask volume (V) to calculate the concentration changes with time (from **Equation 2.5** in **Section 2.2.2**) does not produce the best calibration results. Ritter et al. (1976) found that using the τ_{fit} obtained from the fit of the exponential decay of the instrument signal vs time (**Equation 3.15**) gave improved results since this way the τ_{fit} is a function of the flow through the flask, the detector linearity and the analyte(s) involved. In order to achieve linearity in calibrations, the τ_{fit} obtained had to be close to $\tau_{\text{predicted}}$ ($\tau_{\text{predicted}} = 5$ minutes in this case). It can be seen in **Figure 3.17 a** and **b** that this agreement between the τ_{fit} and $\tau_{\text{predicted}}$ was better in smaller compounds such as methanol

($\tau_{\text{fit}} = 5 \text{ min}$) and then increased in deviation for larger compounds, as seen for cycloheptanone ($\tau_{\text{fit}} = 6.3 \text{ min}$).

$$\text{signal} = \text{signal}_0 \exp \frac{-\text{time}(t)}{\tau_{\text{fit}}} \quad \text{Equation 3.15}$$

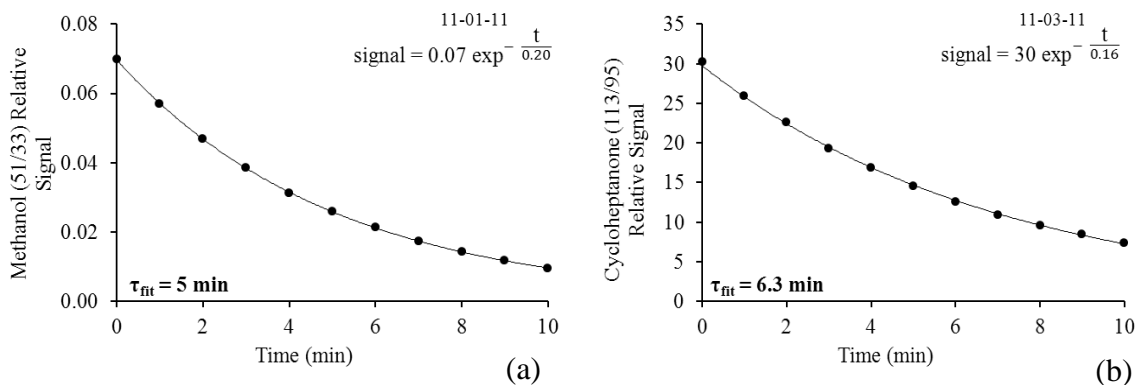


Figure 3.17

(a) Exponential decay of the relative signal of methanol SRM pair 51/33 vs time

(b) Exponential decay of the relative signal of cycloheptanone SRM pair 113/95 vs time

This difference in τ_{fit} was more drastic in initial set-ups, for example, τ_{fit} for cycloheptanone was as high as 9.3 min, but was successfully decreased to the more acceptable values by adding additional dilution at the flask output as seen in **Figure 2.8** in **Section 2.2.2**. It is perhaps seen with the improvement of τ_{fit} for the bigger compounds with increased dilution prior to introduction into the APCI ion source that the depletion of protonating water clusters at increased analyte concentration is the problem. These larger compounds are the ones that have bigger gas phase basicities and therefore cause larger proton depletion. This proton depletion can be drastic enough that even taking the signal relative to the protonating agent is not enough to restore the linearity in

the detector response and therefore drastically hinder the expected exponential signal decay.

Despite variations in τ_{fit} , using this method the calibration curves of relative signal vs. concentration for the compounds sampled all had a coefficient of determination (R^2) value of greater than 0.99 indicating good linearity. A summary of all the τ_{fit} values can be found in **Appendix F**. Examples of these calibration curves for methanol and cycloheptanone are seen in **Figure 3.18 a** and **b**. The relative sensitivities obtained for all the alcohols and ketones from the slopes of these types of calibration curves are summarized in **Table 3.6** for different days.

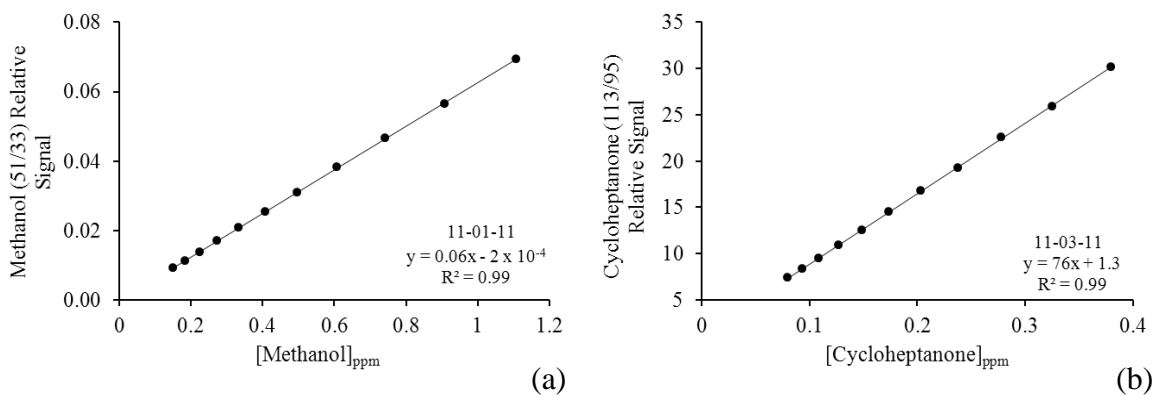


Figure 3.18

- (a) Calibration curve from the relative signal of methanol SRM pair 51/33 vs time obtained by the EDF method
- (b) Calibration curve from the relative signal of cycloheptanone SRM pair 113/95 vs time obtained by the EDF method

Table 3.6 Summary of sensitivities obtained from EDF calibration of alcohols and ketones

- = no data

Date		8-16-11	9-22-11	10-04-11	10-05-11	10-06-11	10-11-11	11-1-11	
Compound	GB	Sensitivity based on Relative Signal							Average Sensitivity
Methanol	724.5	0.06	0.13	0.08	0.15	0.05	0.06	0.06	0.08
Ethanol	746	1.11	2.2	4.1	5.0	-	1.5	1.3	2.1
n-Propanol	756.1	4.10	4.7	8.1	5.3	5.4	1.9	4.9	4.6
n-Butanol	758.9	7.92	11.7	13.5	34.1	30.6	20.9	15.0	17.0
i-Butanol	762.2	-	7.5	-	54.1	20.1	22.2	4.8	15.4
2-Propanol	762.6	6.82	5.2	8.0	-	8.7	14.2	11.9	8.6
t-Butanol	772.2	-	37.0	-	55.1	81.5	70.1	49.9	56.6
Date		8-25-11	9-16-11	9-18-11	9-26-11	10-05-11	10-11-11	10-20-11	
Acetone	782.1	11.00	6.90	11.40	12.00	9.65	12.00	10.00	10.27
Cyclopentanone	794	26.00	20.60	95.00	22.00	50.00	28.00	23.00	32.22
2-Pentanone	800.9	49.00	33.00	-	69.00	-	-	49.00	48.35
3-Pentanone	807	45.00	24.00	88.90	43.00	-	-	41.00	44.23
Cyclohexanone	811.2	172.00	72.00	135.00	93.00	186.00	63.00	95.00	108.15
Cycloheptanone	815.9	74.00	67.00	-	103.00	-	-	108.20	86.22

3.4.3. Applying the ln(Sensitivity) vs. Gas Phase Basicity (GB) Relationship

To test the relationship between the sensitivity and GB, the sensitivities obtained from the alcohol and ketone EDF calibrations and the literature GB values were plotted. The data plotted in these curves is summarized in **Appendix G (Table F.1 and Table G.2)**. To minimize the error associated with extrapolation of the y-intercept it was decided that the ln(sensitivities) needed to be plotted relative to Δ GB rather than absolute GB values. The two functional groups were plotted on the same graph (**Figure 3.19**), however it was clear that two distinct slopes were present. In addition to this observation, the slopes were both different from the theoretical slope of 0.40 mol kJ^{-1} as predicted in **Equation 3.14** and calculated in **Equation 3.16**. The two functional groups were plotted separately (**Figure 3.20** for alcohols and **Figure 3.21** for ketones). The two separate graphs had improved R^2 values of 0.97 (alcohol) and 0.90 (ketone) compared to the 0.76 seen for the combined graph (summarized in **Table 3.7**). In all plots the error bars were based on the individual standard deviations from the respective average lnS values.

Table 3.7 Summary of calibration results for ln(sensitivity) vs. GB using the sensitivity obtained from using calibrations made from the signal of the most abundant ion

Compound used in Calibration	slope (m) (mol kJ^{-1})	y-intercept	R^2
Alcohols + Ketones	0.06 ± 0.01	-0.51 ± 0.60	0.76
Alcohols	0.14 ± 0.01	-2.43 ± 0.40	0.97
Ketones	0.064 ± 0.01	2.50 ± 0.20	0.90

$$\text{theoretical slope} = \frac{1}{RT} = \frac{1}{(8.314 \times 10^{-3} \text{ kJ mol}^{-1} \text{ K}^{-1})(300 \text{ K})} = 0.40 \text{ mol kJ}^{-1} \quad \text{Equation 3.16}$$

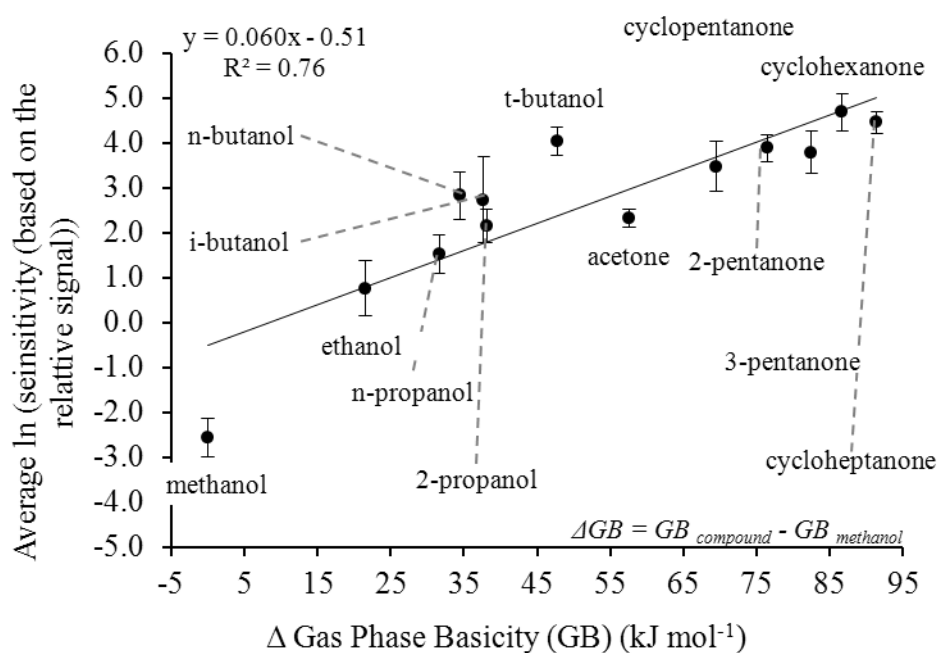


Figure 3.19 Graph of $\ln(\text{sensitivity})$ vs. ΔGB for alcohols and ketones

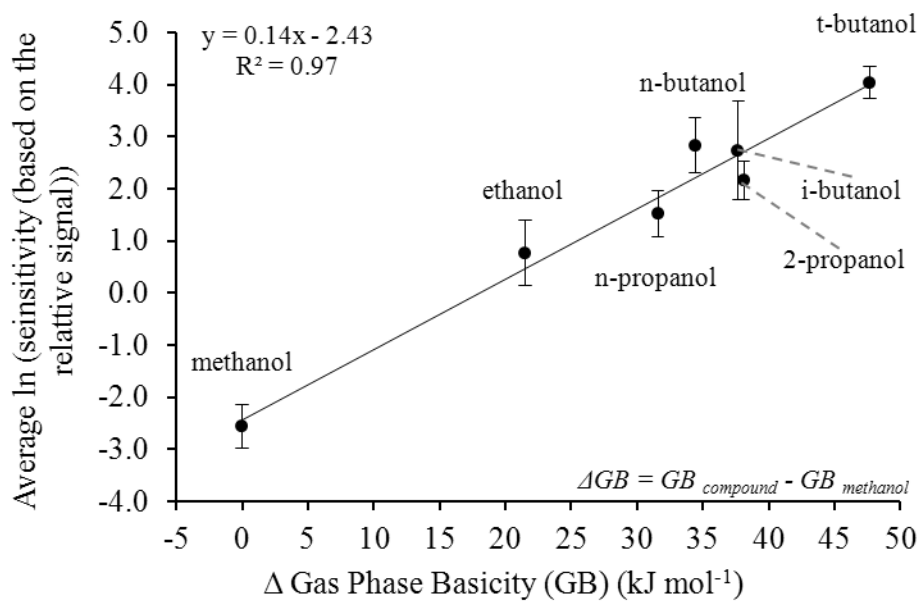


Figure 3.20 Graph of $\ln(\text{sensitivity})$ vs. ΔGB for alcohols

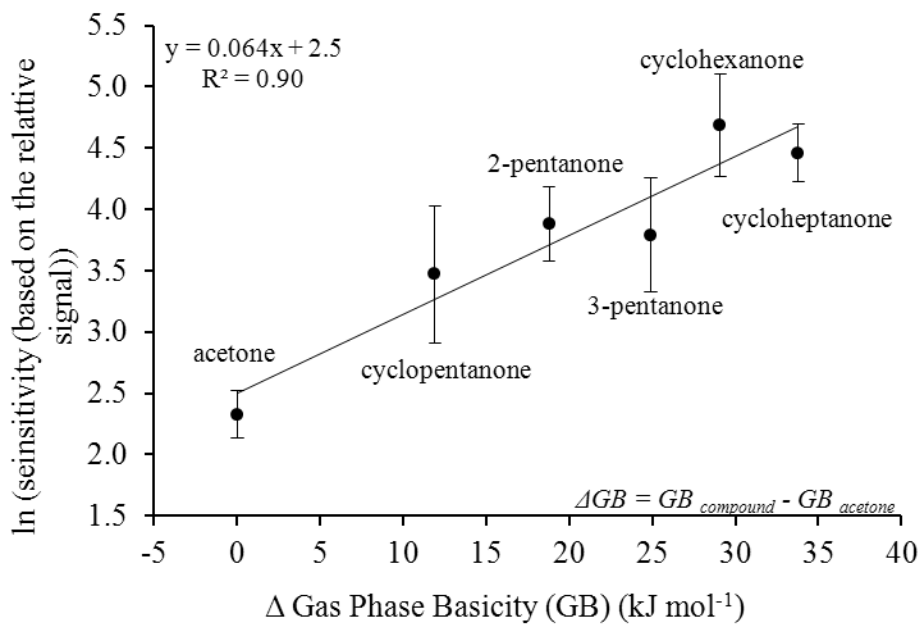


Figure 3.21 Graph of $\ln(\text{sensitivity})$ vs. ΔGB for ketones

3.4.3.1. Plotting Alcohol and Ketone ln (Sensitivity) vs. Δ GB Graphs Separately

3.4.3.1.1 Deviation of ln(Sensitivity) vs. Δ GB Ketone and Alcohol Slopes from the Theoretical Slope

Plotted separately, the alcohol and ketone graphs had different slopes at $(0.14 \pm 0.01) \text{ mol kJ}^{-1}$ and $(0.064 \pm 0.01) \text{ mol kJ}^{-1}$ respectively, and were still very different than the theoretical slope of 0.40 mol kJ^{-1} . It was not clear why the slopes were different from each other or from the theoretical slope. The only deviation from the theoretical slope would be due to temperature fluctuations since all other differences including instrumental condition changes are reflected in the y-intercept term of $\ln(\kappa)$ (**Equation 3.14**). Temperature fluctuations were not expected to exceed $\pm 5^\circ\text{C}$ which translated to very small changes in the slope (maximum of 2% change). At this time the reasons for the deviation from the theoretical slope are not known.

3.4.3.1.2 Differences Between the ln(Sensitivity) vs. Δ GB Ketone and Alcohol Slopes

As for the differences between the ketone and alcohol slopes, one theory was that it was due to the fact that the ion types used for calibrations were different for the two functional groups. The most abundant ion was used for both calibrations; in the case of the ketones it was always the peak associated with the $(\text{M}+\text{H})^+$ ion and for the alcohols it was the peaks attributed to the $(\text{M}+\text{H}+\text{H}_2\text{O})^+$ ion and the $(\text{M}+\text{H}-\text{H}_2\text{O})^+$ ion (for n and t butanol). This theory was tested by plotting the average ln(sensitivity) values based on the relative sensitivities of the sum of the three most abundant ions seen for the alcohols and ketones (**Appendix A**) rather than one ion. The plots are in **Figure 3.22** for the alcohols) and **Figure 3.23** for the ketones. However, as seen in **Table 3.8** that this did

not show any statistical difference in the slopes (new slopes: 0.013 ± 0.02 for alcohols and 0.066 ± 0.01 for ketones). The same statement was true for the y-intercept values (Table 3.7 and Table 3.8). These observations were not surprising since the most abundant ion for both the alcohols and ketones tends to heavily dominate the spectra during calibrations. This showed that comparing sensitivities between compounds based on their one most abundant ion is sufficient to evaluate their sensitivities but the use of different ions for calibrations does not explain the difference between the slopes of the alcohols and ketones.

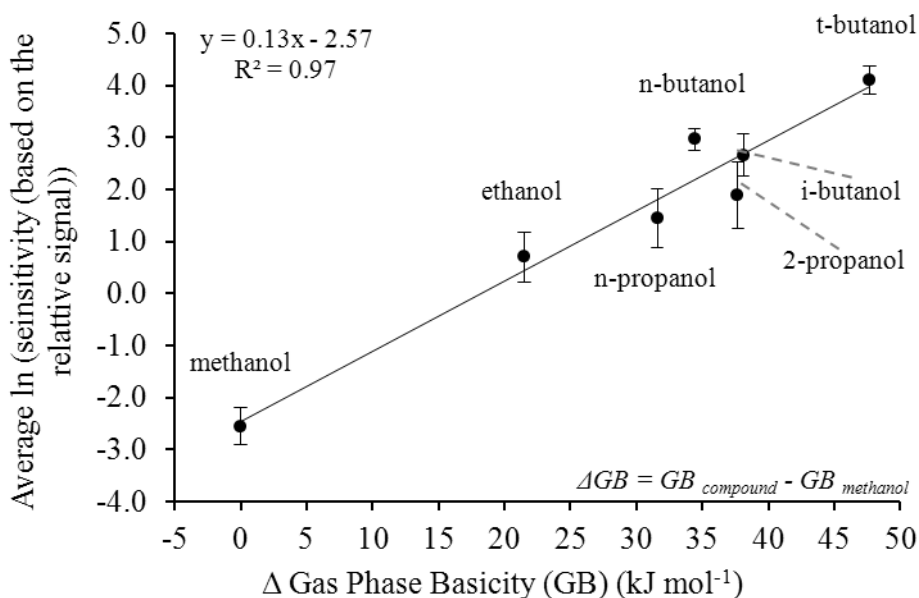


Figure 3.22 Graph of $\ln(\text{sensitivity})$ vs. ΔGB for alcohols using the sum of the signals of the three most abundant ions

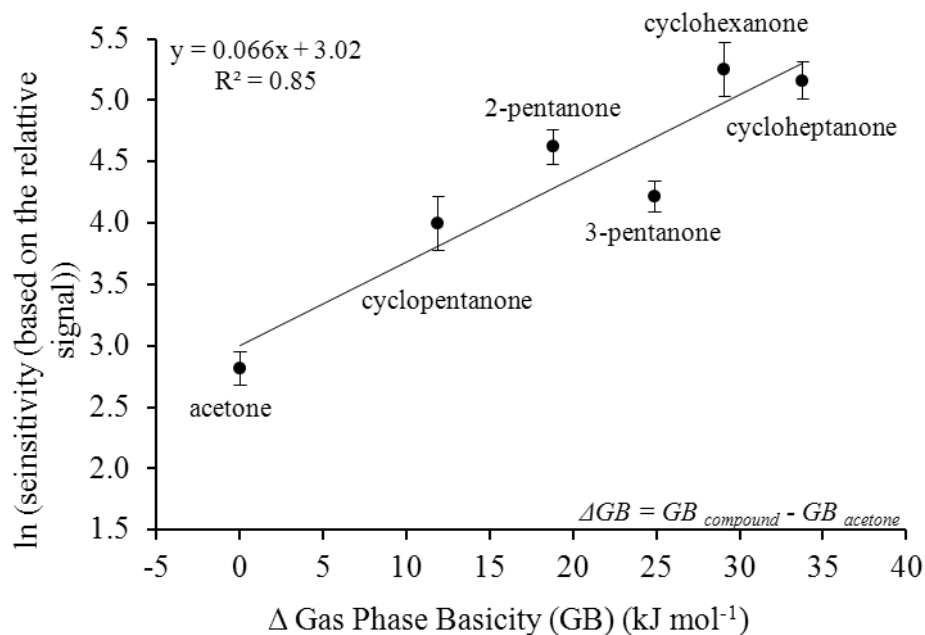


Figure 3.23 Graph of $\ln(\text{sensitivity})$ vs. ΔGB for ketones using the sum of the signals of the three most abundant ions

Table 3.8 Summary of calibration results for $\ln(\text{sensitivity})$ vs. GB using the sensitivity obtained from using calibrations made from the sum of the signals of the three most abundant ions

Compound used in Calibration	slope (m) (mol kJ ⁻¹)	y-intercept	R ²
Alcohols	0.13 ± 0.02	-2.57 ± 0.40	0.97
Ketones	0.066 ± 0.01	3.02 ± 0.30	0.85

The other theory for the difference between slopes was that the two types of functional groups undergo two different processes in the protonation; which somehow is reflected in their $\ln(\text{sensitivity})$ vs. ΔGB relationship. These processes are outlined in a schematic in **Figure 3.24** [Bouchoux, 2007].

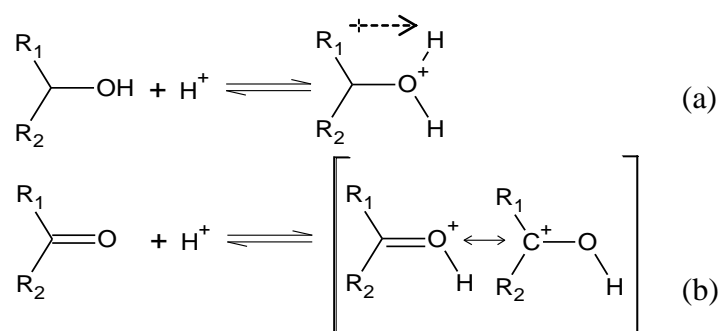


Figure 3.24 schematic of preferred protonation (a) alcohols (b) ketones

There was no way to confirm if these differences were a factor but it was decided that it was best to use the calibration curves individually. For compounds with a hydroxyl group the alcohol curve would be used and for ones with a carbonyl group the ketone graph would be used to evaluate the instrument sensitivity relative to GB.

3.4.3.2. Accuracy of $\ln(\text{Sensitivity})$ Estimated from $\ln(\text{Sensitivity})$ vs. ΔGB Graphs Calibration Curve and Average Experimental $\ln(\text{Sensitivity})$

To get an idea of the accuracy of the ketone and alcohol calibration curves as they pertain to the compounds used for calibrations the absolute differences were calculated (**Equation 3.6**) and are summarized in **Table 3.9** and **Table 3.10**. Two $\ln(\text{sensitivity})$ values were compared, the first was the $\ln(\text{sensitivity})$ calculated by substituting the appropriate ΔGB value into the equation of the ketone or alcohol $\ln(\text{sensitivity})$ vs. ΔGB calibration curve line equation. The second $\ln(\text{sensitivity})$ value was the average

ln(sensitivity) that was experimental measured from the various compound relative signal vs. concentration calibration curves.

$$\text{absolute difference } (\Delta \ln S) = \left| \begin{array}{c} \text{average experimental } \ln S - \\ \ln S \text{ calculated from the slope of the } \ln S \\ \text{vs. } \Delta GB \text{ calibration} \end{array} \right| \quad \text{Equation 3.17}$$

The absolute difference ($\Delta \ln S$) was low for the ketones (less than 0.31) which indicated that the calibration estimated sensitivities agreed well with the experimentally determined values. However, for the alcohols the percent errors ranged from low (less than 0.15) for methanol, i-butanol and t-butanol and to higher (0.29-0.62) values for ethanol, n-propanol, n-butanol and 2-propanol). The results were a bit surprising since the alcohol calibration curve had a better R^2 value than the ketone curve. But visually looking at the graphs it is seen that in the alcohol case (**Figure 3.20**) the line of best fit is anchored by the three compounds with the best percent error while in the ketone case (**Figure 3.21**) the line of best fit is more equidistant between all the calibration points and therefore more representative of the overall ln(sensitivity) vs. ΔGB relationship.

Based on these results it is shown that both calibration curves can use ΔGB values from the compounds involved in the calibration to produce comparable values to those obtained experimentally. With the ketone graph more representative than the alcohol graph. For both graphs, adding more compounds to the calibration curve would allow to better define the ln(sensitivity) vs. ΔGB relationship.

Table 3.9 Absolute differences ($\Delta \ln S$) between the $\ln(\text{sensitivity})$ or $\ln S$ calculated from ketone $\ln S$ vs. ΔGB calibration and experimentally measured $\ln S$

where: $\Delta GB = GB_{\text{compound}} - GB_{\text{acetone}}$

Compound	ΔGB	$\ln S$ calculated from the slope of the $\ln S$ vs. ΔGB calibration	Average Experimental $\ln S$	$\Delta \ln S$
Acetone	0	2.50	2.33	0.17
Cyclopentanone	11.9	3.26	3.47	0.21
2-Pentanone	18.8	3.71	3.88	0.17
3-Pentanone	24.9	4.10	3.79	0.31
Cyclohexanone	29.1	4.37	4.68	0.31
Cycloheptanone	33.8	4.67	4.46	0.21

Table 3.10 Absolute differences ($\Delta \ln S$) between the $\ln(\text{sensitivity})$ or $\ln S$ calculated from alcohol $\ln S$ vs. ΔGB calibration and experimentally measured $\ln S$

where: $\Delta GB = GB_{\text{compound}} - GB_{\text{acetone}}$

Compound	ΔGB	$\ln S$ calculated from the slope of the $\ln S$ vs. ΔGB calibration	Average Experimental $\ln S$	$\Delta \ln S$
Methanol	0	-2.43	-2.56	0.14
Ethanol	21.5	0.47	0.76	0.29
n-Propanol	31.6	1.83	1.52	0.31
n-Butanol	34.4	2.21	2.83	0.62
i-Butanol	37.7	2.65	2.73	0.08
2-Propanol	38.1	2.71	2.16	0.55
t-Butanol	47.7	4.00	4.04	0.04

3.5. Testing the Validity of the Calibrations for Chamber Reaction Relevant Compounds

For both the compound specific calibrations obtained using the syringe pump and the general instrument sensitivity obtained using EDF calibrations it was important to test not only the precision of the results but also the accuracy. It was previously shown that the syringe pump calibration using a proper set-up can provide reproducible sensitivity results; particularly over the course of a day (**Table 3.4** in **Section 3.3.1.3**). And in the case of the EDF results the relative sensitivity of compounds in relation to their gas phase basicity for the same type single functional groups was also reproducible (**Table 3.6**). Some accuracy testing was done for the EDF calibrations in **Section 3.4.3.2** in which it was tested for the compounds involved in the calibration. The main goal of this study is to use these calibrations for chamber reaction relevant compounds so tests were done for both calibration cases to see how the respective calibration curves could be of use to predict a concentration from a measured signal of a beta-pinene/HO reaction product (nopinone).

3.5.1. Syringe Pump Accuracy Results

3.5.1.1. Data Acquisition and Evaluation Procedure

For the case of the syringe pump, the injection of the nopinone was done by standard addition. In the standard addition the calibration set-up was as described in **Figure 3.11** in **Section 3.3.1.3**; and such that the chamber sampling was always part of the calibration set-up. The nopinone (0.2 ppm) was injected into the chamber and allowed to mix for at least one hour. After the mixing time and once a stable nopinone

SRM signal was attained, increasing amounts of known nopinone were injected via syringe pump into the calibration set-up in order to generate a calibration curve. This way the sensitivity of the instrument was evaluated in the same sample matrix as experienced in the chamber.

Table 3.11 describes the concentration results from the standard addition calibrations. In this case sensitivities for four individual nopinone SRM pairs (m/z 139/121, 157/139, 157/121 and 277/139) were determined (**Table 3.12**). These sensitivities were used to solve for the concentration of the 0.2 ppm of injected nopinone. The agreement between the actual injected and calculated values was evaluated by calculating their percent (%) errors (**Equation 3.18**).

Table 3.11 Nopinone concentrations obtained from calibrations (actual nopinone injection value = 0.2ppm). The sensitivities used to calculate the concentrations are in **Table 3.12**.

Date	m/z 139/121 Concentration (ppm)	% Error	m/z 157/139 Concentration (ppm)	% Error	m/z 157/121 Concentration (ppm)	% Error	m/z 277/139 Concentration (ppm)	% Error
01-13-11	0.22 ± 0.07	10	0.17 ± 0.02	15	0.13 ± 0.02	35	0.09 ± 0.02	55
02-02-11	0.20 ± 0.12	0	0.20 ± 0.12	0	0.18 ± 0.12	10	0.41 ± 0.01	105
03-02-11	0.16 ± 0.02	20	0.15 ± 0.01	25	0.13 ± 0.01	35	0.13 ± 0.01	75

*Errors on the concentration are based on the calibration regression fit

Table 3.12 Sensitivities obtained from standard addition calibrations

Date	Sensitivity 139/121	Sensitivity 157/139	Sensitivity 157/121	Sensitivity 277/139
01-13-11	336.3	39.3	4.0	64.9
02-02-11	273.6	36.8	4.2	91.8
03-02-11	544.5	66.6	8.0	100.6

$$\text{percent (\%) error} = \frac{|\text{calibration concentration result} - \text{injected value}|}{\text{injected value}} \quad \text{Equation 3.18}$$

Across most of the SRM pairs there was generally good agreement with the 0.2 ppm of injected with the exception of the dimer pair of m/z 277/139 nopinone (the results for the dimer are discussed separately in **Section 3.5.1.2** below). The m/z 139/121 pair had the most accurate results i.e. the smallest calculated percent errors (0-20%) over the three days. Taking also into account the errors that arise from the regression fits on the calibration curves, all pairs provided a range of values which covered the expected value of 0.2 ppm. This indicated that this syringe pump standard addition method of calibration could be used to provide both accurate and precise results.

3.5.1.2. The Poor Accuracy of the Nopinone Dimer SRM Pair

Out of all the nopinone SRM pairs tested for accuracy, the dimer pair (m/z 277/139) displayed the least accurate results. The dimer pair gave very inconsistent results (0.09-0.41 ppm) with large % errors (55-105%). The dimer calibrations were done based on the relationship defined in **Equation 3.5** of **Section 3.2.1**. This relationship was derived in our group and was not previously presented in literature material. Despite the fact that all calibration curves were linear ($R^2 > 0.99$) it seemed that these calibration curves do not properly define its behaviour. Perhaps treatment of the dimer behaviour based on that of the monomer does not fully predict its concentration/SRM signal relationship. These observations were also consistent with other quantification attempts done by our group [Aljawhary, 2011]. For these reasons it

was concluded that at this time the dimer signal cannot accurately predict nopinone concentration from its signal and was not used in elucidating any other quantitative nopinone information.

3.5.2. Exponential Dilution Flask (EDF) Results

3.5.2.1. Direct EDF Sampling of Nopinone Problems

Attempts to sample nopinone by the EDF method were unsuccessful as no exponential decay could be achieved. Nopinone is expected to have a larger GB value than the other sampled compounds. As shown in **Section 3.4.2.1** there was improvement to other larger GB compounds (e.g. cycloheptanone) when they were introduced at a lower initial concentration. The lowest concentration that could be achieved for nopinone was done by tracking it as a known impurity (Sigma-Aldrich, personal communication) in commercially available beta-pinene. Beta-pinene was injected into the EDF flask at the lowest amount the current set-up would allow. As seen in **Figure 3.25a** and **b** the beta-Pinene decay (**a**) proceeded close to the predicted (**Section 3.4.2.1**) exponential decay ($\tau_{\text{predicted}} = 5 \text{ min}$) with a τ_{fit} of 4.5 min while the τ_{fit} for the nopinone decay, **Figure 3.25b**, was undefined; which means that sensitivity of beta-pinene could be determined by this method while that of nopinone could not. With these two compounds being sampled at the same time with such drastically different results it supported the thought that the problem was compound specific rather than the general set-up. One explanation could be that Nopinone is of too low volatility or too polar resulting in it settling or depositing on the walls of the flask leading to incomplete mixing

with the airflow passing through the flask. This results in a slow/unstable increase in concentration at the flask output and a disruption to the exponential dilution decay.

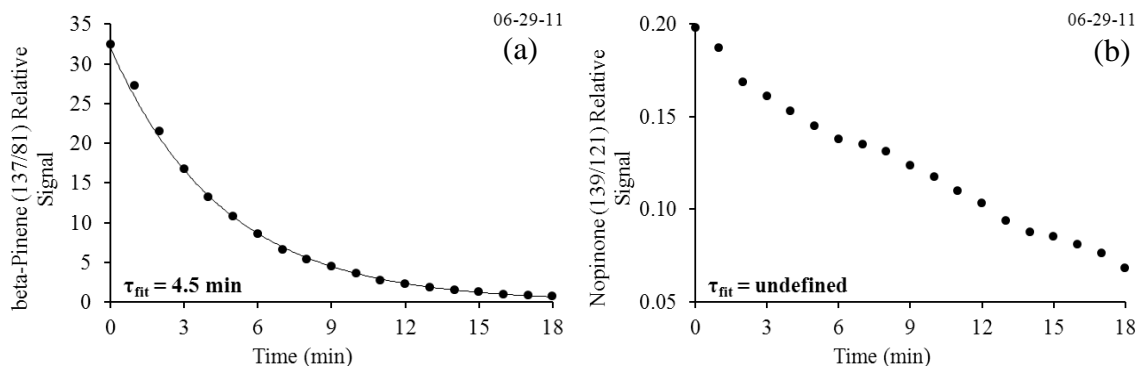


Figure 3.25 The EDF exponential decays for (a) beta-pinene (b) its nopinone impurity over time

3.5.2.2. Nopinone Sensitivity Estimation

To overcome the sampling problem associated with nopinone but to still test the accuracy of the EDF calibration results, the $\ln(\text{sensitivity})$ vs. ΔGB graph was used in order to estimate the sensitivity for nopinone. Only the ketone graph (**Figure 3.21**) was used because it was determined that there were differences in the slopes between the alcohol graph and the ketone graph (**Section 3.4.3.1.1**). Since the compound tested for (nopinone) was a ketone appropriately the ketone curve was used. Unfortunately the GB of nopinone has not been reported in literature sources, but it was thought that a very similarly structured compound could be used as a surrogate. The closest shaped compound to nopinone with an available literature GB was camphor (**Figure 3.26a**). The GB of camphor is reported to be 827 kJ mol^{-1} [Hunter et al., 1998]. Camphor has one additional methyl group in comparison to the nopinone structure (**Figure 3.26b**) which is

expected to give it a slightly higher GB due to the structure having higher polarizability from the methyl group and therefore able to transfer more electron density to the oxygen and stabilize the oxygen-hydrogen bond that is formed upon protonation [Taft, 1983].

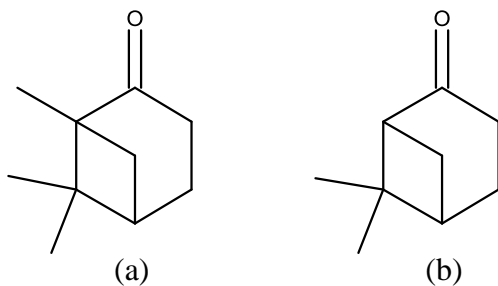


Figure 3.26 The structures of (a) camphor (b) nopinone

Using the slope of the ketone $\ln(\text{sensitivity})$ vs. ΔGB graph and the GB of camphor, the sensitivity of nopinone was calculated as outlined in **Equation 3.19**. To get an idea of the error on this calculated sensitivity; the upper (max) and lower (min) ranges of the sensitivity were obtained. To get these ranges the standard deviation of the slope based on the regression fit was used ($\sigma_{\text{slope}(m)} = \pm 0.01$ (**Table 3.7**)). This was either added to or subtracted from the slope and then this new slope was used in the same calculation as in **Equation 3.19**. This gave either a maximum sensitivity (added σ_m) or a minimum sensitivity (subtracted σ_m). The calculated sensitivity and obtained ranges are summarized in **Table 3.13**. The error on the intercept was not taken into account in these range calculations since the equations with the original fitted slope and the slopes obtained by adding and subtracting σ_m are all independent linear systems with the intercept as a common point.

$$\ln(\text{Sensitivity})_{\text{nopinone}} = 0.064 \text{ mol kJ}^{-1} \left(827 \text{ kJ mol}^{-1} - \text{GB}_{\text{acetone}} \right) + 2.5$$

Where $\text{GB}_{\text{acetone}} = 782.1 \text{ kJ mol}^{-1}$

Equation 3.19

Table 3.13 Calculated sensitivities of nopinone and calculated errors on the sensitivity (set-up A). The upper and lower ranges (min and max of the sensitivity) are also listed.

		Slope (mol kJ ⁻¹)	Sensitivity
Fit	slope (m)	0.064	217.2
Min	m - σ_m	0.054	135.0
Max	m + σ_m	0.075	349.5

3.5.2.3. Nopinone Sensitivity Accuracy Testing: Set-Up A Results

In order to test the accuracy of the calculated sensitivity, 0.2 ppm of nopinone was injected into the chamber in the manner previously described in **Section 3.5.1.1**. The chamber was then sampled in place of the EDF flask, while the rest of the conditions around the APCI source used for EDF sampling remained the same (Set-up A, **Figure 3.27**). Once the signal for nopinone was stabilized, its concentration was calculated based on the sensitivities calculated in **Table 3.13**. Only the signal of the most abundant ion pair for nopinone (*m/z* 139/121) was used since the ketone calibration curve was based on sensitivities obtained from the single most abundant respective ion pairs.

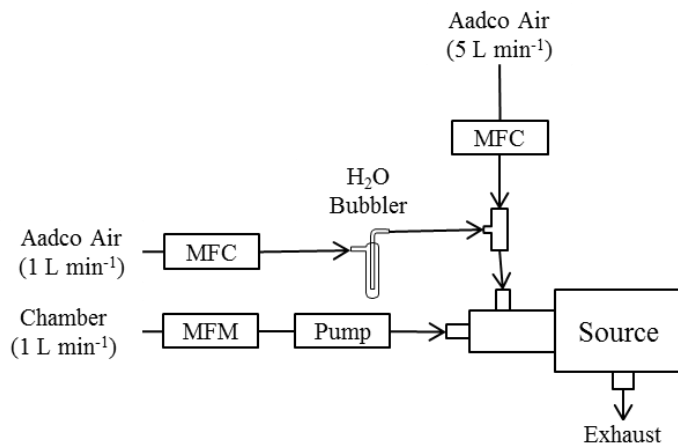


Figure 3.27 Schematic of chamber sampling set-up to test the EDF calibration results (set-up A)

Table 3.14 outlines the results of applying the sensitivities obtained to calculate the nopinone concentration based on the measured SRM signal. The range (0.2-0.5ppm) obtained from the calibration did cover the expected 0.2 ppm however the % error calculated from the calculated slope became progressively larger on tested days starting at 20% and rising up to 85%. This demonstrates that extrapolating the sensitivity from the ketone calibration curve using this sampling set-up can give some idea of the concentration values of nopinone however with very large error. There was worry that this set-up could have the same issue at the chamber set-up done with syringe pump (**Figure 3.9** in **Section 3.3.1.3**) where calibration and chamber sampling were done separately. The problem in the syringe pump case was that the sensitivity of the instrument changed during the switching between the sampling set-ups (**Figure 3.10** in **Section 3.3.1.3**) if this was also the case here with the EDF/chamber sampling then the sensitivities obtained by the EDF may have not been representative of the ones during the

chamber sampling leading to an improper conversion of signal to concentration. Therefore another sampling set-up was attempted.

Table 3.14 The signal obtained for the 0.2 ppm of injected nopinone and the concentration calculated based on the sensitivity obtained from the slope of the ketone $\ln(\text{sensitivity})$ vs. GB plot (set-up A). The concentration calculated from the upper and lower ranges (max and min) of the sensitivity are also listed.

Date	10-27-11	%Error	10-28-11	%Error	10-31-11	%Error
Relative SRM Signal (139/121)	7.47		9.35		11.5	
Sensitivity_{fit} = 217.2	0.24	20	0.30	50	0.37	85
Sensitivity_{min} = 135.0	0.39		0.48		0.60	
Sensitivity_{max} = 349.5	0.15		0.19		0.23	
Range	0.1-0.4		0.2-0.5		0.2-0.6	

3.5.2.4. Nopinone Sensitivity Accuracy Testing: Set-Up B Results

To try and minimize the change around the source conditions that could occur during the switching of the EDF and chamber sampling; the chamber sampling was integrated into the calibration. This was similar to the standard addition set-up that was used for the syringe pump calibrations (**Figure 3.11** in **Section 3.3.1.3**) the set up for the EDF flask and chamber is shown in **Figure 3.28**. In this way the chamber was sampled during the EDF calibrations and the EDF flask output was flowing when the chamber data (nopinone signal from the 0.2 ppm injection) was obtained. The full results of the calibrations are outlined in **Appendix H**. In this set-up, the slope of the ketone $\ln(\text{Sensitivity})$ vs. ΔGB was increased slightly to $0.066 \text{ mol kJ}^{-1}$ and the intercept was also increased from 2.50 to 2.80 which lead to a higher sensitivity based on the fitted

slope (**Table 3.15**). The error on the slope (σ_m) was also larger at ± 0.014 leading to a larger range of min/max sensitivities.

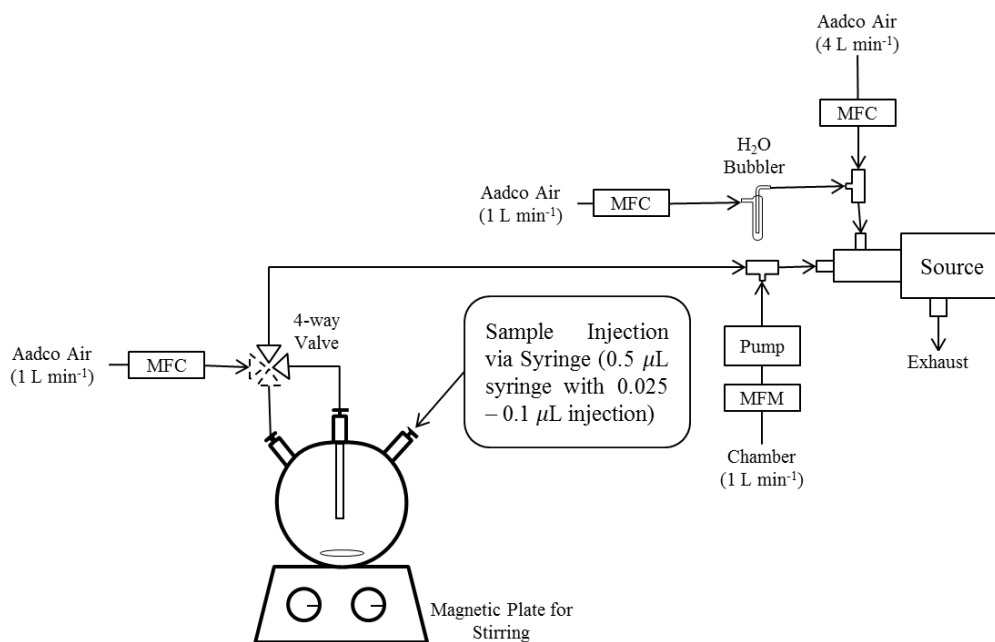


Figure 3.28 Schematic of chamber sampling set-up to test the EDF calibration results (set-up B)

Table 3.15 Calculated sensitivities of nopinone and calculated errors on the sensitivity (set-up B). The upper and lower ranges (max and min) of the sensitivity are also listed.

		Slope (mol kJ^{-1})	Sensitivity
Fit	slope (m)	0.066	314.5
Min	m - σ_m	0.052	167.8
Max	m + σ_m	0.080	589.5

When these newly calculated slopes were used to use the obtained signal from the 0.2 ppm injection, they gave improved results to the data that was obtained through set-up A (**Table 3.16**) (decrease in % error of 5-30% over the 20-85% previously calculated in **Section 3.5.2.3**) However, when additional nopinone injection tests were done with set-up B (**Table 3.17**) (days 11-2-11 to 11-7-11) the % errors were once again extremely large 75-115% and larger error range of 0.2-0.8ppm. So although this set-up B gave some minor improvement over the % error over that seen for set-up A; this improvement was not always seen and came with the additional disadvantage of having a larger error on the slope. This indicated that the ln(sensitivity) vs. Δ GB calibrations plots thus far obtained using the EDF method (using set-up A or B) cannot provide reproducible and sufficiently accurate results for nopinone. And based on the current results cannot be used to estimate the sensitivities of chamber relevant compounds based on their available or estimated GB values.

Table 3.16 The signals obtained from set-up A re-calculated with set-up B sensitivities

Date	10-27-11	%Error	10-28-11	%Error	10-31-11	%Error
<i>Set-Up A 0.2 ppm Injections re-Calculated with Set-Up B Sensitivities</i>						
Relative SRM Signal (139/121)	7.47		9.35		11.50	
Sensitivity_{fit} = 314.5	0.17	15	0.21	5	0.26	30
Sensitivity_{min} = 167.8	0.31		39		0.48	
Sensitivity_{max} = 589.5	0.09		0.11		0.14	
Range	0.1-0.3		0.1-0.4		0.1-0.5	

Table 3.17 The signal obtained for the 0.2 ppm of injected nopinone and the concentration calculated based on the sensitivity obtained from the slope of the ketone $\ln(\text{sensitivity})$ vs. ΔGB plot (set-up B). The concentration calculated from the upper and lower ranges (max and min) of the sensitivity are also listed.

Date	11-02-11	%Error	11-04-11	%Error	11-07-11	%Error
<i>Set-Up B 0.2 ppm Injections</i>						
Relative SRM Signal (139/121)	15.80		18.78		19.36	
Sensitivity _{fit} = 314.5	0.35	75	0.42	110	0.43	115
Sensitivity _{min} = 167.8	0.66		0.78		0.81	
Sensitivity _{max} = 589.5	0.19		0.22		0.23	
Range	0.2-0.7		0.2-0.8		0.2-0.8	

3.5.2.5. Possible Problems Associated with Estimation of Sensitivities from the Ketone Calibration

Both the set-ups attempted to combine $\ln(\text{sensitivity})$ vs. GB ketone graph calibrations and chamber sampling and relate APCI signal to nopinone concentration were unsuccessful. The results showed poor accuracy (high % error) and a wide range of sensitivities. There could have been several reasons of why these results were seen and these are discussed in **Section 3.5.2.5.1** and **3.5.2.5.2** below.

3.5.2.5.1 Shortcomings of Camphor as a Surrogate for Nopinone GB

The first is that the gas phase basicity of nopinone is not known and camphor was used as a surrogate to estimate this value. As seen in **Figure 3.26** the structures of the two compounds differ by one methyl group. Although there is no value reported of how much this one group would affect the GB, some idea can be gained by looking at other compounds that differ by a methyl group whose GB's are known. Some of these are

seen in **Table 3.5** in **Section 3.4**, for example cyclohexanone ($811.2 \text{ kJ mol}^{-1}$) and cycloheptanone ($815.9 \text{ kJ mol}^{-1}$). For the most part this GB difference is less than 10 kJ mol^{-1} . Unfortunately even this small difference can lead to a potentially large difference in calculated sensitivity and therefore concentration. Calculated sensitivities from these differences from camphor GB are shown in **Table 3.18**. And as seen from this a difference in GB by 10 kJ mol^{-1} can lead to an almost 50% difference in sensitivity. So despite Camphor being the closest surrogate to nopinone that has a GB reported, it could still not closely predict the nopinone sensitivity and experimental or theoretical determination of nopinone GB may be required to fully assess its actual sensitivity.

Table 3.18 Calculation of sensitivity changes with changes of GB (using set-up A data as starting comparison sensitivity)

GB Difference (kJ mol^{-1})	Sensitivity when GB Difference is <i>subtracted</i> from camphor GB (827 kJ mol^{-1})
0	217.2
2	191.3
5	158.2
10	115.3

3.5.2.5.2 Problems in the $\ln(\text{Sensitivity})$ vs. ΔGB Calibration

Some problems could also be attributed to the calibration. The first could be that the concentrations in the calibration are not accurately determined due to not knowing the exact initial concentration in the flask. As seen in **Equation 2.5** in **Section 2.2.2** the initial concentration is used to calculate the rest of the concentrations during the exponential dilution so if it is not correct, then all the concentrations are not correct. Problems with

the initial concentration could be due to sample lost during sampling in the experimental apparatus. Checking of the initial concentration was not done in these experiments but could be done in future experiments by using an additional sample introduction method (e.g. syringe pump) and comparing signals.

Another problem with the calibration was that it has a limited range of compounds. The GB of camphor is 11 kJ mol^{-1} higher than GB of cycloheptanone, which was the highest GB compound for which a calibration was done for. Camphor could not be sample by the current EDF set-up since it is a solid at room temperature and would be required to be heated or made into a solution prior to sampling. Therefore camphor's sensitivity could not be experimentally determined and compared to the calculated value from the ketone $\ln(\text{sensitivity})$ vs. GB calibration. Further modification would need to be done to the set-up or a different mode of calibration would need to be used to allow for sampling of such higher GB and often lower vapour pressure compounds so that their sensitivity could be experimentally determined. This would also show if this calibration of simple ketones is representative of more complex ketone structures.

3.5.3. Nopinone Yield Measurements

Smog chamber experiments using beta-pinene and the hydroxyl radical (HO) were done in order to obtain nopinone yields. The conditions for these experiments are outlined in **Section 2.3**. Once the reaction was initiated an experimental time profile of nopinone could be obtained using its SRM signal. Since the SRM signal m/z 139/121

was common to both the syringe pump and EDF calibrations, its signal was used and is shown in **Figure 3.29**. As mentioned earlier the beta-pinene concentration was tracked using its signal in the GC-FID instrument (**Section 2.2.3 and 2.3**).

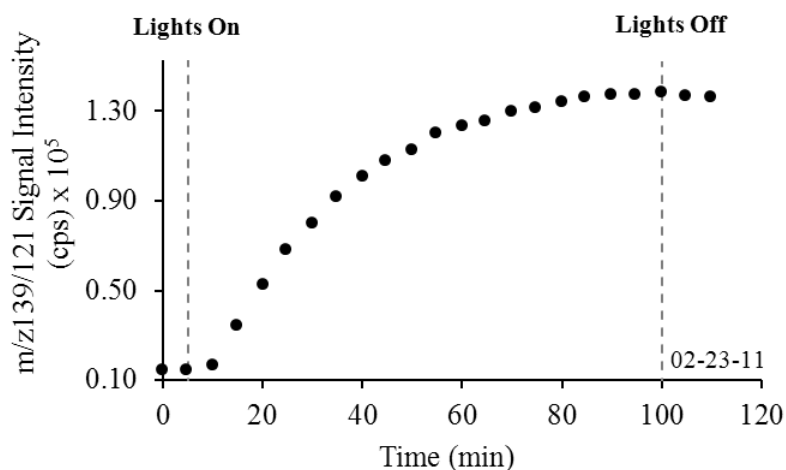


Figure 3.29 Reaction time profile of m/z 139/121 over the course of a smog chamber experiment

Once the appropriate sensitivity was applied to the generated SRM signal, then a plot was made between the nopinone amount produced and the beta-Pinene amount consumed. If a linear relationship was observed then the slope allowed the yield to be calculated using a least squares regression analysis. This slope represented the relationship outlined in **Equation 3.20**.

$$\alpha = \frac{[\text{Nopinone}]_{\text{ppm}}}{\Delta[\text{beta-Pinene}]_{\text{ppm}}} \quad \text{Equation 3.20}$$

It was noted that nopinone itself has the ability to react with HO at a rate of approximately 20% that of beta-Pinene with a rate constant of $1.4 \times 10^{-11} \text{ cm}^3 \text{ molecule}^{-1}$

$s^{-1}(k_{NP,HO})$ vs. the $7.9 \times 10^{-11}(k_{bP,HO})$ [Atkinson, 1997] for beta-pinene. For this reason a correction was made to the nopinone yield calculated. This correction was modeled based on an expression derived by Atkinson et al. (1982) and is summarized in **Equation 3.21** below. Although, nopinone can also react with the nitrate (NO_3) radical and ozone (O_3) their rate of reaction is not expected to be significant enough to contribute to extensive nopinone loss. This is because their rate constants: $k_{NP,NO_3} = 2 \times 10^{-15} \text{ cm}^3 \text{ molecule}^{-1} \text{ s}^{-1}$ and $k_{NP,O_3} = 5 \times 10^{-21} \text{ cm}^3 \text{ molecule}^{-1} \text{ s}^{-1}$ [Calogirou et al., 1999] are lower than that with HO and their concentration is expected to be very low over the course of the reaction time frame of these experiments.

$$\alpha_{\text{corrected}} = F * \alpha$$

Equation 3.21

$$\text{Correction Factor (F)} = \left(\frac{k_{bP,HO} - k_{NP,HO}}{k_{bP,HO}} \right) \left(\frac{1 - ([bP]_t/[bP]_0)}{([bP]_t/[bP]_0)^{k_{NP,HO}/k_{bP,HO}} - ([bP]_t/[bP]_0)} \right)$$

3.5.3.1. Nopinone Yield Measurements Using the Syringe Pump Calibration Method

For nopinone yields obtained using the syringe pump calibrations, the nopinone concentration was measured in the same way as was done for the 0.2 ppm nopinone injections in **Section 3.5.1.1** during the course of the chamber reaction. Since the calibration sensitivity obtained would be used to calculate the nopinone throughout the course of the reaction it was important to see if there were any major influences of the matrix on the instrument sensitivity toward nopinone over the entire course of the reaction time. For this reason two calibrations were done. One calibration was done prior to the experiment, using output from a flushed chamber. And a second calibration

was done after the chamber lights were turned off, 90 minutes into the chamber experiment reaction. As seen in **Figure 3.29** turning off the lights stopped reactions involving nopinone and beta-pinene resulting in a fairly stable background signal required for the calibration.

Table 3.19 Slopes from standard addition syringe pump calibrations from chamber experiments

Date	2-14-11	2-23-11	2-28-11
1 st Calibration	522	561	484.0
2 nd Calibration	534	531	481.0
% Difference between 1 st and 2 nd calibrations	2	5	1
*2 nd calibration slope used in the yield calculation			

As shown in **Table 3.19** there were minor changes (5% or less) in sensitivity between the two calibrations indicating that the matrix had minor influences on the instrument sensitivity toward nopinone. This is similar to the results seen by Herrera et al. (2008) as they investigated matrix effects on compounds of different proton affinities and found that matrix effects for compounds with high proton affinities and therefore high sensitivities were minor.

A plot was made between the nopinone produced and the beta-Pinene consumed (**Figure 3.30**) and showed a good linear relationship between the two variables; this allowed the yield to be calculated using a least squares analysis for the slope of the line representing this relationship as described in **Section 3.5.3**. (**Equation 3.20** and **Equation 3.21**).

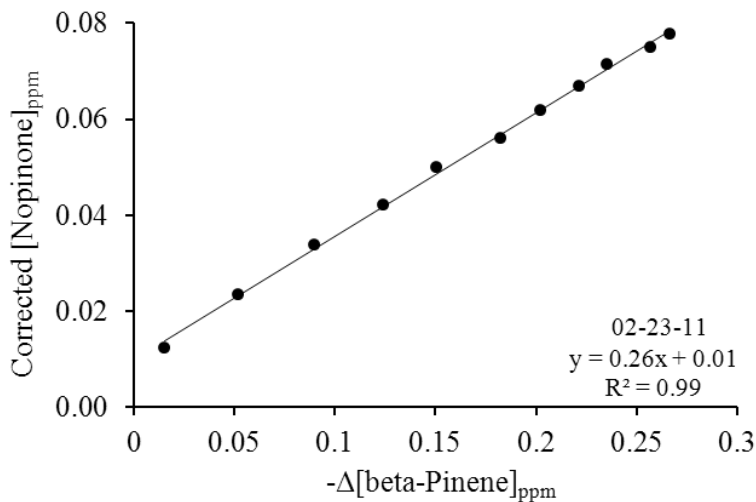


Figure 3.30 Plot of nopinone formed, corrected for the reaction with HO radical plotted against beta-pinene consumed

The yields obtained on different days of these experiments are shown in **Table 3.20**. There were some variations among the results obtained for the different nopinone pairs used. The best agreement between the different experiment days was shown by SRM pair m/z 139/121. While SRM pairs m/z 157/139 and 157/121 showed slightly more variation between experiment days and amongst themselves; perhaps resulting from minor contributions to the pairs from other species. The errors in the yields do not cover the observed differences between the days but these could also be due to slightly varying daily instrument sensitivities (**Table 3.19**). Overall the average yield obtained was $24 \pm 5\%$.

Table 3.20 Nopinone product yields (%) using syringe pump calibrations

Date	2-14-11	2-23-11	2-28-11	Average	Standard Deviation
<i>m/z</i> 139/121	23 ± 0.3	26 ± 0.4	26 ± 0.2	25	2
<i>m/z</i> 157/139	19 ± 0.3	30 ± 0.2	27 ± 0.3	25	6
<i>m/z</i> 157/121	16 ± 0.3	28 ± 0.2	25 ± 0.3	23	6
				24 ±	5

*Errors on the yield are based on the error on the regression fit of the sensitivity of the Corrected [Nopinone]_{ppm} vs. -Δ[beta-pinene]_{ppm} graph

3.5.3.2. Nopinone Yield Measurements Using Sensitivities of ln(Sensitivity) vs. ΔGB Graph of Ketones

Even though **Sections 3.5.2.3** and **3.5.2.4** showed that the ketone graph of lnS vs. ΔGB did not give particularly accurate results in predicting nopinone concentrations, yield measurements were still attempted to see the range that would be obtained. Since set-up B gave lower errors in predicting the nopinone concentration it was used for the yield measurements. The yield measurements were obtained in the same way as described in **Sections 3.5.3** and **3.5.3.1** except the nopinone concentration was calculated with the sensitivity of EDF set-up B calibrations (**Table 3.15**). **Table 3.21** summarizes the yield results obtained. It shows that the average yield from the regression fit sensitivity was $72 \pm 6\%$. An average range of 40-140% yield was obtained taking into account the errors of the fitted slope. This is much higher than the yield results obtained through the syringe pump calibrations (**Section 3.5.3.1**), unrealistically high values of greater than 100% yields and a very wider range of error on the yield.

Table 3.21 Nopinone product yields (%) obtained from the sensitivities of the ln(sensitivity) vs. ΔGB graph of ketones

Date	11-02-11	11-04-11	11-07-11	11-11-11	Average	Standard Deviation
Sensitivity _{fit} = 314.5	65	67	77	80	72	6
Sensitivity _{min} = 167.8	122	125	144	151	135	12
Sensitivity _{max} = 589.5	35	35	41	43	39	3
Range	40-120	40-130	40-140	40-150	40-140	

3.5.3.2.1 Estimation of Instrument Sensitivity and Yield Calculation from a One-Point Calibration

There was an opportunity to do a one-point calibration immediately following the completion of a beta-pinene/HO chamber experiment. In this calibration, an injection of 0.2 ppm of nopinone was made into the chamber to measure the instrument response to the known concentration injection (visually show in **Figure 3.31**). This was used to give an idea of how much the nopinone yield was overestimated by the ln S vs. ΔGB calibration method. To get the yield, **Equation 3.22** was used to calculate the instrument sensitivity. Using this sensitivity, the nopinone (corrected) concentration was estimated throughout the course of the beta-pinene reaction. The yields calculated in this manner are summarized in **Table 3.22**. The average calculated yield was $35 \pm 3\%$. This yield value is much lower than those estimated by the lnS vs. ΔGB and is only moderately higher than that of the syringe pump calibration method (**Table 3.20**). This calibration may have been a better determinant of the yield over the ln S vs. ΔGB calibrations since this calibration, like the syringe pump standard addition calibrations (**Section 3.5.3.1**), was done directly following the completion of the beta-pinene/HO chamber experiment,

so it was more likely to be applicable. This is in contrast with the $\ln S$ vs. ΔGB calibrations which may not sufficiently account for the day to day variation in instrument sensitivity. This is also in addition to the problems identified for the $\ln S$ vs. ΔGB calibrations in **Section 3.5.2.5** that could also explain the incorrect yield results.

$$\frac{\text{observed relative SRM signal } (m/z 139/121) \text{ for theoretical 0.2ppm injection}}{\text{theoretical injection concentration (0.2ppm)}} = \frac{\text{observed relative SRM signal } (m/z 139/121) \text{ during a chamber experiment}}{\text{corrected [nopinone]_{ppm} during a chamber experiment}} \quad \text{Equation 3.22}$$

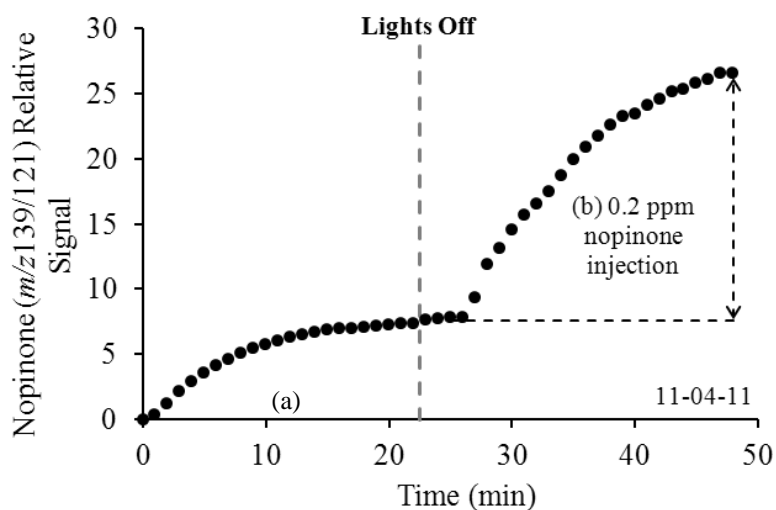


Figure 3.31

- (a) Nopinone (m/z 139/121) relative signal over the course of a beta-pinene chamber experiment
- (b) Nopinone (m/z 139/121) relative signal after a 0.2ppm injection into the chamber (with the lights off)

Table 3.22 Nopinone product yields (%) obtained from the instrument response to a 0.2 ppm nopinone injection following a beta-pinene chamber experiment

Date	11-02-11	11-04-11	11-07-11	Average	Standard Deviation
Relative SRM signal					
<i>m/z</i> from 0.2 ppm	15.8	18.8	19.4		
Injection into Chamber					
Estimated Yield (%)	37	32	36	35	± 3
Error on Estimated	0.7	0.3	0.5		

*Errors on the yield are based on the error on the regression fit of the sensitivity of the Corrected [Nopinone]_{ppm} vs. -Δ[beta-pinene]_{ppm} graph

3.5.3.3. Comparison to Literature Reported Gas Phase Nopinone Yields

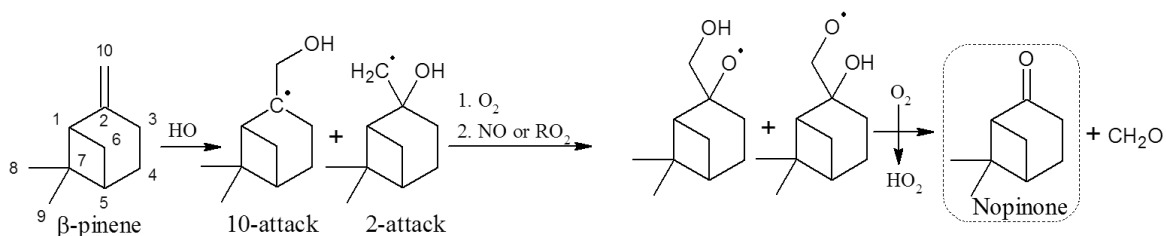
The nopinone gas phase yields reported in literature are summarized in **Table 3.23** and center around 25% with the yield reported by Lee et al. (2006) at 17% on the lower end and the 78% reported by Hatakeyama et al. (1991) being much higher than the rest. Larsen et al. (2001), Jaoui et al. (2001) and Wisthaler et al. (2001) speculated that the results by Hatakeyama et al. (1991) are overestimated due to the poor selectivity that can be displayed by the FT-IR measurement technique and possible interferences by other carbonyl species at the absorption band of 1700 cm⁻¹ used. In fact Wisthaler et al. (2001) did simultaneous PTR-MS and FT-IR nopinone yield measurements. Although yield numbers for the FT-IR were not reported; they did find that during the first 10 minutes of the reaction the nopinone concentration measured by the FT-IR was a factor of 2-3 times higher than that measured by the PTR-MS. In addition, the PTR-MS showed peaks that could correspond to carbonyl compounds (not identified) in the early part of the reaction that could explain the FT-IR observations. However, the yield by Hatakeyama et al.

(1991) still gets mentioned due to the fact that the majority of reported beta-pinene/HO reaction mechanisms (Master Chemical Mechanism (MCM)) state that nopinone is the first formed major product, as well as, being the starting point for many other second generation products (e.g. pinic acid). Since the initial reaction of HO with beta-pinene is proposed to occur through the addition of HO to the double bond (Atkinson 1989), which is followed by a series of reactions that favour the formation of nopinone. This is shown visually in **Figure 3.32**.

The yields found in this study are also shown in **Table 3.23**. Both the yields obtained from the syringe pump calibration and estimated from the instrument sensitivity towards the 0.2 ppm injection are in general agreement with the other nopinone yields reported in literature. From the results seen (**Sections 3.5.2.3** and **3.5.2.4**) it was expected that the results from the EDF/lnS vs. Δ GB ketone calibrations were to be higher than the other yield results.

Table 3.23 Literature reported gas phase nopinone yields

Yield (%)	HO Source	Method	NOx Level	Reference
78 ± 8	H ₂ O ₂	FT-IR	varied	Hatakeyama et al. 1991
25 ± 5	H ₂ O ₂	FT-IR	ppt	Larsen et al. 2001
25 ± 3	CH ₃ ONO	PTR-MS	low ppm	Wisthaler et al. 2001
17	HONO	PTR-MS	varied	Lee et al. 2006
27 ± 0.04	CH ₃ ONO	GC-FID	low ppm	Hakola et al. 1994
30 ± 5	CH ₃ ONO	GC-FID	low ppm	Arey et al. 1990
<i>This Study</i>				
24 ± 5	IPN	APCI-MS/MS	low ppm	Syringe pump calibration
72 ± 6	IPN	APCI-MS/MS	low ppm	Sensitivity from ketone lnS vs. ΔGB graph
35 ± 3	IPN	APCI-MS/MS	low ppm	Estimated from instrument sensitivity to 0.2 ppm injection

**Figure 3.32** Proposed nopinone formation mechanism [MCM]

3.5.4. Applying Calibrations to Evaluate Concentration from Signal and Determining Yields

The two calibration methods developed in this study were tested for their ability to accurately determine the concentration of nopinone, a chamber reaction relevant compound, from its SRM signal. Syringe pump calibrations, although the more time consuming of the two methods, were able to predict the concentration of an injected 0.2 ppm nopinone concentration in the chamber with reasonable accuracy (**Section 3.5.1**). These calibrations also gave yield results that were consistent with previously reported literature values (**Table 3.23**).

On the hand the calibration results, in which the sensitivity of nopinone was determined from the ketone $\ln(\text{sensitivity})$ vs. ΔGB calibration (**Figure 3.21**) and the GB of camphor, were less positive. In both nopinone chamber sampling set-ups attempted, (**Section 3.5.2.3** and **3.5.2.4**) the accuracy results were poor with high percent errors calculated when comparing the concentration obtained from the calibration to the actual injected nopinone concentration of 0.2 ppm (**Table 3.14**, **Table 3.16** and **Table 3.17**). As expected from the accuracy testing results, this calibration approach also gave yield results that deviated from reported literature data (**Table 3.23**). A few problem areas were identified with implementation of the $\ln(\text{sensitivity})$ vs. ΔGB calibration approach, which are summarized in **Section 3.5.2.5** and are left to be addressed in the future.

4. Conclusions

There were two main objectives in this study. The first was to replace the older APCI-MS/MS instrument, TAGA 6000E, with the newer API 365. This meant establishing an effective smog chamber and other analyte sampling system with the API 365 and the testing of consistency between previously gained TAGA 6000E data with that acquired by the new instrument. The second objective was to establish a quantitative data acquisition method to be eventually incorporated into chamber experiments to enrich our data and knowledge gained from these experiments, as well as, to increase the general usefulness of the APCI-MS/MS for future experiments. This additional quantitative information would allow us to calculate product yields that pertain to our experimental conditions, potentially obtain product distributions in both the gas and particle phase and gain a better understanding of the instrument's sensitivity toward different classes of compounds.

4.1. Qualitative Data Acquisition

The replacement of the TAGA 6000E with the API 365 APCI-MS/MS ran into some initial issues (**Section 3.1.1**). First was the fact that the API 365 instrument APCI ion source, unlike the TAGA 6000E, was not isolated from the external lab environment. This created problems since our set-up relied heavily on controlled airflow movement in the ion source which was not only important in sampling analyte ions but also in consideration for future planned quantitative experiments where the accurate knowledge of source analyte concentration was vital. Additionally, contamination from lab air was observed. This problem was attributed to the fact that the API 365 is designed to be used

primarily with an ESI ion source in which analyte ion movement is mostly controlled via an electric field between the ESI capillary needle tip and the curtain plate (**Section 3.1.1.1**); while the APCI source was added as a post-production accessory. The solution to this problem was to place an EPDM rubber cord in lieu of a “real” O-ring in the leaking area that was identified in the interface region of the instrument (**Figure 3.2**).

The second issue was the previous use of an in-line quartz fiber filter prior to the sample entering the ion source. This filter was used to remove particle phase products prior to gas phase sampling by the APCI-MS/MS. However, experiments done by the API 365 without the in-line filter revealed that the filter contributed to delays to SRM time profiles of some beta-pinene/HO chamber reaction products (**Figure 3.3**). This observation was attributed to previously reported issues with Teflon filter adsorption [Kirchstetter et al., 2001] (**Section 3.1.1.2**). Due to this problem, the filter was not be used in the gas phase chamber sampling by the API 365 described here. The APCI source’s ability to only ionize gas phase analytes, as well as the operation of the ion source at room temperature, was decided to be sufficient in separating products in the two phases.

The proper sealing of the APCI ion source of the API 365 and the elimination of the in-line Teflon filter during gas phase smog chamber sampling allowed qualitative data acquisition. Several beta-pinene/HO chamber reaction relevant compounds, which were qualitatively characterized by the TAGA 6000E APCI-MS/MS, were also able to be defined by similar terms with the API 365 (summary in **Table 3.2**) and therefore further work (e.g. quantification) could be done.

4.2. Quantitative Data Acquisition

Once the API 365 was properly equipped to sample the desired analytes and was successfully tested for its ability to give qualitative experimental data, experimental set-ups were developed to establish calibration procedures to obtain quantitative data.

4.2.1. Compound Specific Calibrations

Quantification in the APCI-MS/MS instrument posed some problems since the relationship between concentration and instrument signal deviated from linearity in the positive ion ionization mode (**Section 2.1.1**) when too much of the protonating reagent ($((M+H)(H_2O)_m)^+$) was depleted (i.e. at higher analyte concentrations) Sunner et al. (1988a,b), (**Section 3.2**). It was found that to get around this issue the ion signal that is related to the analyte of interest had to be plotted as a signal that is relative to the signal(s) of the protonating reagent ions ($((M+H)(H_2O)_m)^+$). An expression was derived to relate this relative signal to analyte concentration to be used in calibrations (**Equation 3.4**).

Initial calibration attempts were designed to be compound specific. Two compounds that were representative of products seen for the beta-pinene/HO reaction in the chamber were chosen; these were nopinone (for gas phase products) and pinic acid (for particle phase products). In these calibrations the variable concentration of analyte introduced into the APCI-MS/MS was controlled via the introduction of the analyte in liquid form with a syringe pump into an Aadco air stream. For nopinone both a methanol solution and pure nopinone was tested in the syringe. It was found that the methanol solution gave inconsistent results between trials and therefore only the pure nopinone was

used in future trials (**Section 3.3.1.1** and **Section 3.3.1.2**). Consistent calibrations could be achieved with the pure nopinone and syringe pump but two set-ups had to be attempted when the calibration was incorporated with chamber sampling (**Section 3.3.1.3**). The first set-up (**Figure 3.9**) involved the calibration being done with one set-up and then a different set-up for chamber sampling was used. It was found that with this set-up that calibrations done before and after chamber sampling produced different sensitivities; making it difficult to know the sensitivity during chamber sampling (**Figure 3.10**). For this reason a second set-up was attempted (**Figure 3.11**). In this set-up calibration and chamber data acquisition was done using the same sampling set-up. In this set-up the calibrations were done in a standard addition manner (**Figure 3.12**). This manner of calibrations gave much more consistent sensitivities and was used for subsequent experiments involving syringe pump calibrations and the chamber.

The calibration set-up was less successful when dealing with lower vapour pressure compounds like pinic acid. These compounds are solid at room temperature and had to be dissolved in water prior to utilization in the syringe pump. They needed to be heated to effectively get them into the gas phase and diluted with air and introduced into the APCI ion source. However, despite best attempts to use variable syringe types, flow rates and heated sampling set-ups to encourage effective sample evaporation into the gas phase, a stable, usable signal in the APCI-MS/MS could not be consistently seen. An effective calibration set-up for these lower vapour pressure products was not found in these experiments.

4.2.2. General Instrument Sensitivity Evaluation

The other calibration attempt was to get an idea of the general APCI-MS/MS instrument sensitivity. An attempt was made to relate gas phase basicity (GB), a quantity that is either available in literature or is calculated, to instrument sensitivity. GB, measured in kJ mol^{-1} , is the negative free energy change of the proton transfer reaction in **Reaction 3.5**. The GB of an analyte needs to be higher than that of protonated water and its clusters $((\text{M}+\text{H})(\text{H}_2\text{O})_m)^+$, in order for the analyte to undergo proton transfer and form positive quasimolecular ions in the APCI ion source. The higher the GB of a compound, the greater its ability to compete with other analytes in the source for available protonating reagents and therefore compounds with higher GB's have higher sensitivities. An expression was derived to relate GB and sensitivity which can be summarized as: $\ln(\text{sensitivity})$ vs. ΔGB (where $\text{sensitivity} = \text{relative sensitivity} = \frac{\text{relative signal}}{\text{concentration}}$) and $\Delta\text{GB} = \text{GB}_{\text{compound}} - \text{GB}_{\text{ref}}$ where ref = acetone for ketones and ref = methanol for alcohols or alcohol/ketone calibrations ; **Section 3.4.1**).

To test this GB and sensitivity relationship; simple (seven alcohols and six ketones) compounds were chosen since beta-pinene/HO reaction relevant compounds were of higher functionality and often without literature reported GB values. The individual calibrations for these compounds were done using the exponential dilution flask (EDF) method (**Section 2.2.2**) rather than syringe pump since this method has the ability to generate many calibration points in a short amount of time. After some adjustments all thirteen compounds had calibration curves with R^2 values greater than

0.99; indicating good linearity in the calibration. The $\ln(\text{sensitivities})$ for the alcohols and ketones were plotted relative to ΔGB . Unfortunately the linearity of this calibration was relative poor ($R^2 = 0.76$) but greatly improved when the alcohol and ketones were plotted on separate graphs ($R^2 = 0.97$ for alcohols and $R^2 = 0.90$ for ketones). These two graphs were thought to be of use individually for compounds of those two unique functionalities.

4.2.3. Calibration Accuracy and Yield Testing

The accuracy and yield measuring abilities of the individual compound, syringe pump calibrations and the EDF based general instrument sensitivity calibrations using the $\ln(\text{sensitivity})$ vs. ΔGB relationship, were tested. For the testing, a known amount of nopinone (0.2 ppm) was injected into the smog chamber and the relative ability of the calibrations to predict this concentration from the measured APCI-MS/MS SRM signal was studied. The yield measurements were done by following the nopinone SRM signal over the course of a chamber beta-pinene/HO experiment and applying the calibration to predict the yield.

The syringe pump calibrations were able to predict the injected 0.2 ppm of nopinone with fairly good accuracy (0-35%) (**Table 3.11**). This was with the exception of the SRM pair that represented the dimer ion of nopinone (m/z 277/139); which gave very inconsistent results and was deemed not suitable to be used as a signal in calibrations at this time (**Section 3.5.1.2**). The syringe pump calibrations had an average yield result of $(24 \pm 5)\%$ which was generally consistent with the majority of previously reported literature yields (17-30 %) (**Table 3.23**).

For the $\ln(\text{sensitivity})$ vs. ΔGB calibration, the application of the calibration was a bit more complicated. Firstly, it was found that the sensitivity of nopinone could not be measured using the EDF calibration method due to its higher polarity and lower volatility relative to other compounds sampled in the calibration (**Section 3.5.2.1**). To deal with this, its sensitivity was estimated from the ketone $\ln(\text{sensitivity})$ vs. ΔGB graph since it has ketone functionality. Additionally, the GB of nopinone was not reported in literature and a surrogate had to be used for its GB. The closest found surrogate was camphor with a GB of 827 kJ mol^{-1} (**Figure 3.26**).

The accuracy testing for this $\ln(\text{sensitivity})$ vs. ΔGB calibration was done using two different set-ups. In one set-up the calibration and chamber sampling was done separately while in another set-up both were done in the same assembly. These tests showed that these calibrations, regardless of set-up, did an insufficient job of predicting nopinone concentration, with percent error values ranging from an acceptable 5% to the in-majority, unusable greater than 50% error. Not surprisingly, the yield results deviated from previously reported literature data with an average value of $(72 \pm 6)\%$ and with some individual yield results exceeding 100%. Some points of concern for these type of calibrations were identified (**Section 3.5.2.5**) and perhaps if addressed could make these calibrations more feasible in the future.

5. Future Work

5.1. Low Vapour Pressure Compound Calibrations

In this work there were successful set-ups achieved for the calibrations of higher vapour pressure compounds. Syringe pump calibrations were done for nopinone and methanol (**Section 3.3.1.1**) and these results showed promise for other compounds of similar volatility. The exponential dilution flask (EDF) calibrations experienced difficulty in calibrating for nopinone (**Section 3.5.2.1**) but were successful for a variety of other higher volatility compounds (**Section 3.4.2.1**). However, as seen for unsuccessful syringe pump calibration attempts for pinic and pinonic acid (**Section 3.3.2**) (lower vapour pressure compounds) other means of analyte introduction should be explored for future calibration attempts for these types of compounds. Being able to calibrate for low vapour pressure compounds would allow quantitative information regarding particle phase products from chamber reactions to be obtained. Two alternative sample introduction set-ups are suggested for future use here: a diffusion tube and a heated nebulizer.

5.1.1. Diffusion Tube Sample Introduction

One low cost set-up that could be used for low vapour pressure compound calibrations is the use of a diffusion tube. An example of a diffusion tube is shown in **Figure 5.1**. It is a set-up that is well suited for low vapour pressure liquid or solid analytes that are available in their pure form. For calibrations the set-up needs to be kept under stringent temperature control (within 0.1 °C); so that a constant vapour source can be achieved in the analyte reservoir [McKinley et al., 2010]. A large partial pressure

difference is maintained between the reservoir and capillary outlet by having a dilution gas flow pass over the precision bore capillary opening. With this pressure difference, and provided the sides of the capillary are kept very clean, the vapour from the reservoir can travel with a consistent diffusion rate up the capillary and into the dilution gas flow to proceed to be used in a calibration. The emission rate from the diffusion tube is defined by the diffusion coefficient, compound molecular weight, total pressure, vapour partial pressure, temperature, capillary tube cross section and diffusion path length. This emission rate is estimated using equations in **Appendix J (Equation J.1, Equation I.2 and Equation I.3)** [Nelson, 1971]. However, accurate emission rate information is determined gravimetrically by weighing the diffusion tube periodically after it has operated at steady operating conditions. To calculate this Equation I.4 is used [McKinley et al., 2010].

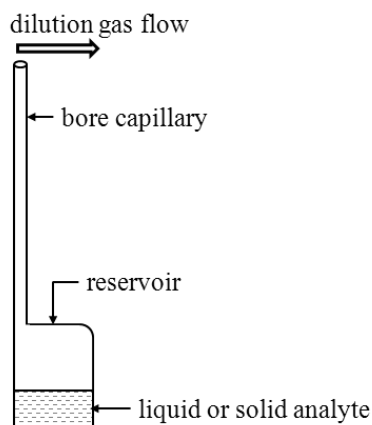


Figure 5.1 Schematic of a diffusion tube

5.1.2. The Use of a Heated Nebulizer

The heated nebulizer as was briefly mentioned in **Section 3.3.2.1**, is another way that calibrations with the APCI-MS/MS could be attempted for lower vapour pressure compounds. One such heated nebulizer comes as an accessory with the API-365 and is shown in **Figure 5.2**. In this set-up a liquid or a liquid in a solution (e.g. of water or methanol) is introduced into the set-up via liquid injection into a stainless steel capillary with a small internal diameter (e.g. 120 μm). The liquid is pumped through the capillary and is met at the tip by a nebulizing (NEB) gas (e.g. N_2). The capillary and the nebulizing gas are also enclosed in a quartz tube that is heated and contains an auxiliary (AUX) gas (e.g. N_2 or Aadco air). The combination of an appropriate solvent, flow rate, nebulizing gas and temperature help the sample exiting the capillary disperse into a fine mist. This mist mixes with the auxiliary gas and ideally proceeds as a gas phase analyte to be ionized in the corona discharge region (**Figure 2.1**). In contrast to the heated set-up that was attempted with the syringe pump in **Section 3.3.2** (**Figure 3.14**) in this set-up the heater, nebulizing and auxiliary gases aid with the transfer of the solution into the gas phase. Also, the sample gets heated very close to the ionization region so there is less chance of temperature gradients and sample loss as might have been the case in the set-up of **Figure 3.14**.

Although not discussed here in detail, calibration attempts with this heated nebulizer (**Figure 5.2**) were briefly attempted in this study. The problems that were found with this particular nebulizer were that the flow rates (of liquid and gases) did not allow for the generation of calibrations in the appropriately low concentration ranges. The liquid input

for this nebulizer is meant to come from an LC (liquid chromatography) column at flow rates of $200 \mu\text{L min}^{-1}$ to 1 ml min^{-1} . Pure and dilute solution sample introduction attempts via syringe pump at flow rates out of the above range were unsuccessful. This was in addition to the fact that this particular nebulizer was heavily contaminated from previous use and cleaning attempts with solvents and heating did not improve the conditions; making calibrations difficult in the face of a large number of contamination peaks.

However, this technique is a valid approach for low vapour pressure compound calibration attempts in the future. Similar set-ups have been used in studies (e.g. Warscheid et al. (2001) and Hoffmann et al. (2002)) for these types of analytes. If modifications could be made to the nebulizer in **Figure 5.2** or if a set-up with similar components could be developed; then it could very plausibly be integrated for use in the acquisition of quantitative, chamber particle phase APCI-MS/MS data.

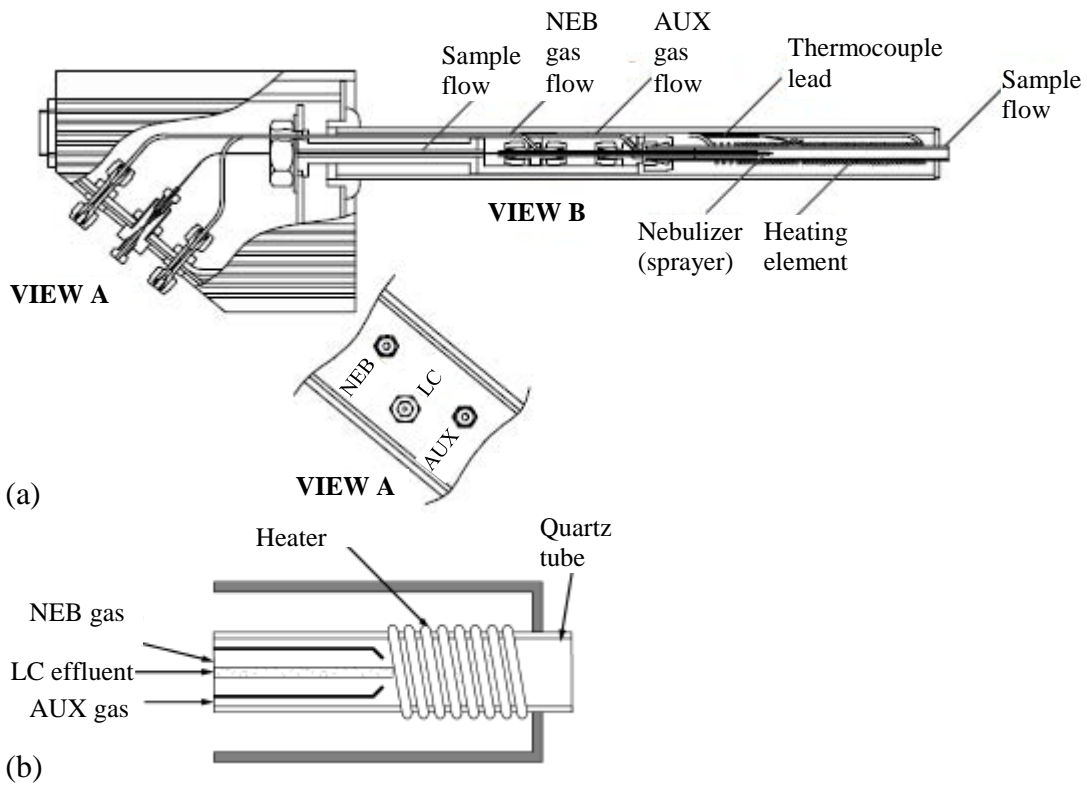


Figure 5.2

(a) Heated nebulizer probe cross section

(b) Close up schematic of tip of heated nebulizer

(Figure from: PE Sciex API System Reference Manual)

5.2. More work on $\ln(\text{Sensitivity})$ vs. $\Delta\text{Gas Phase Basicity (GB)}$ Calibrations

Another area that could be explored in the future is the further development of the $\ln(\text{Sensitivity})$ vs. ΔGB calibration curves for the evaluation of the general sensitivity of the API-365 instrument discussed in this work. The results seen in **Section 3.5.2.3** and **Section 3.5.2.4** do reveal that these calibrations show poor accuracy when used to predict the sensitivity of a chamber beta-pinene/HO reaction product (nopinone). However, the calibrations for both the sampled simple alcohols and ketones (**Table 3.6**) did show good linearity (**Figure 3.20** and **Figure 3.21**) and the experimental determined sensitivities agreed fairly well with the sensitivities predicted by the calibration (**Table 3.9** and **Table 3.10**). Several points of further work were identified in regards to these calibrations (**Section 3.5.2.5**).

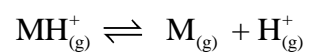
The first is that the individual compound sensitivities in these calibrations were obtained using the EDF method (**Section 2.2.2**). This method relies heavily on having an accurate knowledge of the initial analyte concentration in the flask since all other concentrations over the exponential decay are calculated based on this value (**Equation 2.5**). In this work these initial concentrations were not checked but could be done in the future by using an additional calibration method (e.g. using a syringe pump) to check for agreement in sensitivity results.

Secondly these calibrations were done using simple compounds having a single functionality in order to do initial tests to this $\ln(\text{sensitivity})/\Delta\text{GB}$ relationship. This relationship could be better defined by including additional simple (straight chained, small branched, single ringed, etc.) compounds to the calibration curve(s). As well as,

expanding it further and including more complicated reagents (e.g. more branched linear structures; single or multi ringed compounds with alkyl group substituents or bridged structures). And continue building up these calibrations with the goal to ultimately to include more chamber reaction relevant and multifunctional compounds.

Lastly, these calibrations depend on knowledge of the compound GB in order for its sensitivity to be estimated from $\ln(\text{Sensitivity})$ vs. ΔGB calibration curves. Unfortunately, experimentally determined GB values of most beta-pinene/HO reaction products are not reported in the literature. And although it is beyond the scope of this work it would be of interest to be able to calculate these values and one could explore sources/individuals that could be collaborated with in order to do this. The proton affinity (PA) or GB values of compounds could be theoretically determined with computational means in several ways. Most of these approaches use Gn (Gaussian) methods. Depending on the computation time and memory requirements, these approaches can have varying accuracies [Bouchoux, 2007]. But in general these methods take a basis set (the 6-311G(*d,p*) basis set is commonly used [Curtiss et al., 1991]) to describe molecular orbitals and have the electrons non-correlated (e.g. self-consistent field (SCF) method) or correlated (Møller-Plesset (MP) theory). With this orbital and electron information, the molecule equilibrium geometry, followed by its electronic and vibrational energies can be calculated. The information could then be further applied to calculate several parameters including individual heats of formation. For example, the heats of formation of the species in **Reaction 5.1**, where M is the analyte of interest could

be calculated [Nicolaidis et al., 1996]. These individual heats of formation could be used to calculate proton affinity (PA) and GB (**Section 3.4.1**):



Reaction 5.1

Appendix A. Calibration Compounds Information

Table A.1 SRM pairs used to calibrate compounds

Compound	Nominal Mass (<i>u</i>)	Precursor/Product ion pairs	Precursor/Product ion pairs	Precursor/Product ion pairs	Precursor/Product ion pairs	Precursor/Product ion pairs	
Suspected identity of the precursor ion		[M+H] ⁺	% [*]	[M+H+H ₂ O] ⁺	% [*]	[M ₂ +H] ⁺	% [*]
Methanol	32	33/15	-	51/33	<u>97</u>	65/47	29
Ethanol	46	47/29	41	65/47	<u>46</u>	93/57	13
n-Propanol	60	61/43	21	79/43	<u>42</u>	121/43	37
2-Propanol	60	61/43	<u>39</u>	79/43	31	121/103	30
n-Butanol**	57	57/41	<u>52</u>	93/57	42	149/57	6
t-Butanol**	57	57/41	<u>57</u>	93/57	36	149/57	7
Acetone	58	59/41	<u>71</u>	77/59	7	117/59	22
Cyclopentanone	84	85/67	<u>54</u>	103/85	34	169/85	12
2-Pentanone	86	87/45	<u>67</u>	105/87	7	173/87	26
3-Pentanone	86	87/45	<u>83</u>	105/87	4	173/87	13
Cyclohexanone	98	99/81	<u>52</u>	117/99	8	197/99	40
Cycloheptanone	112	113/95	<u>65</u>	131/113	5	225/131	30

*Where the % is the relative abundance of the ion from the three most abundant observed ions (unless specified, the SRM ion pair with the highest relative abundance (%) (bold/underlined) was used in the calibrations)

** the pair used for these is *m/z* 57/41 with a suspected identity of [M+H-H₂O]⁺ since 75/57 ([M+H]⁺) had minimal detectable signal

Table A.2 SRM pairs followed for pinonic and pinic acid calibrations (CE 10)

<i>m/z</i> of precursor/product ion pairs	Mass loss (<i>u</i>) from precursor	Suspected identity of the observed precursor ion and its mass loss
Pinonic Acid Pairs (M= nopinone with nominal mass of 184 <i>u</i>)		
185/167	-18	[M+H] ⁺ with (1 x H ₂ O) loss
185/139	-46	[M+H] ⁺ with <i>m/z</i> 46 loss
Pinic Acid Pairs (M= nopinone with nominal mass of 186 <i>u</i>)		
187/169	-18	[M+H] ⁺ with (1 x H ₂ O) loss
187/141	-46	[M+H] ⁺ with <i>m/z</i> 46 loss

Appendix B. Calculation of Analyte Concentration at the APCI Ion Source

Parameters Used

pressure = 1 atm

temperature = 273.15 K

gas constant = 0.0821 L atm mol⁻¹K⁻¹

$$\text{Aadco air}_{\text{mol min}^{-1}} = \frac{\text{pressure}}{\text{temperature} \times \text{gas constant}} \times \text{Aadco air flow rate} \quad \text{Equation B.1}$$

$$\text{analyte}_{\text{mol min}^{-1}} = \frac{\text{density}}{\text{molecular weight}} \times \text{syringe pump flow rate} \quad \text{Equation B.2}$$

$$\text{analyte concentration}_{\text{ppm}} = \frac{\text{analyte}_{\text{mol min}^{-1}}}{\text{Aadco air}_{\text{mol min}^{-1}}} \times 10^6 \quad \text{Equation B.3}$$

$$\text{concentration at the source} = \text{analyte concentration}_{\text{ppm}} \times \text{dilution factor} \quad \text{Equation B.4}$$

$$\text{dilution factor}_{\text{based on the input flows at the ion source (* point in Figure B.1)}} = \quad \text{Equation B.5}$$

$$\frac{\text{flow of analyte input}}{\text{flow of analyte input} + \text{total dilution input}}$$

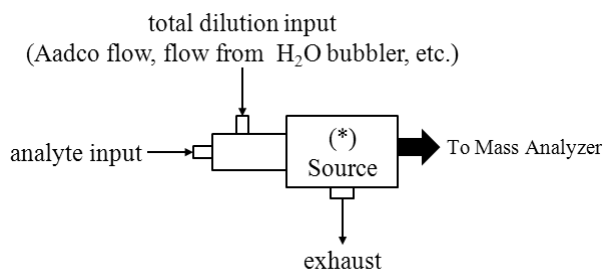


Figure B.1 APCI source flow inputs and (*) as the area in the source at which concentration calculated for use in calibrations

*****The concentrations stated were estimated to have an error of 10-15% due to errors in factors such as the syringe volume, syringe pump rate, Aadco flow rate, operator error, etc.**

Appendix C. Other Instrument Data from beta-Pinene/HO Chamber Experiments

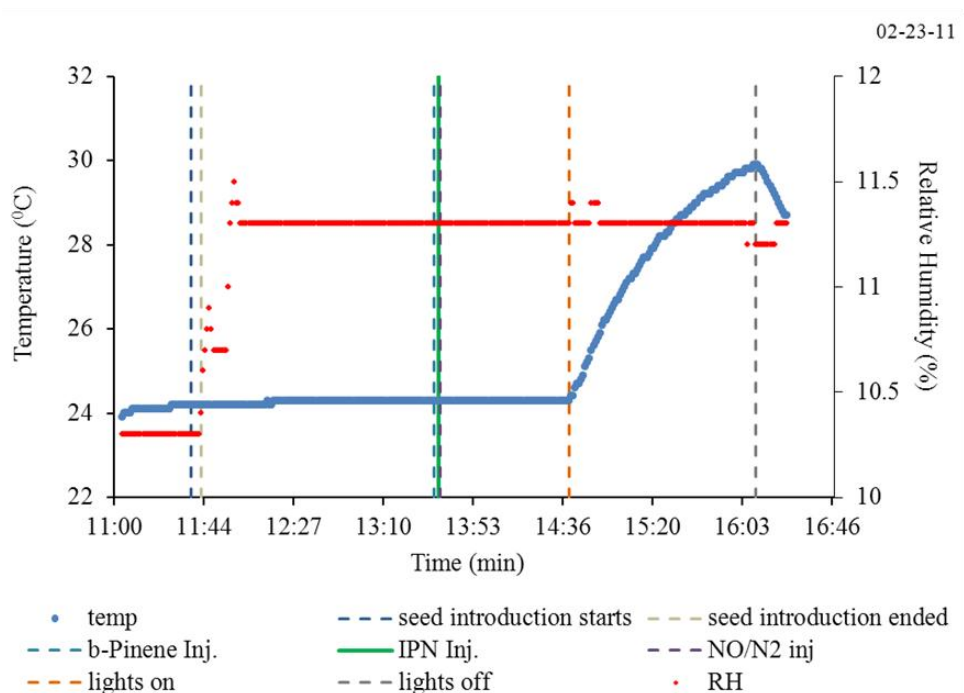


Figure C.1 Typical temperature and relative humidity time profile during a beta-pinene/HO experiments

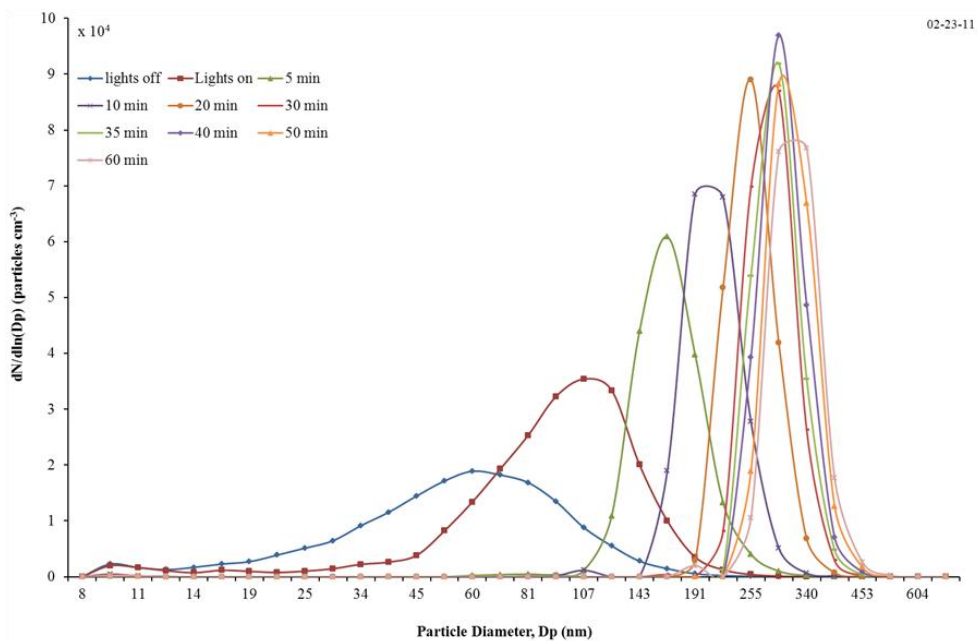


Figure C.2 Example of a beta-Pinene/HO experiment particle size distribution

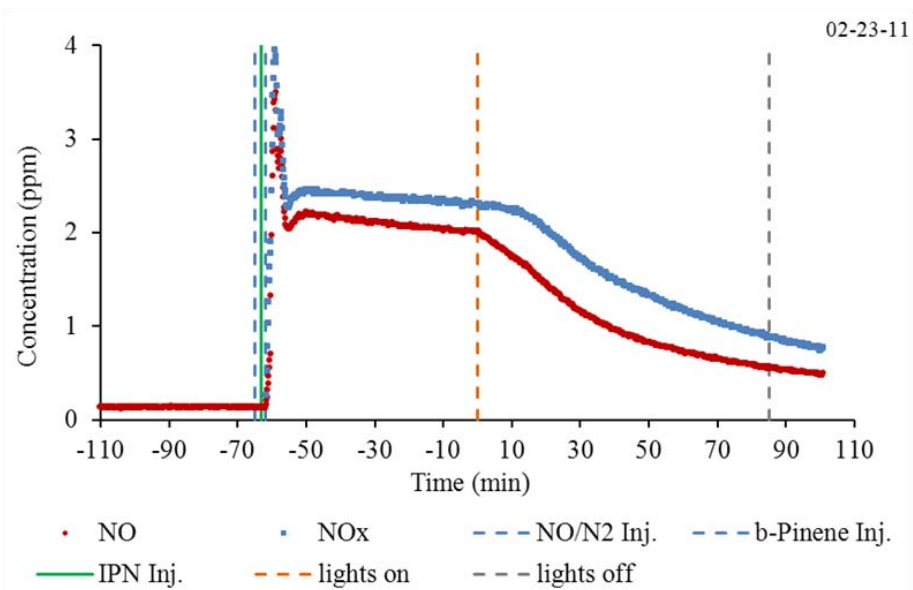


Figure C.3 Example NO and NOx time profile during a beta-pinene/HO chamber experiment

Appendix D. Sample Saturation Mixing Ratio Calculation for Pinic Acid

$$\ln\left(\frac{P_2}{P_1}\right) = \frac{\Delta H_{\text{vap}}}{R} \left(\frac{1}{T_1} - \frac{1}{T_2}\right) \text{ Clausius-Clapeyron Relation} \quad \text{Equation D.1}$$

Where:

$$\Delta H_{\text{vap}} = 109 \text{ kJ mol}^{-1}$$

$$P_{296\text{K}} = 3.2 \times 10^{-5} \text{ Pa [Bilde et al., 2001]}$$

Which makes $P_{373\text{K}} = 0.3 \text{ Pa}$

And lead to saturation mixing ratios of:

$$c_{\text{pinic acid, 296K}} = \frac{3.2 \times 10^{-5} \text{ Pa}}{1.01 \times 10^5 \text{ Pa}} \times 10^9 = 0.3 \text{ ppb} \quad \text{Equation D.2}$$

$$c_{\text{pinic acid, 373K}} = \frac{0.3 \text{ Pa}}{1.01 \times 10^5 \text{ Pa}} \times 10^6 = 3 \text{ ppm} \quad \text{Equation D.3}$$

Appendix E. Sample water droplet formation and evaporation rate for syringe

Done for a flow rate (Q_L) of $0.7 \mu\text{L min}^{-1}$ and temperature (T) of 100°C :

$$\phi = 4\pi a D \left(\frac{P_{\text{vapour}} MW}{RT} \right) \quad \text{Equation E.1}$$

Evaporation rate was equal to mass per unit time and liquid flow rate (Q_L)

$$\therefore Q_L \rho = 4\pi a D \left(\frac{P_{\text{vapour}} MW}{RT} \right) \quad \text{Equation E.2}$$

and the time (t) to evaporate the droplet would be = $\frac{\text{volume droplet}}{Q_L} =$ Equation E.3

$$\frac{\frac{4}{3}\pi a^3}{Q_L}$$

Where:

D = diffusion coefficient = $0.1 \text{ cm}^2\text{s}^{-1}$ (estimated) $P_{\text{vapour}} = \text{vapour pressure} = 1\text{atm}$

$\rho_{100^\circ\text{C}} = 0.96 \text{ g cm}^{-3}$ T = temperature = 373K

R = gas constant = $0.0821 \text{ L atm mol}^{-1} \text{ K}^{-1}$ MW = molecular weight = 18gmol^{-1}

$\Phi = \text{evaporation rate (mass time}^{-1}\text{)}$ a = droplet radius at tip of syringe

$Q_L = \text{Liquid flow rate (volume time}^{-1}\text{)}$

Using these calculations the radius of the droplet and time (t) to evaporate it would be:

a = $150\mu\text{m}$ t = 1.2 seconds

[Ahmad, 2010]

Appendix F. Time Constants of EDF Calibrations

Table F.1 Time constant (τ_{fit}) for alcohols based on relative signal

- = no data

Date	8-16-11	9-22-11	10-04-11	10-05-11	10-06-11	10-11-11	11-1-11
Compound	$\tau_{\text{relative signal}}$						
Methanol	4.8	4.3	4.3	4.4	4.6	5.0	5.0
Ethanol	4.7	4.7	5.1	4.3	-	5.2	5.2
n-Propanol	4.8	-	5.4	4.5	4.6	5.1	5.2
n-Butanol	4.6	5.0	5.1	4.8	4.7	4.5	5.0
i-Butanol	-	5.0	-	4.6	4.9	5.2	4.7
2-Propanol	4.8	5.2	4.6	-	5.0	4.4	4.8
t-Butanol	-	4.3	-	4.7	4.7	4.6	4.5

Table F.2 Time constant (τ_{fit}) for ketones based on relative signal

- = no data

Date	8-25-11	9-16-11	9-18-11	9-26-11	10-05-11	10-11-11	10-20-11
Compound	$\tau_{\text{relative signal}}$						
Acetone	5.1	6.2	4.7	4.8	4.6	5.2	4.8
Cyclopentanone	5.2	5.3	5.3	4.7	4.7	7.1	4.2
2-Pentanone	5.1	5.5	-	5.1	-	-	4.8
3-Pentanone	4.7	4.8	4.5	4.5	-	-	4.7
Cyclohexanone	4.7	5.3	-	5.1	5.4	6.6	4.7
Cycloheptanone	6.4	7.1	-	5.5	-	-	4.4

Appendix G. $\ln(\text{sensitivity})$ vs. Gas Phase Basicity (GB) data used for plotting calibration curves

Table F.1 Summary of alcohol $\ln(\text{sensitivity})$ values vs. ΔGB

where: $\Delta\text{GB} = \text{GB}_{\text{compound}} - \text{GB}_{\text{methanol}}$

S = sensitivity based on relative signal - = no data

Date		8-16-11	9-22-11	10-04-11	10-05-11	10-06-11	10-11-11	11-1-11		
Compound	ΔGB	$\ln\text{S}$							Average $\ln\text{S}$	Standard Deviation
Methanol	0	-2.90	-2.04	-2.53	-1.90	-2.94	-2.81	-2.81	-2.56	0.43
Ethanol	21.5	0.10	0.79	1.40	1.61	-	0.41	0.26	0.76	0.62
n-Propanol	31.6	1.41	1.55	2.09	1.67	1.69	0.64	1.59	1.52	0.44
n-Butanol	34.4	2.07	2.46	2.60	3.53	3.42	3.04	2.71	2.83	0.53
i-Butanol	37.7	-	2.01	-	3.99	3.00	3.10	1.57	2.73	0.96
2-Propanol	38.1	1.92	1.65	2.08	-	2.16	2.65	2.48	2.16	0.37
t-Butanol	47.7	-	3.61	-	4.01	4.40	4.25	3.91	4.04	0.31
Graph Data for $\Delta\ln\text{S}_{\text{individual days}}$ vs. ΔGB										
Individual Slope		0.134	0.111	0.131	0.131	0.153	0.150	0.137		
Individual y-intercept		-2.84	-1.92	-2.16	-1.64	-2.88	-2.90	-2.75		
Individual R^2		0.99	0.95	0.92	0.91	0.95	0.94	0.95		

Table G.2 Summary of ketone $\ln(\text{sensitivity})$ values vs. ΔGB

Date		8-25-11	9-16-11	9-18-11	9-26-11	10-05-11	10-11-11	10-20-11		
Compound	ΔGB	$\ln\text{S}$							Average $\ln\text{S}$	Standard Deviation
Acetone	0	2.40	1.93	2.43	2.48	2.27	2.48	2.30	2.33	0.19
Cyclopentanone	11.9	3.26	3.03	4.55	3.09	3.91	3.33	3.14	3.47	0.56
2-Pentanone	18.8	3.89	3.50	-	4.23	-	-	3.89	3.88	0.30
3-Pentanone	24.9	3.81	3.18	4.49	3.76	-	-	3.71	3.79	0.47
Cyclohexanone	29.1	5.15	4.28	4.91	4.53	5.23	4.14	4.55	4.68	0.42
Cycloheptanone	33.8	4.30	4.20	-	4.63	-	-	4.68	4.46	0.24
Graph Data for $\Delta\ln\text{S}_{\text{individual days}}$ vs. ΔGB										
Individual Slope		0.049	0.049	0.061	0.049	0.078	0.044	0.052		
Individual y-intercept		2.40	1.93	2.66	2.38	2.25	2.46	2.20		
Individual R^2		0.74	0.88	0.88	0.89	1.00	1.00	0.93		

Appendix H. EDF set-up B calibration data summary

Table H.1 Ketone Δ GB values and lnS values for individual days and lnS taken as an average for EDF (set-up B (**Figure 3.28** in **Section 3.5.2.4**))

where: Δ GB = GB_{compound} - GB_{acetone}

S = sensitivity based on relative signal - = no data

Date		11-3-11	11-4-11	11-7-11	11-11-11		
Compound	Δ GB	lnS				Average lnS	Standard Deviation
Acetone	0	2.52	2.79	2.73	2.60	2.66	0.12
Cyclopentanone	11.9	4.14	4.06	4.06	4.01	4.07	0.05
2-Pentanone	18.8	3.19	-	-	4.42	3.80	0.87
3-Pentanone	24.9	4.07	-	-	3.97	4.02	0.07
Cyclohexanone	29.1	4.86	-	-	5.24	5.05	0.27
Cycloheptanone	33.8	4.82	5.36	4.86	4.96	5.00	0.25
		Graph Data for Δ lnS _{individual days} vs. Δ GB					
Individual Slope		0.064	0.074	0.060	0.068		
Individual y-intercept		2.67	2.94	2.97	2.85		
Individual R ²		0.73	0.97	0.91	0.82		

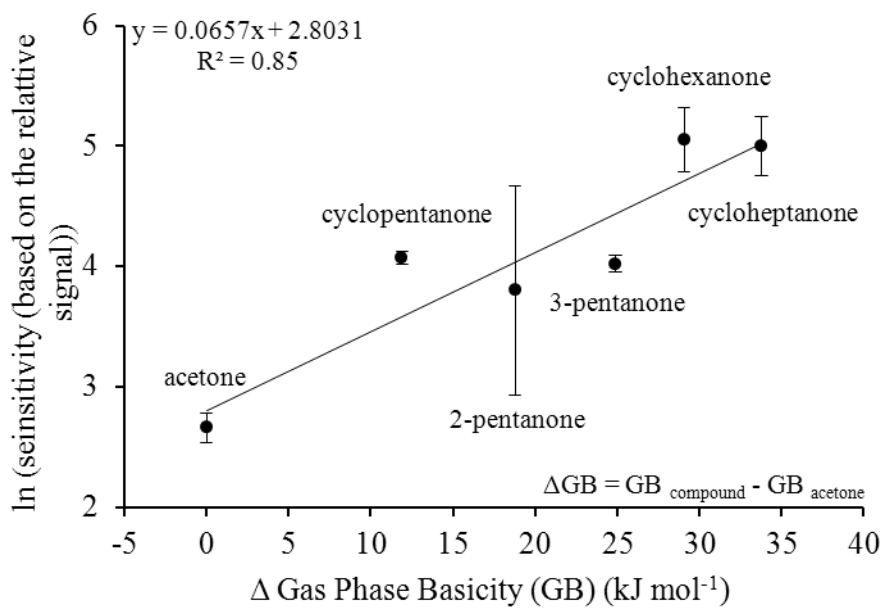


Figure H.1 lnS vs. ΔGB of Ketones using EDF Set-Up B (**Figure 3.28**)

Appendix I. Diffusion Tube Calculations [Nelson, 1971]

$$C = 10^6 \times \frac{q_d}{Q} \quad \text{Equation I.1}$$

Where:

C = concentration (ppm)

q_d = diffusion rate (ml min⁻¹)

Q = dilution gas flow rate (ml min⁻¹)

$$q_d = \left(\frac{D * M * P * A}{T * L * R} \right) \log \left(\frac{P}{P - P_V} \right) \quad \text{Equation I.2}$$

Where:

q_d = diffusion rate (g sec⁻¹)

D = diffusion coefficient (cm² sec⁻¹)

M = molecular weight of diffusing vapour (g mol⁻¹)

P = pressure in the capillary tube (atm)

A = capillary cross section (cm²)

T = temperature (K)

L = diffusion path length (cm)

P_V = partial pressure of the diffusing vapour (atm)

R = molar gas constant (ml atm mol⁻¹ K⁻¹)

$$D = D_0 \left(\frac{T}{T_0} \right)^m \left(\frac{P_0}{P} \right) \quad \text{Equation I.3}$$

Where:

D_0 = diffusion coefficient at standard conditions (cm² sec⁻¹)

T_0 = 273 K

P_0 = 1 atm

m = constant (usually 1.75-2)

$$C_i = \frac{q_{d,i} K}{F} \quad \text{Equation I.4}$$

Where:

C_i = concentration of analyte (ppm)

$q_{d,i}$ = emission rate (ng min⁻¹)

F = dilution flow (ml min⁻¹)

K = conversion factor (g sec⁻¹ to L sec⁻¹ at STP)

References

- Advanced Chemistry Development (ACD/Labs) Software (1994-2012 ACD/Labs)
- Ahmad, A. (2010). Characterization and Calibration of an Ion-Trap Time of Flight Mass Spectrometer. M.Sc. Annual Research Evaluation Report, York University.
- Aljawhary, D. (2011). Product Yields from the Gas-Phase Ozonolysis of Isobutene Using APCI-MS/MS. Chem 4000 Undergraduate Research Thesis Project Report, York University.
- Ambrose, J. L., K. Haase, R. S. Russo, Y. Zhou et al. (2010). An Inter comparison of GC-FID and PTR-MS Toluene Measurements in Ambient Air Under Conditions of Enhanced Monoterpene Loading. *Atmos. Meas. Tech. Discuss.*, 3: 1.
- Arey, J., R. Atkinson, and S. M. Aschmann (1990). Product Study of the Gas-Phase Reactions of Monoterpenes with the OH Radical in the Presence of NO_x. *J. Geophys. Res.*, 95: 18539.
- Atkinson, R. (2000). Atmospheric chemistry of VOCs and NO_x. *Atmos. Environ.*, 34: 2063.
- Atkinson, R. (1997). Gas-Phase Tropospheric Chemistry of Volatile Organic Compounds: 1. Alkanes and Alkenes. *J. Phys. Chem. Ref. Data.*, 26: 215.
- Atkinson, R., S. M. Aschmann, W. P. L. Carter, A. M. Winer et al. (1982). Alkyl Nitrate Formation from the Nitrogen Oxide (NO_x)-Air Photooxidations of C₂-C₈ n-Alkanes. *J. Phys. Chem.*, 86: 4563.
- Auld, J. (2009). A smog Chamber Study of Mechanisms for beta-Pinene Oxidation by Hydroxy Radicals. Ph.D., York University.
- Badjagbo, K., S. Sauvé, and S. Moore (2007). Real-Time Continuous Monitoring Methods for Airborne VOCs. *TrAC, Trends Anal. Chem.*, 26: 931.
- Barbu, A., M. (2003). Smog Chamber Studies of Aromatic Hydrocarbon Photooxidation by Hydroxyl Radicals. M.Sc., York University.
- Bauer, S. E. and S. Menon (2012). Aerosol Direct, Indirect, Semidirect, and Surface Albedo Effects from Sector Contributions Based on the IPCC AR5 Emissions for Preindustrial and Present-Day Conditions. *J. Geophys. Res. Atmos.*, 117: D01206.

- Bennett, J. F., F. Collin, and D. R. Hastie (2009). A Laboratory Flow Reactor with Gas Particle Separation and On-Line MS/MS for Product Identification in Atmospherically Important Reactions. *Atmos. Meas. Tech.*, 2: 813.
- Bienenstock, Y. S. (2001). Chamber Studies of Particulate Production from Hydroxyl Reactions with Toluene. M.Sc., York University.
- Bilde, M. and S. Pandis (2001). Evaporation Rates and Vapor Pressures of Individual Aerosol Species Formed in the Atmospheric Oxidation of alpha and beta-Pinene. *Environ. Sci. Technol.*, 35: 3344.
- Blake, R. S., P. S. Monks, and A. M. Ellis (2009). Proton-Transfer Reaction Mass Spectrometry. *Chem. Rev.*, 109: 861.
- Bouchoux, G. (2007). Gas-phase Basicities of Polyfunctional Molecules. Part 1: Theory and Methods. *Mass Spectrom. Rev.*, 26: 775.
- Cadle, S. H., P. J. Groblicki, and P. A. Mulawa (1983). Problems in the Sampling and Analysis of Carbon Particulate. *Atmos. Environ.*, 17: 593.
- Calogirou, A., N. R. Jensen, C. J. Nielsen, D. Kotzias et al. (1999). Gas-Phase Reactions of Nopinone, 3-Isopropenyl-6-oxo-heptanal, and 5-Methyl-5-vinyltetrahydrofuran-2-ol with OH, NO₃, and Ozone. *Environ. Sci. Technol.*, 33: 453.
- Cao, X. and C.N., Hewitt. (1999). The sampling and Analysis of Volatile Organic Compounds in the Atmosphere. *Reactive Hydrocarbons in the Atmosphere.*, edited by C. N. Hewitt. Academic Press, San Diego, U.S.A.
- Curtiss, L. A., K. Raghavachari, G. W. Trucks, and J. A. Pople (1991). Gaussian-2 Theory for Molecular Energies of First and Second-Row Compounds. *J. Phys. Chem.*, 94: 7221.
- de Gouw, J. A., P. D. Goldan, C. Warneke, W. C. Kuster et al. (2003). Validation of Proton Transfer Reaction-Mass Spectrometry (PTR-MS) Measurements of Gas-Phase Organic Compounds in the Atmosphere during the New England Air Quality Study (NEAQS) in 2002. *J. Geophys. Res.*, 108: 4682.
- De Hoffmann, E. and V, Stroobant. (2008). *Mass spectrometry: Principles and Applications* (3rd ed.). Wiley, New Jersey, U.S.A.
- Dickerson, R. R., S. Kondragunta, G. Stenchikov, K. L. Civerolo et al. (1997). The Impact of Aerosols on Solar Ultraviolet Radiation and Photochemical Smog. *Science.*, 278: 827.

- Downard, K. (2004). *Mass spectrometry: A foundation Course*. The Royal Society of Chemistry, Cambridge, U.K.
- Finlayson-Pitts, B.,J. and J.N.,Pitts Jr. (2000). *Atmospheric chemistry: Fundamentals and Experimental Techniques*. John Wiley & Sons, San Diego, U.S.A.
- Gauderman, W., G. Gilliland, H. Vora, E. Avol et al. (2002). Association Between Air Pollution and Lung Function Growth in Southern California Children - Results from a Second Cohort. *Am. J. Respir. Crit. Care Med.*, 166: 76.
- Glasius, M., M. Duane, and B. Larsen (1999). Determination of Polar Terpene Oxidation Products in Aerosols by Liquid Chromatography Ion Trap Mass Spectrometry *J. Chromatogr. A.*, 833: 121.
- Greenhouse, S. and F. Andrawes (1990). Generation of Gaseous Standards using Exponential Dilution Flasks in Series. *Anal. Chim. Acta*, 236: 221.
- Grosjean, D., E. L. Williams, E. Grosjean, J. M. Andino et al. (1993). Atmospheric Oxidation of Biogenic Hydrocarbons: Reaction of Ozone with beta-Pinene, D-Limonene and trans-Caryophyllene. *Environ. Sci. Technol.*, 27: 2754.
- Gross, J.H. (2010). *Mass spectrometry: a Textbook* (2nd ed). Springer, London, U.K.
- Guenther, A., C. Geron, T. Pierce, B. Lamb et al. (2000). Natural Emissions of Non-Methane Volatile Organic Compounds, Carbon Monoxide, and Oxides of Nitrogen from North America. *Atmos. Environ.*, 34: 2205.
- Hallquist, M., J. C. Wenger, U. Baltensperger, Y. Rudich et al. (2009). The Formation, Properties and Impact of Secondary Organic Aerosol: Current and Emerging Issues. *Atmos. Chem. Phys.*, 9: 5155.
- Harris, D. C. (2006). *Quantitative Chemical Analysis* (7th ed). W. H. Freeman, New York, U.S.A.
- Hatakeyama, S., K. Izumi, T. Fukuyama, H. Akimoto et al. (1991). Reactions of OH with α -Pinene and β -Pinene in Air: Estimate of Global CO Production from the Atmospheric Oxidation of Terpenes. *J. Geophys. Res.*, 96: 947.
- Herrera, L., J. Grossert, and L. Ramaley (2008), Quantitative Aspects of and Ionization Mechanisms in Positive-Ion Atmospheric Pressure Chemical Ionization Mass Spectrometry. *J. Am. Soc. Mass. Spectrom.*, 19, 1926.

- Hoffmann, T., R. Bandur, S. Hoffmann, and B. Warscheid (2002). On-line Characterization of Gaseous and Particulate Organic Analytes using Atmospheric Pressure Chemical Ionization Mass Spectrometry. *Spectrochim. Acta, Part B.*, 57: 1635.
- Hunter, E. P. L. and S. G. Lias (1998). Evaluated Gas Phase Basicities and Proton Affinities of Molecules: An Update. *J. Phys. Chem., Ref. Data*, 27: 413.
- Inman, E. L., E. Voigtman, and J. D. Winefordner (1982). Calibration Curve Preparation of Analytes in Liquid Solutions by Means of an Exponential Dilution Flask. *Appl. Spectrosc.*, 36: 99.
- Jaoui, M. and R. M. Kamens (2001). Mass Balance of Gaseous and Particulate Products Analysis from α -Pinene/NO_x/air in the Presence of Natural Sunlight. *J. Geophys. Res.*, 106: 12541.
- Jayne, J., D. Leard, X. Zhang, P. Davidovits et al. (2000). Development of an Aerosol Mass Spectrometer for Size and Composition Analysis of Submicron Particles. *Aerosol Sci. Technol.*, 33: 49.
- Jost, C., D. Sprung, T. Kenntner, and T. Reiner (2003). Atmospheric Pressure Chemical Ionization Mass Spectrometry for the Detection of Tropospheric Trace Gases: the Influence of Clustering on Sensitivity and Precision. *Int. J. Mass spectrom.*, 223-224: 771.
- Kansal, A. (2009). Sources and Reactivity of NMHCs and VOCs in the Atmosphere: A Review. *J. Hazard. Mater.*, 166: 17.
- Kawai, Y., S. Yamaguchi, Y. Okada, K. Takeuchi et al. (2003). Reactions of Protonated Water Clusters H⁺(H₂O)_n (n=1–6) with Dimethylsulfoxide in a Guided Ion Beam Apparatus. *Chem. Phys. Lett.*, 377: 69.
- Kebarle, P. (1977). Ion Thermochemistry and Solvation from Gas-Phase Ion Equilibria. *Annu. Rev. Phys. Chem.*, 28: 445.
- Kelly, F. (2003). Oxidative Stress: its Role in Air Pollution and Adverse Health Effects. *Occup. Environ. Med.*, 60: 612.
- Kirchstetter, T. W., C. E. Corrigan, and T. Novakov (2001). Laboratory and Field Investigation of the Adsorption of Gaseous Organic Compounds onto Quartz Filters. *Atmos. Environ.*, 35: 1663.

- Larsen, B. R., D. Di Bella, M. Glasius, R. Winterhalter et al. (2001), Gas-Phase OH Oxidation of Monoterpenes: Gaseous and Particulate Products. *J. Atmos. Chem.*, 38, 231.
- Lee, A., A. H. Goldstein, J. H. Kroll, N. L. Ng et al. (2006). Gas-phase Products and Secondary Aerosol Yields from the Photooxidation of 16 Different Terpenes. *J. Geophys. Res.*, 111: D17305.
- Lovelock, J. E. (1961). Ionization Methods for the Analysis of Gases and Vapors. *Anal. Chem.*, 33: 162.
- March, R.E. and R.J., Hughes. (1989). *Quadrupole Storage Mass Spectrometry.*, Vol. 102. John Wiley and Sons, New York, U.S.A.
- Mauderly, J. L. and J. C. Chow (2008). Health Effects of Organic Aerosols. *Inhal. Toxicol.*, 20: 257.
- McKinley, J. and R.E.,Majors. (2000). The Preparation of Calibration Standards for Volatile Organic Compounds - A Question of Traceability. *LC.GC. North Am.*, 18: 1024.
- McMurry, P. H. (2000). A Review of Atmospheric Aerosol Measurements. *Atmos. Environ.*, 34: 1959.
- Nelson, G. O. (1971). *Controlled Test Atmospheres: Principles and Techniques.* Ann Arbor Publishers, Ann Arbor, U.S.A.
- Nicolaides, A., A. Rauk, M. N. Glukhovtsev, and L. Radom (1996). Heats of Formation from G2, G2(MP2), and G2(MP2,SVP) Total Energies. *J. Phys. Chem.*, 100: 17460.
- Noyes, W. A. (1936). n-Butyl Nitrite. *Org. Synth.*, 16: 7.
- Orlando, J. J., B. Nozière, G. S. Tyndall, G. E. Orzechowska et al. (2000). Product Studies of the OH and Ozone Initiated Oxidation of Some Monoterpenes. *J. Geophys. Res.*, 105: 11561.
- Pilling, M. (2009). The Master Chemical Mechanism. <http://mcm.leeds.ac.uk/MCM/>
- Possanzini, M., A. Febo, and A. Liberti (1983). New Design of a High-Performance Denuder for the Sampling of Atmospheric Pollutants. *Atmos. Environ.*, 17: 2605.
- Proctor, C. J. and J. F. J. Todd (1983). Atmospheric Pressure Ionization Mass Spectrometry. *Org. Mass Spectrom.*, 18: 509.

- Ritter, J. J. and N. K. Adams (1976). Exponential Dilution as a Calibration Technique. *Anal. Chem.*, 48: 612.
- Ruiz, P. A., J. E. Lawrence, S. T. Ferguson, J. M. Wolfson et al. (2006). A Counter-Current Parallel-Plate Membrane Denuder for the Non-Specific Removal of Trace Gases. *Environ. Sci. Technol.*, 40: 5058.
- Sarrafzadeh, M. (2012). A Chamber Study of the Aging of Reaction Products Formed by Photo-Oxidation of beta-Pinene. Ph.D. Annual Research Evaluation Report., York University.
- Seinfeld, J. H. and S.N., Pandis. (2006). *Atmospheric Chemistry and Physics - From Air Pollution to Climate Change* (2nd Ed.). John Wiley & Sons, New Jersey, U.S.A.
- Seinfeld, J. H. and J. F. Pankow (2003). Organic Atmospheric Particulate Material. *Annu. Rev. Phys. Chem.*, 54: 121.
- Sunner, J., M. G. Ikonomou, and P. Kebarle (1988a). Sensitivity Enhancements Obtained at High Temperatures in Atmospheric Pressure Ionization Mass Spectrometry. *Anal. Chem.*, 60: 1308.
- Sunner, J., G. Nicol, and P. Kebarle (1988b). Factors Determining Relative Sensitivity of Analytes in Positive Mode Atmospheric Pressure Ionization Mass Spectrometry. *Anal. Chem.*, 60: 1300.
- Taft, R. W. (1983). Protonic Acidities and Basicities in the Gas phase and in Solution: Substituent and Solvent Effects. *Progress in Physical Organic Chemistry.*, vol. 14., edited by Department of Chemistry. John Wiley & Sons, Irvine, California.
- Twomey, S. A., Piepgrass, M. and Wolfe, T.L. (1984). An Assessment of the Impact of Pollution on Global Cloud Albedo. *Tellus B*, 36B: 356.
- Wang, H. C. and W. John (1988). Characteristics of the Berner Impactor for Sampling Inorganic-Ions. *Aerosol. Sci. Technol.*, 8: 157.
- Warneck, P. and J. Williams. (2012). *The Atmospheric Chemist's Companion Numerical Data for Use in the Atmospheric Sciences*. Springer, New York, U.S.A.
- Warscheid, B. and T. Hoffmann (2001). On-line Measurements of α -Pinene Ozonolysis Products Using an Atmospheric Pressure Chemical Ionisation Ion-Trap Mass Spectrometer. *Atmos. Environ.*, 35: 2927.

- Warscheid, B., U. Kückelmann, and T. Hoffmann (2003). Direct Quantitative Analysis of Organic Compounds in the Gas and Particle Phase Using a Modified Atmospheric Pressure Chemical Ionization Source in Combination with Ion Trap Mass Spectrometry. *Anal. Chem.*, 75: 1410.
- Wisthaler, A., N. R. Jensen, R. Winterhalter, W. Lindinger et al. (2001). Measurements of Acetone and Other Gas Phase Product Yields from the OH-Initiated Oxidation of Terpenes by Proton-Transfer-Reaction Mass Spectrometry (PTR-MS). *Atmos. Environ.*, 35: 6181.
- Zemp, E., S. Elsasser, C. Schindler, N. Kunzli et al. (1999). Long-Term Ambient Air Pollution and Respiratory Symptoms in Adults (SAPALDIA Study). *Am. J. Respir. Crit. Care Med.*, 159: 1257.